# 九州大学学術情報リポジトリ Kyushu University Institutional Repository

Studies on the Catabolic Pathway of Sterylglucoside and Its Physiological Significance in Cryptococcus neoformans and Saccharomyces cerevisiae

渡邉, 昂

https://doi.org/10.15017/1500796

出版情報:九州大学, 2014, 博士(農学), 課程博士

バージョン:

権利関係:全文ファイル公表済

Studies on the Catabolic Pathway of Sterylglucoside and Its

Physiological Significance in *Cryptococcus neoformans* and

Saccharomyces cerevisiae

Takashi Watanabe

# **CONTENTS**

CHA	PTER 1.	GENERAL INTRODUCTION	1
~~~.			
CHAPTER 2. Sterylglucoside catabolism and its biological significance			
in Cryptococcus neoformans			
2-1.	INTRODUCTION		17
2-2.	MATERIALS AND METHODS		20
2-3.	. RESULTS		28
2-4.	. DISCUSSION		34
2-5.	SUMMARY		37
FIGURES AND TABLES			38
CHAPTER 3. An ergosteryl-β-glucosidase (Egh1) involved in vacuole formation			
	in S	accharomyces cerevisiae	
3-1.	. INTRODUCTION		54
3-2.	MATERIALS AND METHODS		56
3-3.	. RESULTS		62
3-4.	. DISCUSSION		66
3-5.	SUMMARY		70
FIGURES AND TABLES			71
CHAPTER 4. GENERAL DISCUSSION			80
REFERENCES 8			
			00
ACKNOWLEDGMENTS			100

# **ABBREVIATIONS**

CG : cholesterylglucoside

EG : ergosteryl β-glucoside

EGCase : endoglycoceramidase

EGCrP1 : EGCase related Protein 1

EGCrP2 : EGCase related Protein 2

DKO : egcrp1/egcrp2-double-knock-out mutant

FA : fatty acid

GXM : glucuronoxylomannan

GSL : glycosphingolipid

Glc : glucose

GlcCer : glucosylceramide

hFA : 2-hydroxy fatty acid

HSP 70 : heat shock protein 70

IPC : inositol phosphoryl ceramide

1KO : egcrp1-knock-out mutant

2KO : egcrp2-knock-out mutant

LacCer : lactosylceramide

MIPA : micropexophagy-specific membrane apparatus

M(IP)<sub>2</sub>C : mannosyl diinositol phosphorylceramide

4MU : 4-methylumberifellyl or 4-methylumbelliferone

NAT : nourseothricin

NBD : 7-nitro-2,1,3-benzoxadiazole

PI3P : phosphatidylinositol 3-phosphate

 $PI(3,5)P_2$ : phosphatidylinositol 3,5-bisphosphate

PI4P : phosphatidylinositol 4-phosphate

*p*NP : *para*-nitrophenyl or *para*-nitrophenol

SG : sterylglucoside

SGT : sterol glucosyltransferase

SM : sphingomyelin

WT : wild type

# **CHAPTER 1. GENERAL INTRODUCTION**

In this thesis, the author describes the catabolism and functions of a steryl  $\beta$ -glucoside in fungi and yeast. Before the experimental details are discussed, some fundamental background information is provided as part of a general introduction. The scope of this research is also summarized at the end of this section.

# Cryptococcus neoformans

The pathogenic fungus *Cryptococcus neoformans* causes cryptococcosis, an opportunistic infectious disease. The typical symptoms of cryptococcosis are meningitis and pneumonia, and this disease frequently occurs in immunodeficient patients such as those with AIDS. It is estimated that cryptococcosis causes one million infections and 600,000 deaths per year; it is especially prevalent in Africa (1,2).

The most characteristic feature of *C. neoformans* is a thick polysaccharide capsule that surrounds the cell body (Fig. GI-1A). The capsule is composed of glucuronoxylomannan (GXM), which is a very long heteropolysaccharide comprising mannose, xylose, and glucuronic acid (3). The capsule allows *C. neoformans* to invade and remain in hosts (4) because it protects against phagocytosis by macrophages (5). The capsule also allows the fungi to grow in phagocytic cells by protecting against attacks by host cells (6,7). This result was disclosed by an experiment using acapsular mutants of *C. neoformans* that cannot replicate inside phagocytic cells (6-9). Collectively, the polysaccharide capsule was demonstrated to be an important virulence factor that allows *C. neoformans* to infect humans.

C. neoformans was originally divided into four serotypes (A, B, C, and D) (Fig. GI-1B); however, serotypes B and C were classified as C. gattii in 1970 (10). Although C. neoformans is

distributed worldwide, *C. gattii* is restrictively distributed in tropical areas (11-13). *C. neoformans* is primarily an opportunistic pathogen; in contrast, *C. gattii* causes cryptococcosis in immunocompetent individuals (13). In the early 2000, *C. gattii* became well known after an outbreak of infections on Vancouver Island in British Columbia, Canada (14-17).

Cryptococcosis is classified among deep-seated mycoses, and several antibiotics have been developed to treat this serious disease. Amphotericin B, which binds ergosterol and forms pores in the fungal membrane, is frequently used to treat mycoses, including cryptococcosis. Other drugs used for cryptococcosis include fluconazole and flucytosine; the former inhibits ergosterol synthesis, and the latter inhibits DNA synthesis. However, these drugs have caused problems such as severe side effects and the appearance of a highly drug-resistant form of *C. neoformans* (18). Thus, the development of new anti-cryptococcal drugs is urgently required.

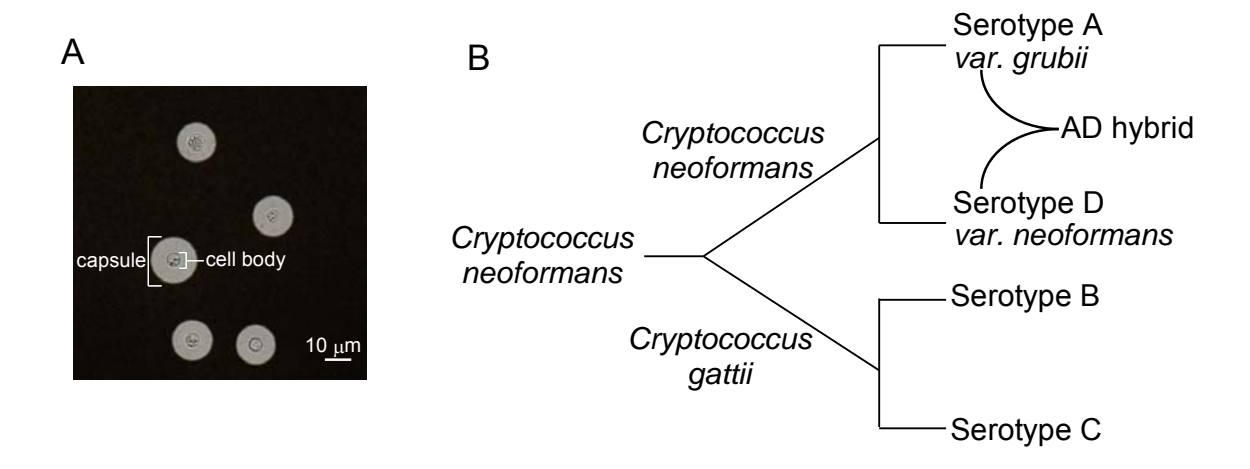


# FIGURE GI -1. Serotype and structure of *Cryptococcus neoformans*.

A, C. neoformans serotype A stained with India ink. After culture at 25°C for 1 day in 10% Sabouraud liquid medium, pH 7.0, cells were stained with India ink. B, C. neoformans is divided into C. neoformans (serotype A, D, and AD hybrid) and C. gattii (serotype B and C).

# Fungal sphingolipids and glycosphingolipids

Sphingolipids are a class of lipids that contain a ceramide or sphingoid base within the molecule. Sphingolipids are mainly classified as glycosphingolipids (GSLs) and phosphosphingolipids; as hydrophilic moieties, the former possesses sugar residues, whereas the latter possesses phosphoryl groups. Sphingolipids, including GSLs, are membrane components and form the lipid microdomain (so-called lipid raft) with cholesterol within the membrane. GSLs and their metabolites are involved in many cellular events such as cell-cell interactions, cell adhesion, cell differentiation, cell growth, and signal transduction (19-23). GSLs are also utilized by pathogens and intestinal bacteria to invade cells or remain at the cell surface (24).

The molecular species of membrane lipids are somewhat different between mammals and fungi. Fungi do not have sphingomyelin (SM); alternatively, they have inositol phosphoryl ceramide (IPC) as their main phosphosphingolipid (25). In fungi, ergosterol is the major sterol, whereas cholesterol is the main sterol in mammals. Sterols are essential for forming lipid microdomains, and ergosterol exhibited stronger domain-promoting activity than cholesterol in *in vitro* experiments (26). It was reported that ergosterol interacts with IPC, mannose-IPC (MIPC), and mannose-(inositol phosphoryl)<sub>2</sub> ceramide (M(IP)<sub>2</sub>C) in the microdomain of fungi, whereas cholesterol interacts with GSLs and SMs in the microdomain of mammals (27-30).

The putative sphingolipid synthesis pathway proposed for fungi (31) is described below. 3-Ketosphinganine is generated from the condensation reaction of L-serine with palmitoyl-CoA that is catalyzed by serine palmitoyl transferase (SPT). 3-Ketosphinganine reductase converts 3-ketosphinganine into dihydrosphinganine. Ceramide synthase (CerS) then transfers the  $\alpha$ -hydroxy fatty acid (hFA) (32,33). Through the overall reaction, dihydroceramide (d18:0/hFA) is synthesized. However, after the synthesis of phytosphingosine (t18:0) by dihydroceramide

C4-hydroxylase (Des2), phytoceramide is synthesized by CerS (34). Phosphosphingolipids such as IPC, MIPC, and M(IP)<sub>2</sub>C are mainly synthesized from the precursor phytoceramide. Dihydroceramide is modified by dihydroceramide Δ4-desaturase (Des1) (35), sphingolipid Δ8-desaturase (36), and sphingolipid C9-methyltranseferase (SMT1) to produce fungal-specific ceramide (d18:2+9Me/hFA), which is very unique in structure because of the presence of not only double bonds at C4 and C8 but also a methyl branch at C9 in the sphingoid base (37-39). The fungal ceramide is then converted to glucosylceramide (GlcCer) by GlcCer synthase 1 (GSC1).

GCS1, which is highly conserved from lower eukaryotes to humans, catalyzes the transfer reaction of glucose (Glc) from UDP-Glc to ceramide. The specificity of GCS1 for lipid moieties is very broad; thus, the enzyme can utilize fungal-specific ceramide as well as ceramide, dihydroceramide, and phytoceramide as a substrate. As a result, both GlcCer with fungal-specific ceramide (d18:2+9Me/hFA) and GlcCer with immature ceramide (d18:2/hFA, d18:1/hFA, d18:0/hFA) were generated via the fungal GlcCer synthesis pathway. In the ceramide synthesis pathway, the fungal-specific ceramide (mature ceramide) is sequentially generated from immature ceramide, which lacks double bond(s) or methyl branch, in the following order: d18:0/hFA  $\Rightarrow$  d18:1/hFA  $\Rightarrow$  d18:2/hFA. Endoglycoceramidase (EGCase)-related Protein 1 (EGCrP1) hydrolyzes immature GlcCer during GlcCer synthesis in *C. neoformans*, resulting in the production of homogeneous GlcCer with homogeneous ceramide moieties (d18:2+9Me/hFA)(40). *C. neoformans* EGCrP1-deletion mutants exhibited GlcCer with heterogeneous ceramide moieties, resulting in incomplete synthesis of the polysaccharide capsule in these mutants. This result may indicate that the quality control of GlcCer ceramide moiety by EGCrP1 is deeply related to capsule formation in *C. neoformans* (40).

GlcCer is thought to be biologically relevant in fungi; this simple GSL is involved in cell division and budding (41-43), interactions between fungi and insects or plants (44), alkaline toler-

ance (45,46), and infection processes in mice and plants (45-47). Notably, however, the budding yeast *Saccharomyces cerevisiae*, which is a subject in Chapter 3, does not contain GlcCer (48).

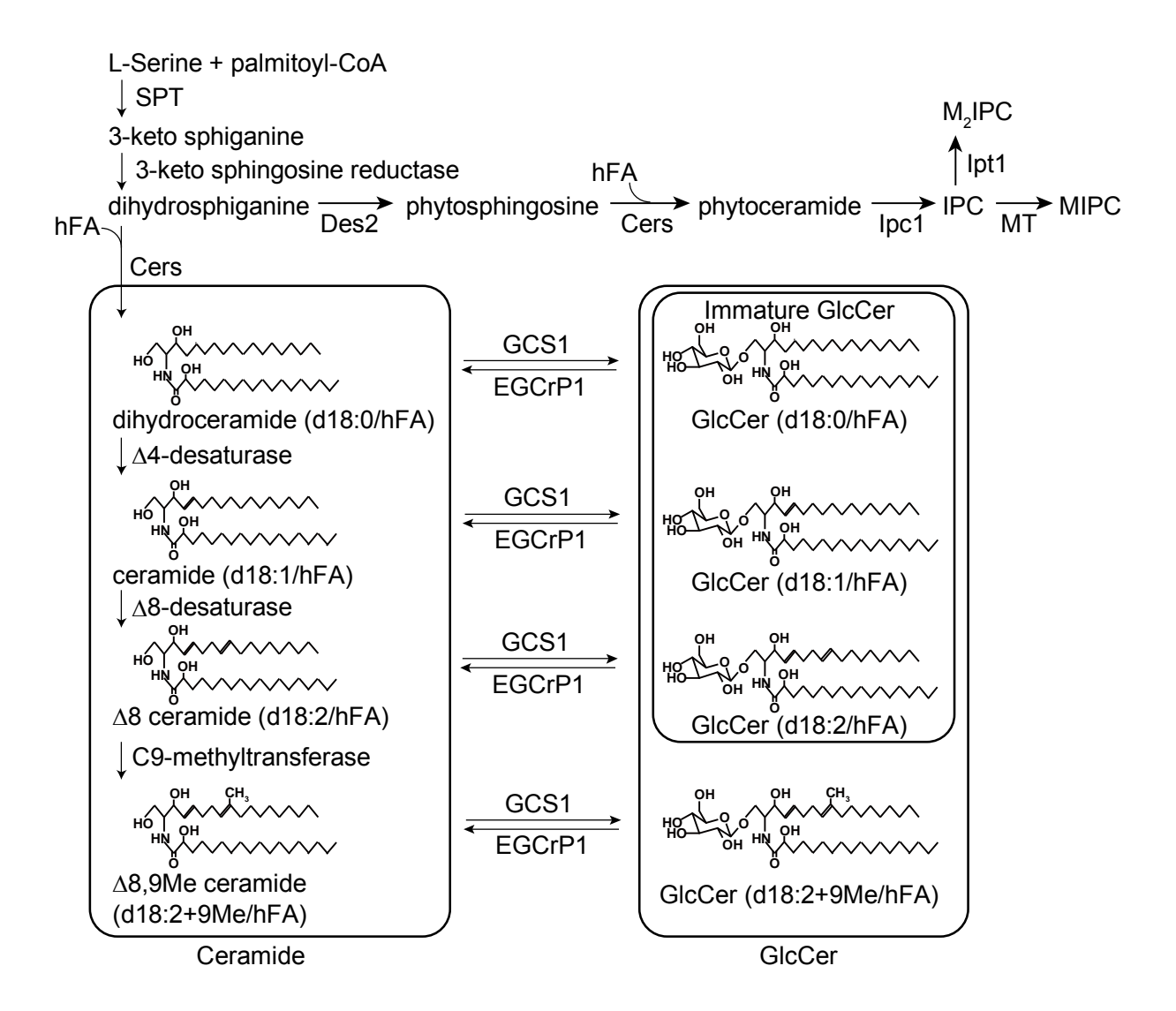


FIGURE GI -2. Hypothetical scheme for the sphingolipid biosynthetic pathway in *C. neoformans*.

# Steryl glucosides

Steryl glucoside (SG) is the most abundant sterol in many organisms (49). However, the abundance of sterols differs in different organisms (Fig. GI-3A); cholesteryl glucoside (CG) (50), sitosteryl glucoside (51), and ergosteryl glucoside (EG) (52) are the major SGs in animals, plants, and fungi, respectively.  $\beta$ -Glc is usually bound to sterol moieties; however,  $\alpha$ -Glc is bound to sterol moieties in *Helicobacter pylori* (53).

In fungi, SG is synthesized by a sterol glucosyltransferase (SGT), which transfers Glc from UDP-Glc to sterols (Fig. GI-3B). For example, Ugt51/Atg26, a homologue of plant Ugt80A1 and 2, appears to be responsible for EG synthesis in fungi and in budding yeast (54-57). However, it remains to be elucidated in yeast whether Ugt51/Atg26 can actually synthesize EGs *in vivo* because EGs cannot be detected in wild type (WT) or *UGT51/ATG26*-mutant yeast. This issue will be discussed in Chapter 3.

The SGT domain structures (PpSGT) have been studied in *Pichia pastoris* (58). PpSGT comprises a PH domain, a GRAM domain, and a catalytic domain. Although the catalytic domain is essential for SG synthesis, the PH and GRAM domains are not required for the catalytic reaction. However, the GRAM domain is necessary for the correct localization of PpSGT. Sakai *et al* clearly indicated that PpSGT was involved in peroxisome degradation through a type of autophagy termed pexophagy (58). At least two patterns of peroxisome degradation have been proposed; macropexophagy and micropexophagy (Fig. GI-4A) (59). During macropexophagy, peroxisomes are individually released from membranes, thereby forming a pexophagosome (Fig. GI-4B). This organelle fuses with the vacuolar membrane, exposing the incorporated peroxisome to vacuolar hydrolases. During micropexophagy, a cluster of peroxisomes is enclosed by vacuolar membrane protrusions and/or segmented vacuoles as well as by a newly formed membrane structure termed 'microp-

exophagy-specific membrane apparatus (MIPA)'. GRAM domain-deleted PpSGT mutants were found to form SGs but not MIPAs *in vivo* (58-60). Catalytic domain-deleted PpSGT mutants were unable to form MIPAs. These results indicated that PpSGT requires not only the catalytic domain but also the GRAM domain to perform pexophagy *in vivo*. In contrast to *P. pastoris*, UGT51/ATG26 was not involved in the process of autophagy in *S. cerevisiae* and *Yarrowia lipolytica* (61,62).

SG synthesis is induced in cells treated with unusually high temperature (heat shock). In human fibroblasts, heat shock induces CG accumulation, followed by expression of heat shock protein 70 (HSP70) (50). Upon adding CG to human fibroblast cultures, HSP70 was induced without heat shock, suggesting that CG is a lipid mediator of stress-induced HSP production (63). Because SG also accumulates in mold cells following heat shock (64), this glycolipid appears to be a signaling molecule in lower eukaryotes as well as in mammals under stress conditions. The GC content is increased not only by heat but also by cold shock; the CG content in the rat stomach is increased under cold conditions, possibly to inhibit ulcer formation (65).

Arabidopsis thaliana has three sterol glucosyltransferases (Ugt80A2, Ugt80B1 and Ugt713B1) (66,67). *Ugt80A2*-deletion mutants showed relatively minor growth effects, whereas *ugt80B1*-deletion mutants exhibited pronounced abnormal phenotypes, including abnormal development, the abnormal accumulation of seed suberin, which is a hydrophobic substance that prevents water from penetrating the tissue, and the abnormal formation of cutin, which is a component of the plant cuticle in the seed coat (66). *S. cerevisiae* expressing recombinant Ugt713B1 synthesized SG; however, it is unlikely to synthesize SG *in vivo* (67). In the plant-pathogenic fungus *Colletotrichum gloeosporioides*, SGT is required for the infection of its natural host, the avocado fruit, although fungal growth and appressorium formation appeared to be normal in SGT-deletion mutants (68). In the cucumber anthracnose fungus *Colletotrichum orbiculare*, SGT is also an essential vir-

ulence factor for host invasion (69). Furthermore, pexophagy is significantly delayed in the SGT-deletion mutants of *C. orbiculare*, and both the GRAM and catalytic domains are required for pexophagy in *C. orbiculare*. *C. orbiculare* SG was also shown to be involved in the infection process; however, this was not the case for the rice pathogen *Magnaporthe oryzae* (70).  $\alpha$ CG-deficient *H. pylori* was found to induce the inflammatory response and was unable to survive in host cells (71). Furthermore, the addition of  $\alpha$ CG but not  $\beta$ CG to *H. pylori* SG-deletion mutant cultures protected against phagocytosis by macrophages, suggesting that  $\alpha$ CG is involved in the suppression of phagocytosis in the host (71).

As described above, the synthesis of SG by SGT and its biological significance have been extensively investigated. However, SG catabolism remains poorly understood because the enzyme responsible for SG degradation *in vivo* has not been identified. *Sinapis alba* seedlings (72), as well as *Sulfolobus solfataricus LacS*, expressed in *E. coli* (73), hydrolyzed SG under acidic conditions. However, it remains unclear whether these enzymes are involved in SG catabolism *in vivo*.

FIGURE GI -3. Structure and metabolic pathway of sterylglucosides.

(EC 2.4.1.173, Ugt51/Atg26)

Steryl β-glucoside

Glc + Sterol

(EC 3.2.1.104)

Steryl-β-glucosidase

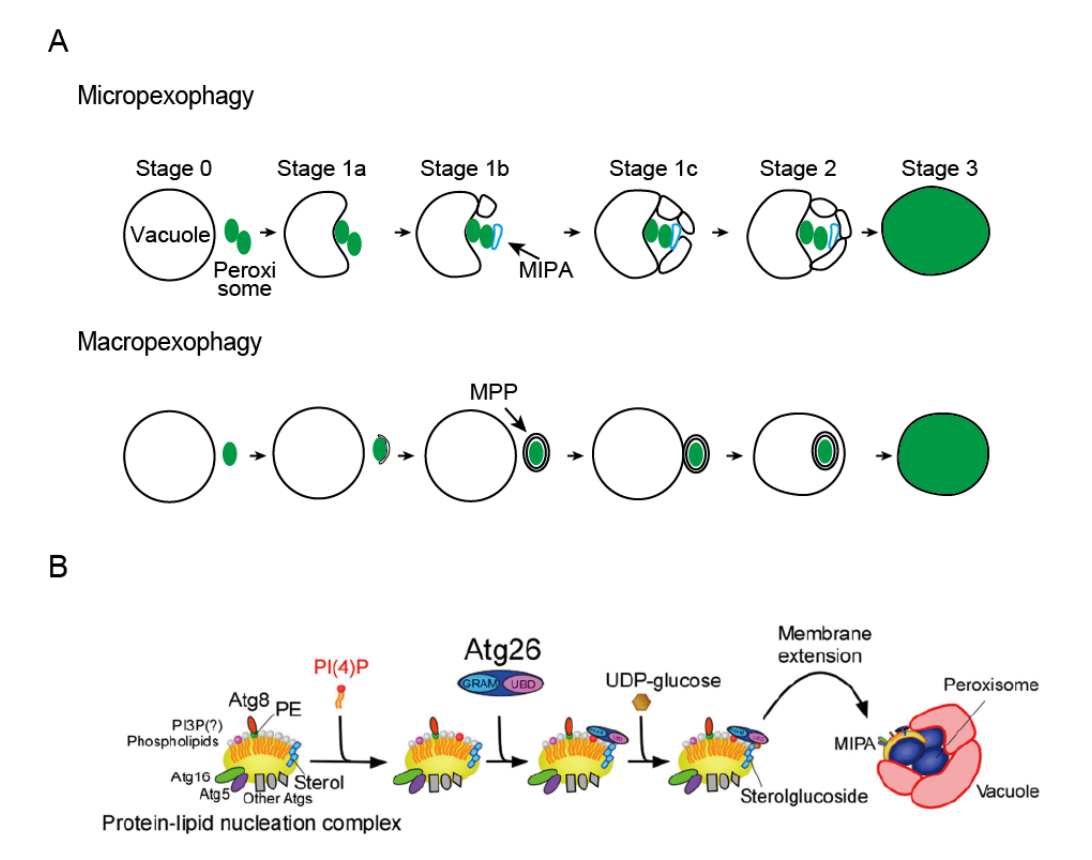


# FIGURE GI-4. Two modes and mechanism of pexophagy.

These figures are from Ref. 59 and 60. MIPA, micropexophasic apparatus; MPP, macropexophagosome; PE, phosphatidylethanolamine; PI(3)P, phosphatidylinositol 3-phosphate; PI(4)P, phosphatidylinositol 4-phosphate.

# **Vacuoles**

Vacuoles are the largest organelles in fungi and yeasts. The basic functions of fungal vacuoles are common to those of mammalian lysosomes and plant vacuoles. They degrade cellular components and pool ions and metabolites to maintain cellular homeostasis (74-77).

The acidic organelles in fungi include vacuoles, early and late endosomes, and the late Golgi apparatus (78). The pH within the vacuoles is acidic (approximately pH 6.0), in contrast to the neutral pH that is maintained in the cytosol (79-82). The major player in acidification is a vacuolar H<sup>+</sup>-ATPase, which transports protons from the cytosol to vacuolar lumen (83). Many vacuolar functions are dependent on its acidity; vacuolar lumenal and membrane enzymes work most efficiently at an acidic pH (80), soluble proteins are efficiently sorted at an acidic pH (84,85), and ions and metabolites are transported across the vacuolar membrane under acidic conditions (86-89). Vacuolar fission and fusion are also regulated by the vacuolar pH (90-92).

The yeast vacuole is a highly dynamic organelle that continuously undergoes fusion and fission. Fusion requires regulatory lipids such as ergosterol, diacylglycerol, phosphatidylinositol 3-phosphate (PI3P) and phosphatidylinositol 4-phosphate (PI4P) (93,94). In cells lacking these lipids, the fragmentation of vacuoles was observed, suggesting that fusion is inhibited. These "regulatory lipids" are necessary for the enrichment of other fusion factors such as SNAREs, Ypt7p1 and HOPS in vacuoles (94). Ergosterol is of special interest because the disruption of genes encoding ergosterol biosynthesis enzymes caused striking vacuole fragmentation despite the presence of ergosterol precursors such as ergostatetraenol and zymosterol (93).

The molecular mechanism of fission of vacuolar vesicles remains largely unknown. Upon cell division, vacuoles are inherited (95). Vac14-, Vac7- or Fab1-deletion mutants, which lack the protein required for PI(3.5)P<sub>2</sub> production, exhibited grossly enlarged vacuoles. PI(3.5)P<sub>2</sub> was

not detectable in the Vac14-, Vac7-, and Fab1-deletion mutants. PI(3,5)P<sub>2</sub> is considered to be a binding site of Atg18, which is a Fab1 effector, on the vacuolar membrane. Atg18 is recruited from the cytosol to the vacuolar membrane in a manner that is dependent on the amount of PI(3,5)P<sub>2</sub> on the vacuolar membrane. Atg18-deletion mutants also exhibited enlarged vacuoles (96), although the PI(3,5)P<sub>2</sub> content in Atg18-deletion mutants was increased. These results may indicate that Atg18 is a "sensor" for PI(3,5)P<sub>2</sub> levels that is related to vesicle fission and membrane recycling in vacuoles (96-98).

# The scope of this study

*C. neoformans* contains large amounts of EG, most popular SG in fungi; thus, the enzymes involved in SG metabolism could be promising targets for the treatment of cryptococcosis; however, the metabolism of fungal SG, especially its catabolism, has yet be fully understood. To develop anti-fungal drugs based on this new concept, it is necessary to elucidate the catabolic pathway of SG in *C. neoformans*.

This thesis addresses the catabolic pathway of SG and its physiological significance in *C. neoformans* (Chapter 2) and *S. cerevisiae* (Chapter 3).

Chapter 2 describes the characterization and functional analysis of an SG-degrading enzyme (steryl-β-glucosidase) in *C. neoformans*. The author and co-workers first tried to identify an EGCrP1 homologue in the genome database of *C. neoformans*. EGCrP1 is a glucocerebrosidase in C. neoformans that participates in GlcCer quality control in vivo (40). Because C. neoformans EGCrP1-deletion mutants still showed glucocerebrosidase activity, the EGCrP1 homologue EGCrP2, was expected to be another glucocerebrosidase. A candidate gene for EGCrP2 was identified in the genome database of C. neoformans, and the gene was disrupted by the split marker method using nourseothricin (NAT)- and hygromycin-resistance genes as selection markers. Recombinant EGCrP2 expressed in E. coli hydrolyzed various SG as well as GlcCer. This result indicated that the specificity of EGCrP2 is completely different than that of EGCrP1 because EGCrP1 is specific to GlcCer and is unable to hydrolyze SGs. Unexpectedly, GlcCer did not accumulate in EGCrP2-deletion mutants; alternatively, an unknown glycolipid accumulated in the mutants. Mass spectrometry and 2-dimensional NMR analyses revealed that this unknown glycolipid was EG, indicating that EGCrP2 is involved in EG catabolism in vivo. This is the first report to identify the steryl-β-glucosidase in fungi. EGCrP2-deletion mutants showed distinct growth arrest, dysfunctional cell budding, and abnormal vacuole morphology, suggesting that EGCrP2 is a potential target for antifungal drugs.

Chapter 3 describes the identification of an EG-degrading enzyme in S. cerevisiae and the functional analysis of the enzyme in relation to vacuole formation. The EGCrP2 homologue Egh1 in budding yeast was found in a genome database of S. cerevisiae; this microorganism is considered to be a powerful tool for investigating the molecular mechanism of vacuole formation. Recombinant EGH1 expressed in E. coli hydrolyzed various β-glucosides, including SGs and GlcCer. EGH1-deletion mutants were generated by homologous recombination using the kanamycin-resistance gene as a selectable marker. The EGH1-deletion mutants accumulated EG similar to C. neoformans, indicating that the EGCrP2 homologues of S. cerevisiae is also involved in EG catabolism in vivo. UGT51/ATG26, which is an SGT in S. cerevisiae, was then disrupted in EGH1-deletion mutants. The double-knockout mutants did not accumulate EG, indicating that EG is synthesized by Ugt51/Atg26 and degraded by Egh1 in S. cerevisiae. In the EGH1-deletion mutants, the fragmentation of vacuoles was observed; this was in contrast to C. neoformans egcrp2-deletion mutants, which displayed enlarged vacuoles. The discrepancy in vacuole morphology in steryl- $\beta$ -glucosidase-deletion mutants may stem from the different EG contents of C. *neoformans* and *S. cerevisiae*. The EG content of *C. neoformans* is  $\geq$ 10 times higher than that of *S.* cerevisiae. Taken together, these results indicate that EG catabolism is deeply related to vacuole formation in fungi and yeasts.

# **CHAPTER 2**

# Sterylglucoside catabolism and its biological significance in *Cryptococcus neoformans*

#### 2-1. INTRODUCTION

Cryptococcosis is an infectious disease caused by pathogenic fungi such as *Cryptococcus* neoformans and *C. gattii*. The prevalence of cryptococcosis has increased over the past 20 years because of the increase in AIDS patients and expanded use of immunosuppressive drugs. More than 600,000 patients with immune deficiencies were reported to have died within 3 months of being infected with *C. neoformans* (1). The highly virulent *C. gattii*, a primary pathogen in healthy individuals and animals, was recently detected in the US and Canada (99). Thus, the development of new drugs against cryptococcosis is urgently needed.

*C. neoformans* synthesizes a glucosylceramide (GlcCer) composed of β-linked glucose and ceramide that possesses a characteristic sphingoid base, which has two double bonds at C4/C8 in the trans conformation and a methyl substitution at C9 (31). Previous studies reported that this fungus-specific GlcCer may be strongly associated with the pathogenicity of *C. neoformans*, and, thus, the enzymes involved in the synthesis of GlcCer, (*e.g.* UDP-glucose:ceramide glucosyltransferase (45,48), sphingoid base C4/C8 desaturase (36,100) and C9 methyltransfearase (37,38) have been intensively studied and the genes responsible for these enzyme activities have also been identified. However, how GlcCer is catabolized in fungi remains unclear because the enzyme(s) responsible for degrading GlcCer in fungi have not yet been identified.

Endoglycoceramidase-related protein 1 (EGCrP1) is a homologue of endoglycoceramidase (EGCase, ceramide glycanase; EC.3.2.1.123), which is an endo-type glycosidase capable of cleaving

the β-glycosidic linkage between the ceramide (Cer) and oligosaccharide of various glycosphingolipids (GSLs) to release an intact oligosaccharide and Cer (101-103). EGCase very weakly hydrolyzes GlcCer, while EGCrP1 specifically hydrolyzes GlcCer, but not oligosaccharide-linked GSLs such as LacCer, GM1a, and Gb3Cer, which are favorite substrates for EGCase. Thus, EGCrP1 was the first identified GlcCer-degrading enzyme (glucocerebrosidase) in fungi (40). Although the disruption of *egcrp1* in *C. neoformans* reduced glucocerebrosidase activity under neutral conditions, the activity remained almost unchanged under acidic conditions, suggesting the presence of other glucocerebrosidase(s) that function in *C. neoformans* under acidic conditions.

Fungi have two major glycolipids: GlcCer and sterylglucoside. The former is related to pathogenicity of fungi (45) and the latter is involved in stress-mediated signal transduction (63). Sterylglucoside synthase (UGT51) was identified in budding yeast (54). However, the enzyme(s) involved in sterylglucoside catabolism have not yet been identified in fungi or yeasts.

The author herein reported the molecular cloning, enzymatic characterization, and physiological relevance of EGCrP2, a homologue of EGCrP1, in *C. neoformans*. The specificity of EGCrP2 for aglycone moiety differed completely from that of EGCrP1; the former hydrolyzed not only GlcCer, but also various  $\beta$ -glucosides including steryl  $\beta$ -glucosides, *para*-nitrophenyl (*p*NP)- $\beta$ -glucoside, and 4-methylumberifellyl (4MU)- $\beta$ -glucoside, while the latter specifically hydrolyzed GlcCer, but not the other  $\beta$ -glucosides tested. Neither EGCrP1 nor EGCrP2 hydrolyzed  $\beta$ -galactosides or  $\alpha$ -glucosides, indicating that both enzymes were  $\beta$ -glucosidases with different aglycone specificities. The disruption of *egcrp2*, but not *egrcp1*, resulted in the accumulation of an unknown glycolipid, which was subsequently identified as an ergosteryl  $\beta$ -glucoside (EG) after purification. EG is a major molecular species of sterylglucoside in fungi and yeasts. These results indicated that EGCrP2 functioned *in vivo* as a steryl- $\beta$ -glucosidase, which is a missing link in sterylglucoside metabolism in fungi. This study also provided evidence to show that EGCrP2 may be a

promising target for the development of anti-fungus drugs for *C. neoformans*.

# 2-2. MATERIALS AND METHODS

#### **Materials**

C6-7-nitro-2,1,3-benzoxadiazole (NBD)-Cer, C6-NBD-GlcCer, and C12-NBD-Gb3Cer were purchased from Matreya, and C6-NBD-LacCer, C6-NBD-GalCer, *p*NP glycosides, 4MU glycosides, and resorufin-β-D-glucopyranoside were from Sigma-Aldrich. C12-NBD-GM1 and C12-NBD-sphingomyelin were prepared using the sphingolipid Cer *N*-deacylase by the method described in (104).

#### **Strain and culture**

C. neoformans var. grubii serotype A strain H99 (ATCC 208821) was purchased from the American Type Culture Collection (ATCC). C. neoformans was cultured at 30°C in YPD medium (2% Glc, 2% peptone, 1% yeast extract).

# **Construction of expression vector**

Total RNA was obtained from fungus cells using Sepasol-RNA I Super G (Nacalai Tesque). First strand cDNA was synthesized from 1 µg of total RNA using PrimeScript Reverse Transcriptase (Takara Bio Inc.). To insert the restriction sites, PCR was carried out using first strand cDNA as a template and the expression primers listed in Table 2-1. Amplification was performed using PrimeSTAR GXL DNA polymerase (Takara Bio Inc.). The amplified product was digested with appropriate restriction enzymes and inserted into the corresponding sites of pET23a (Novagen).

# **Expression of recombinant EGCrP2**

The EGCrP2 gene (egcrp2) of C. neoformans (CNAG 05607) was expressed in Esche-

richia coli BL21 (DE3) by inserting a pET23a vector (Novagen) containing egcrp2. After incubating the transformants at 37°C in Luria-Bertani (LB) medium containing 100 µg/ml of ampicillin until the  $A_{600 \text{ nm}}$  reached  $\sim 0.6$ , isopropyl  $\beta$ -D-thiogalactopyranoside was then added to the culture at a final concentration of 1 mM. After cultivation for 24 h, the cells were harvested by centrifugation (8,000 × g for 15 min), and suspended in 50 mM Tris-HCl buffer, pH 7.5, containing 150 mM NaCl and 20 mM imidazole. The suspension was kept in a sonic bath for 30 sec, this procedure was repeated 4 times to crush the cells, and cell debris was removed by centrifugation (18,000 x g for 15 min). The supernatant was applied to a Ni Sepharose 6 Fast Flow resin (GE Healthcare) packed in a Muromac mini column M (Muromachi Technos), and the column was then washed with 50 mM Tris-HCl, pH 7.5, containing 150 mM NaCl and 40 mM imidazole. Recombinant EGCrP2 was eluted with 50 mM Tris-HCl, pH 7.5, containing 150 mM NaCl and 200 mM imidazole. The purified enzyme was dialyzed against 50 mM Tris-HCl, pH 7.5, containing 150 mM NaCl using Amicon Ultra-4 30k unit (Merck Millipore), and subjected to gel filtration chromatography on a Superdex 200 10/300 GL (GE Healthcare) column equilibrated with 25 mM MES, pH 6.0, containing 100 mM NaCl. EGCrP2 was eluted from the column with the same buffer at a flow rate of 0.5 ml/min, and each 0.5 ml fraction was collected using a fraction collector (GE Healthcare).

#### **Protein assay**

Protein content was determined by Pierce 660 nm Protein Assay Reagent (Thermo Fisher Scientific) with bovine serum albumin as a standard. SDS-PAGE was carried out according to the method of Laemmli (105) with Pre-Stained Protein Markers (Nacalai Tesque) as a standard. Proteins were stained with CBB Stain One (Nacalai Tesque).

# Enzyme assay

An aliquot of each substrate (NBD-labeled GSLs, pNP glycosides, 4MU- $\beta$ -glucosides, and resorufin- $\beta$ -glucoside) was incubated at 30°C for an appropriate period with 100 ng of enzyme in 20  $\mu$ l of 50 mM MES buffer, pH 6.0, containing 0.025% cholic acid. The reaction mixture, dried using a SpeedVac concentrator, was dissolved in 10  $\mu$ l of chloroform/methanol (1:2,  $\nu$ ) and applied to a Silica Gel 60 TLC plate (Merck Millipore), which was developed with chloroform/methanol/water (65:25:4 or 65:16:2,  $\nu$ / $\nu$ / $\nu$ ). NBD-labeled GSLs were visualized using AE-6935B VISIRAYS-B and EZ-capture II (ATTO). The extent of the hydrolysis of NBD-labeled GSLs was calculated as follows: hydrolysis (%) = (peak area for the NBD-Cer generated)  $\nu$  100 / (peak area for the NBD-Cer generated + peak area for the remaining NBD-GSLs). GlcCer and glucose were visualized by spraying the TLC plate with orcinol sulfate reagent.  $\nu$ 0-Nitrophenol released from  $\nu$ 0-P glycosides by the action of the enzyme was measured at 405 nm by Multiskan FC microplate reader (Thermo Fisher Scientific). 4-Methylumbelliferone and resorufin released from 4MU- $\nu$ 2-glucoside and resorufin- $\nu$ 3-glucoside, respectively, were measured at 355/460 nm and 544/590 nm of Ex/Em, respectively, by ARVO MX 1420 fluorescence microplate reader (Perkin Elmer).

# **Characterization of recombinant EGCrP2**

The pH dependency of EGCrP2 activity was determined in a pH range of 4 - 9 using the GTA buffer (3,3-dimethyl-glutaric acid, Tris (hydroxymethyl) aminomethane, and 2-amino-2-methyl-1,3-ropanediol) at a final concentration of 150 mM. Temperature dependency was determined in the range between 15 and 40°C. The effects of DMSO were examined in the range between 0 and 50%. The effects of detergents were examined using sodium cholate and Triton X-100 at the concentration indicated. The kinetic constants of EGCrP2 were measured using various glucosides (Table 2-2) at concentrations ranging between 0.08 and 10 µM. The reaction

product C6-NBD-Cer was separated from C6-NBD-GlcCer on a normal phase HPLC column (Inertsil SIL 150A-5, GL Science) and quantified according to the method described by Hayashi *et al* (106).

# Generation of egcrp1-knockout mutant (1KO)

1KO was generated from C. neoformans var. grubii H99 by the method described in (40).

# Generation of egcrp2-knockout mutant (2KO) and egcrp1/egcrp2 double knockout mutant (DKO)

The *C. neoformans* EGCrP2 gene (*egcrp2*) (locus number CNAG\_05607 in *C. neoformans var. grubii* H99 database) was disrupted with the NAT split marker according to the method described in (40,107). A gene-specific disruption cassette contained approximately 350 bp of the 5'-and 3'-flanking regions of *egcrp2*, an 860-bp fragment of the promoter sequence with the ATG start codon of *C. neoformans* actin gene (108), a 310-bp fragment of the terminator sequence with the stop codon of *C. neoformans* TRP1 (109), and the selectable marker NAT gene (110) (Fig. 2-6). DNA fragments were amplified in the first round of PCR using the primers CN05607N-U and CN05607N-AP-D for the 5'-flanking region, CN05607C-U and CN05607C-D for the 3'-flanking region, ActinP-U and Act-Nat-Down for the actin promoter, and Ttrp-U and Ttrp-CN05607C-D for the TRP1 terminator with genome DNA as a template. Nat-Up and Nat-Ttrp-Down primers were used to amplify the NAT gene with pYL16 (WERNER BioAgents) as a template. The sequences of primers used in this study are summarized in Table 2-1. *C. neoformans* genome DNA was prepared using ISOPLANT II (NIPPON GENE). PCR products were separated on a 1% agarose gel, then extracted from the gel, and used as a template in overlap PCR to combine DNA fragments. All PCR amplifications were performed using PrimeSTAR GXL DNA polymerase (Takara Bio Inc.).

The combined overlap PCR product was then inserted into T-vector pGEM-T Easy to construct pGEM/EGCrP2-5' and pGEM/EGCrP2-3' after adding adenine overhang using 10× A-attachment Mix (TOYOBO) and 2× Ligation Mix (NIPPON GENE). A NAT split marker containing the 200-bp overlapping sequence was amplified by PCR using the primer sets of CN05607N-U and NSL-2 for the 5'-region of NAT, and NSR-2 and CN05607C-D for the 3'-region of NAT with pGEM/EGCrP2-5' and pGEM/EGCrP2-3' as a template, respectively (107). The two PCR fragments were purified, then precipitated onto 500 μg of gold microcarrier beads (0.6 μm; Bio-Rad), and introduced into *C. neoformans* H99 by biolistic transformation, as described previously (111), using a Model PDS-1000/He Biolistic particle delivery system (Bio-Rad). Stable transformants were selected on a YPD agarose plate containing 100 μg/ml nourseothricin (WERNER BioAgents). DKO was generated from 1KO using hygromycin (hyg)-resistant split marker, according to the methods described in (110,111). The gene-specific disruption cassette used was the same as that for the generation of 2KO except for the selectable maker. Hyg-resistant split marker was used instead of NAT split marker for the generation of DKO. The primers used are summarized in Table 2-1.

#### **Southern blot analysis**

It was conducted using 2 μg of genomic DNA digested with *Bam*HI-*Hind*III for *egcrp2* and *Hind*III for *egcrp1*. The gene-specific probes were amplified with primer sets of E2-5SENSE and E2-5ANTISENSE for *egcrp2*, and 3Probe-S and 3Probe-A for *egcrp1* with genomic DNA as a template. The primers used are summarized in Table 2-1.

# **Growth curve**

The growth of *C. neoformans* was examined using a YPD liquid medium at 30°C with shaking (150 rpm). *C. neoformans* (A600nm, 0.02) pre-cultured for 2 days was transferred into fresh

YPD medium and growth was evaluated by measuring  $A_{600 \text{ nm}}$  after the appropriate periods indicated.

# **Extraction of glycolipids**

Total lipids were extracted from *C. neoformans* by chloroform/methanol (1:2, v/v). Total lipids, dissolved in chloroform, were loaded on to a Sep-Pak plus silica cartridge (Waters) equilibrated with chloroform. The glycolipid fraction, which contained GlcCer and ergosterylglucoside, was eluted by acetone. The elution of the glycolipids fraction was monitored by TLC using chloroform/methanol/water (65:16:2, v/v/v) as a developing solution, and stained with orcinol sulfate reagent.

# Purification of the glycolipid that accumulated in 2KO

The glycolipid that accumulated in the 2KO was extracted using the conventional Bligh and Dyer method (112). The lower phase was collected and dried using a Speed Vac concentrator. The dried lipid was dissolved in chloroform, and loaded onto a Sep-Pak plus silica column cartridge equilibrated with chloroform. The glycolipid was eluted from the cartridge by a stepwise elution with chloroform/methanol (98:2, v/v), chloroform/methanol (95:5, v/v), and chloroform/methanol (2:1, v/v). The glycolipid was mainly recovered in the chloroform/methanol (95:5, v/v) fraction. The glycolipid was purified using HPLC (EZChrom Elite, Hitachi) equipped with a Cosmosil 5SL-II column (4.6 x 150 mm, particle size: 5 µm), which was equilibrated and eluted with methanol at a flow rate of 1 ml/min and column temperature of 40°C. The elution of glycolipid was monitored at 278 nm.

# MS spectrometry

An AXIMA-CFR instrument (Shimadzu) was used for the MALDI-TOF-MS analysis.

Mass spectra were acquired in the positive mode and 2,5-dihydroxybenzoic acid was used as the matrix.

# NMR spectroscopy

Spectra were recorded on a Varian INOVA600 spectrometer. The operating conditions were as follows:  $^{1}$ H: frequency, 600 MHz; sweep width, 8 kHz; sampling point, 44 k; accumulation, 128 pulses; temperature 30°C.  $^{13}$ C: frequency, 150 MHz; sweep width, 32 kHz, sampling point 160 k: accumulation, 12000 pulses; temperature 300 k. Chemical shifts were referenced to tetramethylsilane ( $\delta_{H}$ ,  $\delta_{C}$  0) in CD<sub>3</sub>OD and CDCl<sub>3</sub> (1:1, v/v). Conventional pulse sequences were used in the MQ-COSY, TOCSY, NOESY, HSQC and HMBC experiments.

# Flow cytometric analysis

Cells harvested from 3-day cultures were fixed with cold 70% EtOH for 3 h, washed with PBS, and then incubated for 5 min in Hoechst 33342 solution (50  $\mu$ g/ml in distilled water) at room temperature. The samples were placed on ice before the analysis and were then analyzed using an EC800 flow cytometer (Sony). Cell volumes were estimated by the flow cytometer according to the manufacturer's instructions. To eliminate the signals for aggregated cells, Hoechst 33342-based gating was performed in the analysis.

# Vacuole analysis

The vacuole-enriched fraction was isolated from C. neoformans cells by density gradient centrifugation in accordance with Cabrera and Ungermann (113). Typically, a 300-ml culture was subjected to centrifugation at  $4,400 \times g$  for 5 min at room temperature and washed twice with PBS. The pellet was resuspended with spheroplasting buffer containing with 14 ml of McIlvain buffer, 6

ml of 1 M sodium tartrate, and 250 mg of Westase (Takara Bio Inc.), and incubated at 30°C for 2 h sharking at 60 rpm. After centrifuging at 5300 x g, for 5 min at 4°C, the supernatants were discarded. The pellet was dissolved in 2.5 ml of 15% Ficoll in PS buffer (15% w/v Ficoll 400, 20 mM PIPES/KOH, pH 6.8, 200 mM sorbitol), added 200 µl of 0.4 mg/ml DEAE-dextran in PS buffer, and incubated for 5 min on ice, and 30°C for 90 sec. Each 3 ml of the supernatant was transferred into centrifuge tubes, 800 µl of 8% Ficoll in PS buffer (8% w/v Ficoll 400, 20 mM PIPES/KOH, pH 6.8, 200 mM sorbitol) was carefully layered, followed by 800 µl of 4% Ficoll in PS buffer (4% w/v Ficoll 400, 20 mM PIPES/KOH, pH 6.8, 200 mM sorbitol). Finally, 300 µl of 0% Ficoll in PS buffer (20 mM PIPES/KOH, pH 6.8, 200 mM sorbitol) was layered on the top. The tubes were centrifuged using a RPS65T Swing rotor (Hitachi) at 110,000 x g for 90 min at 4°C. The vacuole and lipid droplet fractions were collected from the top to 0%-4% interface using a 1-ml tip. Vacuoles and lipid droplets were separated according to the method described by Zinser et al (114). Lipids were extracted from the lysate and vacuole vesicles (50 µg of protein) by chloroform/methanol (1:2, v/v), and dried under a stream of N2. The lipid was analyzed by TLC using chloroform/methanol/water (65:16:2, v/v/v) as a developing solvent. Vacuoles in cells were visualized with the incorporation of 5-(and-6)-carboxy-2',7'-dichlorofluorescein diacetate (carboxy-DCFDA, Molecular Probes) under microscopy (77).

#### 2-3. RESULTS

# Molecular cloning and characterization of EGCrP2

EGCase, an enzyme capable of cleaving the  $\beta$ -glycosidic linkage between the oligosaccharide and Cer of various GSLs, is distributed in bacteria, actinomycetes and some invertebrates such as jellyfish and hydra (Fig. 2-1). Our group previously reported that the EGCase homologue, EGCrP1, was a glucocerebrosidase of *C. neoformans*, involved in the quality control of GlcCer, possibly associated with the GlcCer synthesis pathway (40). In the present study, the author identified another homologue of EGCase in *C. neoformans* and designated it as EGCrP2. It showed 28% identity to EGCrP1 and rhodococcal EGCase II. The alignment of the deduced amino acid sequence of EGCrP2 with those of EGCrP1 and EGCase II revealed that eight residues, essential for the catalytic activity of glycoside hydrolase (GH) family 5 glycosidases (115), were completely conserved in these enzymes (Fig. 2-2, open circles). Of the 8 residues of EGCrP2, two catalytic glutamates, Glu270 and Glu520, at the end of β-strands 5 and 8, respectively, were thought to be an acid/base catalyst and nucleophile, respectively (Fig. 2-1, closed circles). EGCrP2-like homologues were widely distributed across the phyla/genera of fungi and formed a gene family, which was independent of the EGCrP1 and EGCase families (Fig. 2-1).

To characterize EGCrP2, the *egcrp2* open reading frame encoding 851 amino acid residues was cloned from the complementary DNA of *C. neoformans* and expressed in *E. coli* BL21 (DE3) as a His-tag-fused protein. Recombinant EGCrP2 (rEGCrP2) was purified by affinity chromatography using a Nickel-conjugated Sepharose column and gel filtration using a Superdex 200 10/300 GL column. The purified enzyme showed a single protein band possessing a molecular mass of approximately 120 kDa on SDS-PAGE after staining with Coomassie Brilliant Blue (CBB Stain One) (Fig. 2-3A). Purified rEGCrP2 hydrolyzed C6-NBD-GlcCer to generate C6-NBD-Cer;

however, it did not hydrolyze any of the other NBD-GSLs tested (Fig. 2-3B). rEGCrP2 was also found to hydrolyze native GlcCer, which was not labeled with NBD; however, it did not degrade any other native GSLs (data not shown). The specificity of rEGCrP2 toward GSLs appeared to be identical to that of EGCrP1, but was completely different from that of EGCase, which preferred oligosaccharide-linked GSLs such as LacCer and GM1a (101). Both EGCrP1 and EGCrP2 were β-glucosidases; however, the specificity of EGCrP2 was very broad for aglycone moieties, i.e. EGCrP2 hydrolyzed pNP-β-glucoside (Fig. 2-3C) and 4MU-β-glucoside (Table 2-2), whereas these β-glucosides were completely resistant to hydrolysis by EGCrP1. Neither EGCrP1 nor EGCrP2 hydrolyzed other pNP-glycosides including pNP- $\beta$ -galactoside and pNP- $\alpha$ -glucoside (Fig. 2-3C). Differences in the aglycone specificities of the two EGCrPs were also shown with various β-glycosides, i.e., EGCrP2 hydrolyzed ergosteryl β-glucoside (EG) to generate ergosterol and glucose, but this glycolipid was not degraded by EGCrP1 (Fig. 2-3D). Furthermore, various  $\beta$ -glucosides such as sitostervl  $\beta$ -glucoside, n-octvl  $\beta$ -glucoside, indoxvl  $\beta$ -glucoside, and arbutin were hydrolyzed by EGCrP2 under the conditions used (Fig. 2-3E). Salicin and phloridzin were hydrolyzed by EGCrP2 when the amount of the enzyme was increased 10-fold; however, guercetin-\beta-glucoside was still resistant to hydrolysis by EGCrP2 under the same condition (data not shown). The kinetic parameters of EGCrP2 for various β-glucosides and their structures are summarized in Table 2-2 and Fig. 2-3, respectively.

The maximal activity of EGCrP2 was observed at pH 5.0-5.5 when C6-NBD-GlcCer was used as a substrate, indicating that EGCrP2 was an acid β-glucosidase (Fig. 2-5A). In contrast, the pH optimum of EGCrP1 was previously shown to be approximately 7.5 (40). The optimal temperature of EGCrP2 was found between 32°C and 37°C (Fig. 2-5B), which was a suitable temperature for the growth of *C. neoformans*. The activity of EGCrP2 was enhanced by the addition of sodium cholate at a concentration of 0.025% when C6-NBD-Cer was used as a substrate; however, higher

concentrations of the detergent inhibited activity. Triton X-100 strongly inhibited the activity of EGCrP2 (Fig. 2-5C) and EGCrP1 (40). Although the addition of DMSO did not affect activity up to 30% of the reaction mixture, it inhibited activity at higher concentrations (Fig. 2-5D).

# Generation of egcrp2-knockout mutant (2KO) and egcrp1/egcrp2 double knockout mutant (DKO)

To determine whether EGCrP2 was involved in the catabolism of β-glucosides *in vivo*, 2KO and DKO were generated from *C. neoformans* var. *grubii* serotype A strain H99 (WT) and *egcrp1* knockout mutants (1KO) (12) by gene-targeting homologous recombination using NAT and hygromycin (*hyg*)-resistant gene as a marker, respectively (Fig. 2-6A). Southern blot analysis using the *BamHI-HindIII*-digested genome DNA revealed that the *egcrp2* gene was disrupted by this method in 2KO and DKO, as expected (Fig. 2-6B, left panel), while the *egcrp1* gene was present in WT and 2KO but not 1KO or DKO (Fig. 2-6B, right panel). The β-glucocerebrosidase activity decreased in the cell lysate of 1KO at pH 7.3 but not at pH 5.0 when the activity was measured using C6-NBD-GlcCer, as shown in (12). On the other hand, the activity markedly decreased in the cell lysates of 2KO and DKO when it was measured using C6-NBD-GlcCer at pH 5.0, indicating that EGCrP2 possesses an acid β-glucocerebrosidase activity (Fig. 2-6C, left panel). However, the apparent decrease of β-glucosidase activity of 2KO and DKO was much lower when the activity was measured using 4MU-β-Glc as a substrate at pH 5.0 (Fig. 2-6C, right panel), suggesting the presence of β-glucosidase(s) which may act on 4MU-β-Glc but not C6-NBD-GlcCer under acidic conditions.

# Identification of the lipid that accumulated in 2KO

TLC analysis of cell extracts showed that the accumulation of GlcCer was not significant in 2KO under the conditions used; alternatively, an unknown lipid, whose *Rf* corresponded to that of

sitosteryl β-glucoside (SG), highly accumulated in both 2KO and DKO mutants (Fig. 2-7A lane 4, 5). To clarify its structure, the accumulated lipid was extracted from 2KO, purified as described in the MATERIALS AND METHODS (Fig. 2-7A lane 7), and then analyzed by MALDI-TOF-MS in positive mode using 2,5-dihydroxybenzoic acid as a matrix. The main molecular ion peak, [M+Na]<sup>+</sup>, was observed at m/z 581.4 for the lipid (Fig. 2-7B), which corresponded to the molecular mass of EG (C<sub>32</sub>H<sub>54</sub>O<sub>6</sub>, 558.39). The NMR spectra of the lipid accumulated in 2KO are summarized in Table 2-3. The <sup>1</sup>H NMR spectrum of the purified lipid showed the characteristic signals of a glycoside structure composed by a sterol part and hexopyranose. The <sup>1</sup>H NMR spectrum for the sterol moiety displayed signals for four secondary methyls as a doublet, two tertialy methyls as a singlet, four olefinic protons, and one oxygen-bearing methine proton. In the <sup>13</sup>C NMR spectrum, 28 carbon signals; six methyls, seven methylenes, six methines, two quaternary carbons, two tri-substituted olefins, one di-substituited olefin, and one oxygen-bearing methane, suggested that the sterol moiety could be an ergosterol (Table 2-3). Furthermore, the deshielded signal at  $\delta_C$  78.2 (C-3) in comparison with the ergosterol suggested a glycosidic linkage at C-3. The structure of the sugar moiety was assignable to β-glucopyranoside because of its chemical shift values and the correlation from the H-1 [ $\delta_H$  4.43 (d, J=7.8Hz)] to H<sub>2</sub>-6 ( $\delta_H$  3.73 and 3.87) in the MQ-COSY and TOCSY spectra, and the glycosidic linkage at the C-3 of the ergosterol was also confirmed by the HMBC correlation between the H-1 of Glc ( $\delta_H$  4.43) and C-3 of the ergosterol ( $\delta_C$  78.2). Collectively, the structure of the accumulated lipid was determined to be EG (ergosteryl 3-β-glucoside), a major sterylglucoside in fungi, as shown in Fig 2-7C. EG accumulated in the 2KO in a time-dependent manner; however, the content of this glycolipid was very low and not increased in wild type during the course of cultivation (Fig. 2-7D). These results indicated that EGCrP2 is involved in the degradation of EG in C. neoformans and disruption of egcrp2 resulted in the accumulation of EG.

## Phenotype analysis of 2KO and DKO

To assess the physiological effects of the disruption of the egcrp2 gene, the author compared the cell growth of 2KO and DKO with that of WT and 1KO. The disruption of egcrp2, but not egcrp1, resulted in the arrest of cell growth from the middle log phase to the early stationary phase (Fig. 2-8A). Observations with DIC microscopy revealed that 2KO and DKO cells were larger than WT and 1KO cells possibly due to dysfunction of budding process (Fig. 2-8B). In support of this observation, the flow cytometric analysis revealed that the average cell volumes of 2KO  $(173.82 \mu m^3)$  and DKO  $(191.49 \mu m^3)$  were 5 to 6-fold larger than those of WT  $(31.72 \mu m^3)$  and 1KO (44.27 μm<sup>3</sup>). Small cells (cell volume, ~10 μm<sup>3</sup>) were found in WT and 1KO populations but not in 2KO and DKO populations (Fig. 2-8C). The vacuoles of 2KO were larger than those of WT and 1KO when carboxy-DCFDA was incorporated into these cells as an indicator to visualize vacuoles (Fig. 2-8D). The cell densities of 2KO and DKO were compared with those of WT and 1KO using percoll cell gradient centrifugation. The distribution of cells in the percoll gradient was markedly different, i.e. 2KO and DKO cells were mainly recovered in the 30% percoll fraction (the specific gravity was estimated to be 1.039; blue arrows), whereas WT and 1KO cells were recovered in the 50% (specific gravity, 1.061; yellow arrows) and 80% percoll fractions (specific gravity, 1.094; red arrows). Almost no 2KO and DKO cells were detected in the 80% percoll fraction (Fig. 2-8E). These results indicated that the specific gravities of 2KO and DKO cells were markedly lower than those of 1KO and WT cells.

#### Vacuole analysis of WT and 2KO

The disruption of *egcrp2*, but not *egcrp1*, led to the accumulation of EG (Fig. 2-7A, D) and hypertrophy of cell body (Fig. 2-8B, C) and vacuoles (Fig. 2-8D). EGCrP2 degraded EG most efficiently at an acidic pH (Fig. 2-5A), and, thus, it was hypothesized that EG may be catabolized by

EGCrP2 in acidic compartments in the cell, such as the vacuoles. Vacuoles were thus isolated from WT and 2KO cells using Ficoll gradient centrifugation as described in MATERIALS AND METHODS. The final fractions obtained from both WT and 2KO cells possessed high specific activity for the acid  $\alpha$ -mannosidase, which is a marker enzyme localized in the vacuole, indicating that vacuoles were enriched in these fractions as expected (Fig. 2-9A). The specific activity of the acid  $\alpha$ -mannosidase in the vacuole-enriched fraction of 2KO was markedly higher than that of WT (Fig. 2-9A); however, the specific activity of  $\beta$ -glucosidase was significantly lower in the same fraction of 2KO than that of WT when its activity was measured using C6-NBD-GlcCer (Fig. 2-9B) and 4MU- $\beta$ -glucoside (Fig. 2-9C) as substrates, indicating EGCrP2 was present in the vacuole-enriched fraction. To determine whether EG accumulated in vacuoles, total lipids in the vacuole-enriched fraction were extracted and analyzed by TLC. As shown in Fig. 2-9D, EG was detected in the vacuole-enriched fraction of 2KO, but not in that of WT. These results strongly suggested that EGCrP2 catabolizes EG in the vacuoles of *C. neoformans*.

#### 2-4. DISCUSSION

Since the activity of the glucocerebrosidase did not decrease under acidic conditions after the disruption of *egcrp1* in *C. neoformans* (40), the author searched for glucocerebrosidase(s) capable of working under acidic conditions in this study. EGCrP2, a homologue of EGCrP1, was found to hydrolyze GlcCer *in vitro* and the disruption of *egcrp2* greatly reduced glucocerebrosidase activity when C6-NBD-GlcCer was used as a substrate under acidic conditions (Fig. 2-6C, left). However, the author found that DKO still exhibited glucocerebrosidase activity (Fig. 2-6C, left), suggesting that *C. neoformans* may possess glucocerebrosidase(s) except for EGCrP1 and EGCrP2.

The GlcCer of *C. neoformans* (WT) shows homogeneity in the sphingoid base, which possesses two double bonds at C4/C8 and a methyl substitution at C9 (methyl d18:2) (38,40). However, the EGCrP1-knockout mutant (1KO) accumulated GlcCer possessing several sphingoid bases without methyl substitution (d18:2, d18:1, and d18:0) that are intermediates generated from the pathway of GlcCer synthesis in *C. neoformans* (40). This indicates that EGCrP1 is involved in the quality control of GlcCer in *C. neoformans*. On the other hand, the sphingoid base of GlcCer in 2KO was exclusively methyl d18:2, as in WT (Fig. 2-10), indicating that EGCrP2 is unlikely to participate in the elimination of aberrant GlcCer found in 1KO. This discrepancy in the physiological role of EGCrPs may stem from the different localization of each EGCrP. The different pH optimum for each enzyme may support this hypothesis; however, the precise localization of EGCrPs in *C. neoformans* remains to be elucidated.

EGCrP2 seems to be a major EG-degrading enzyme in *C. neoformans* because *egcrp2*-disrupted mutants leaded to the significant accumulation of EG (Fig. 2-7A, D), a major sterylglucoside in fungi and yeast (49). Sterylglucosides, sterol-containing glucosides, are a major class of glycolipids in fungi; however, they are also found in algae, plants, and animals (49). Sterol

3-β-glucosyltransferase (SGT, EC 2.4.1.173), an enzyme that catalyzes the transfer of glucose from UDP-glucose to sterols, has been found in *Candida albicans* (54), *Colletotrichum gloeosporioides* (68), *Fusarium graminearum* (49), *Leptosphaeria maculans* (116), *Saccharomyces cerevisiae* (54), and *P. pastoris* (54). The SGT-deficient mutants of *P. pastoris* were found to lack pexophagy, which is a process for the degradation of peroxisomes in vacuoles, while SGT did not appear to be essential for pexophagy in *S. cerevisiae* and *Y. lypolytica* (58,61,62). It remains unclear whether the accumulation of EG affects pexophagy in *C. neoformans*. In the present study, the accumulation of EG due to a dysfunction in *egcrp2* may have led to the abnormal cell proliferation (Fig. 2-8A-C) and vacuole morphology (Fig. 2-8D) in *C. neoformans*; however, the mechanism responsible remains unknown.

Although both EGCrP1 and EGCrP2 are  $\beta$ -glucohydrolases belonging to GH family 5, the specificity of both enzymes completely differs for the aglycone moiety; EGCrP1 only cleaved the  $\beta$ -glucosidic linkage of GlcCer among the substrates tested (40), while EGCrP2 hydrolyzed various  $\beta$ -glucosides including GlcCer, steryl  $\beta$ -glucosides, and artificial substrates such as pNP- $\beta$ -glucoside and 4MU- $\beta$ -glucoside (Fig. 2-3, Table 2-2). A comparison of the primary structure of EGCrP2 with EGCrP1 revealed the presence of several inserts in EGCrP2 between possible  $\beta$ -strands 6 and 7,  $\beta$ -strand 9 and  $\alpha$ -helix 11, and the carboxy-terminus region (Fig. 2-2). Further studies are required to elucidate the relationship between the structures and aglycone specificities of EGCrPs. X-ray crystal analysis of EGCrP1 and EGCrP2 could provide valuable information on mutual relationships, and experiments are ongoing.

In the present study, the author identified EGCrP2 as the first steryl-β-glusosidase in fungi. Similar activity was found in *Sinapis alba* (72) and *Sulfolobus solfataricus* (73); however, these enzymes show no sequence homology with EGCrP1/EGCrP2. In addition, it remains unclear whether these plant and archaea enzymes are actually involved in sterylglucoside metabolism *in vivo* be-

cause knockout of the corresponding genes in plants and archaea has not been reported.

EGCrP2 appeared to localize to the vacuole because β-glucosidase activity was detected in the vacuole-enriched fraction and its activity was decreased in the fraction after the disruption of *egcrp2* in *C. neoformans* (Fig. 2-9B, C). The optimum pH of EGCrP2 was found to be 5.0-5.5 (Fig. 2-5A), which approximately corresponded to the vacuole pH determined in *C. neoformans* strain H99 (117). The expression of GFP-tagged EGCrP2 could help to estimate the intracellular localization of EGCrP2; however, the expression of GFP-EGCrP2 has yet to be successfully achieved in *C. neoformans*.

The abnormal morphology of vacuoles in *Candida albicans* mutants led to a decrease in pathogenicity in a mouse model (89,118-120), and, thus, the vacuole proteins of this fungi are now being considered as targets for the development of anti-fungal drugs (121). In this context, EGCrP2 could be a promising candidate for the development of anti-Cryptococcus drugs because a dysfunction in EGCrP2 resulted in an abnormal morphology in the vacuoles (Fig. 2-8D). One of the reasons for this abnormality could stem from the accumulation of EG in the vacuoles; however, the molecular mechanism responsible remains unknown.

Taken together, the author herein uncovered the missing link in sterylglucoside metabolism in *C. neoformans* by identifying the enzyme responsible for degrading EG *in vivo* and *in vitro*.

#### **2-5. SUMMARY**

Cryptococcosis is an infectious disease caused by pathogenic fungi such as Cryptococcus neoformans and Cryptococcus gattii. The ceramide structure (methyl-d18:2/h18:0) of C. neoformans glucosylceramide (GlcCer) is characteristic and strongly related to its pathogenicity. Our group recently identified that endoglycoceramidase-related protein 1 (EGCrP1) as a glucocerebrosidase in C. neoformans and showed that it was involved in the quality control of GlcCer by eliminating immature GlcCer during the synthesis of GlcCer (Ishibashi et al, J. Biol. Chem., 2012). The author herein identified and characterized EGCrP2, a homologue of EGCrP1, as the enzyme responsible for sterylglucoside catabolism in C. neoformans. In contrast to EGCrP1, which is specific to GlcCer, EGCrP2 hydrolyzed various β-glucosides including GlcCer, cholesteryl β-glucoside, ergosteryl  $\beta$ -glucoside, sitosteryl  $\beta$ -glucoside, and para-nitrophenyl  $\beta$ -glucoside, but not  $\alpha$ -glucosides or β-galactosides, under acidic conditions. Disruption of the EGCrP2 gene (egcrp2) resulted in the accumulation of a glycolipid, and the structure of which was determined following purification to ergosteryl 3-\(\beta\)-glucoside, a major sterylglucoside in fungi, by mass spectrometric and two-dimensional nuclear magnetic resonance analyses. This glycolipid accumulated in vacuoles and EGCrP2 was detected in vacuole-enriched fraction. These results indicated that EGCrP2 was involved in the catabolism of ergosteryl β-glucoside in the vacuoles of C. neoformans. Distinct growth arrest, a dysfunction in cell budding, and an abnormal vacuole morphology were detected in the egcrp2-disrupted mutants, suggesting that EGCrP2 may be a promising target for anti-cryptococcal drugs. EGCrP2, classified into glycohydrolase family 5, is the first steryl-β-glucosidase identified as well as a missing link in sterylglucoside metabolism in fungi.

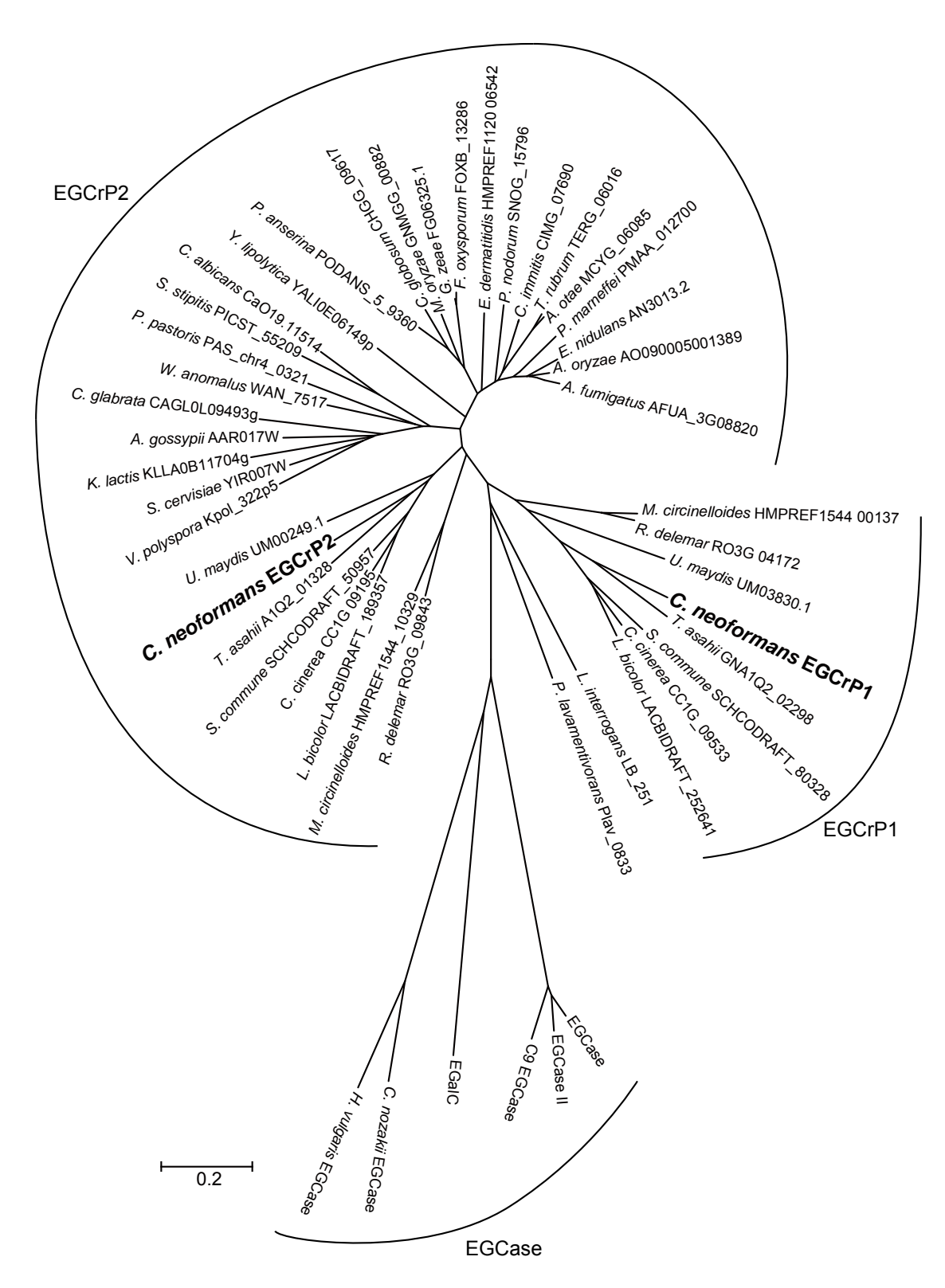
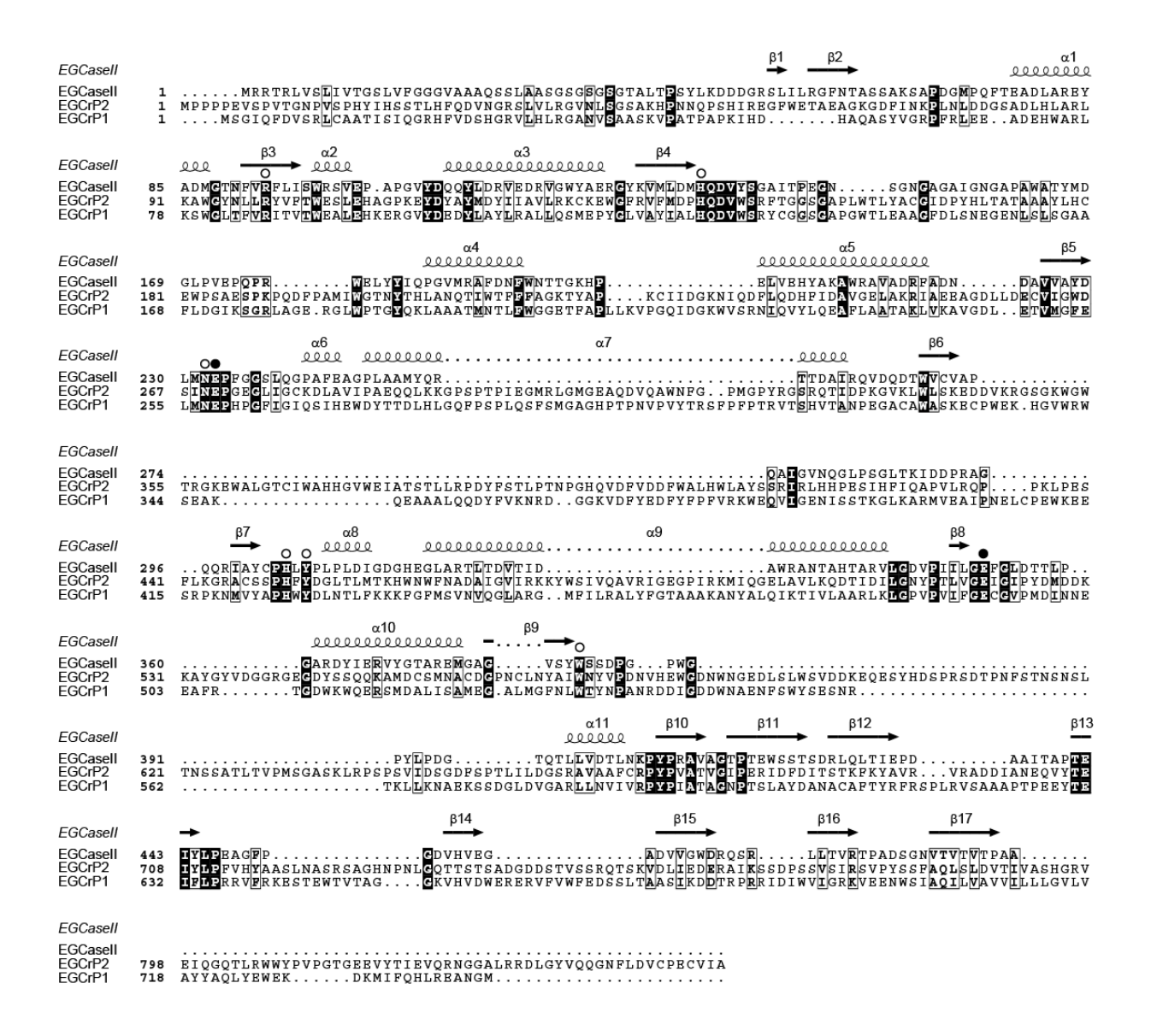


FIGURE 2-1. Phylogenetic tree of EGCrP1, EGCrP2, and EGCase.

The amino acid sequences of EGCrPs and EGCases were reconstructed using the neighbor-joining method (122). The scale bar represents 0.2 amino acid substitutions per site.



## FIGURE 2-2. Alignments of EGCrP1 and EGCrP2 with EGCase II.

The amino acid sequences of *Rhodococcus* EGCase II (EGCase, accession: AAB67050.1), *C. neoformans* EGCrP1 (accession: BAL46040.1), and *C. neoformans* EGCrP2 were aligned using ClustalW (123) and ESPript (124). White letters on a black background and black letters in an open box show identical and similar residues, respectively. Open circles indicate amino acid residues conserved in GH family 5 glycosidase. Two glutamates, the Glu258 and Glu492 of EGCrP1 (40) and Glu270 and Glu520 of EGCrP2, are indicated by closed circles as possible acid/base catalyst and nucleophile, respectively. The secondary structural elements are shown above the amino acid sequence of EGCase II (125).

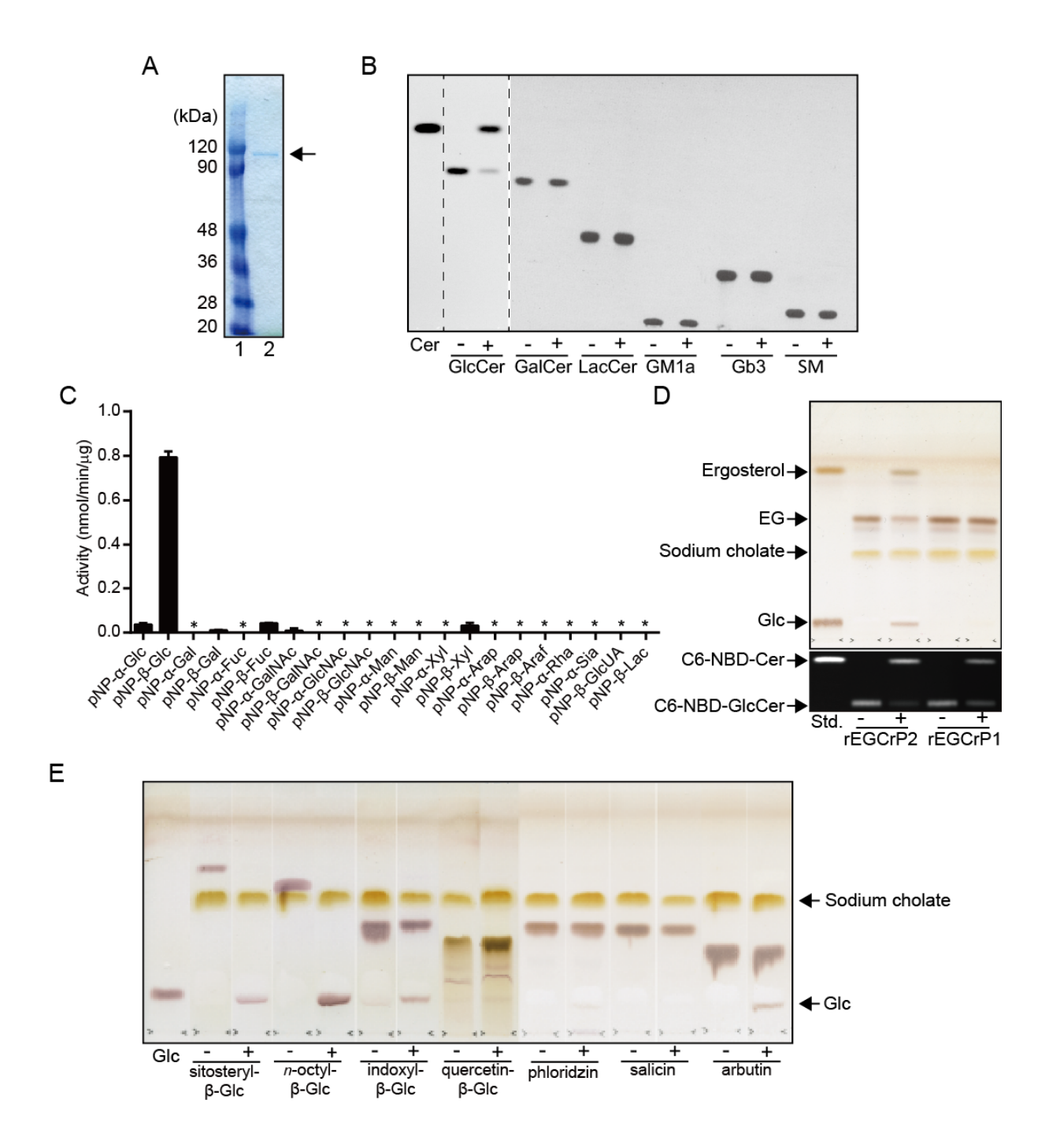


FIGURE 2-3. Purification and characterization of the recombinant EGCrP2.

A, Final preparation of rEGCrP2 on 10% SDS-PAGE. The protein eluted from the Ni-Sepharose column was purified using Superdex 200 10/300 GL. *Lane 1*, protein marker; *lane 2*, final preparation. B, TLC showing the specificity of EGCrP2 toward various C6-NBD-GSLs. Each C6-NBD-GSL (100 pmol) was incubated in 20  $\mu$ l of 50 mM MES buffer, pH 6.0, with 100 ng of rEGCrP2 (+) or heat-inactivated EGCrP2 (-)

at 30°C for 16 h, except for C6-NBD-GlcCer, which was incubated at 30°C for 1 h. Samples were loaded onto a TLC plate, which was developed with chloroform/methanol/water (65:25:4, v/v/v). *C*, Hydrolysis of *p*NP substrates by rEGCrP2. Error bars represent the mean  $\pm$  S.D. of three experiments. An asterisk indicates no hydrolysis of *p*NP substrates. *D*, Upper TLC shows hydrolysis of ergosteryl 3- $\beta$ -glucoside (EG) by rEGCrP2. Fungal EG, purified from 2-mg dry cells of 2KO, was incubated at 30°C for 18 h with 40  $\mu$ g of EGCrP1 or 20 ng of EGCrP2. TLC was developed with chloroform/methanol/water (65:16:2, v/v/v), and stained with orcinol sulfate reagent. Lower TLC shows C6-NBD-Cer released from C6-NBD-GlcCer by rEGCrP1 and 2. Fifty pmol of C6-NBD-GlcCer was incubated at 30°C with 40  $\mu$ g of rEGCrP1 and 20 ng of rEGCrP2 for 18 h. +, with EGCrP1, 2; -, without EGCrP1, 2. *E*, TLC showing the hydrolysis of various  $\beta$ -glucosides by rEGCrP2. Each 100 nmol of substrate was incubated at 30°C with 100 ng of enzyme for 18 h. Samples were loaded onto a TLC plate, which was developed with chloroform/methanol/water (65:25:4, v/v/v) and visualized by orcinol sulfate reagent. Glc shows glucose released from various  $\beta$ -glucosides by rEGCrP2, -, without EGCrP2, -, without EGCrP2.

## Fluorescent substrates

## Color substrate

oh HO 
$$O$$
  $O$   $O$   $NO_2$   $pNP-\beta$ -Glc

## Non-fluorescent substrates

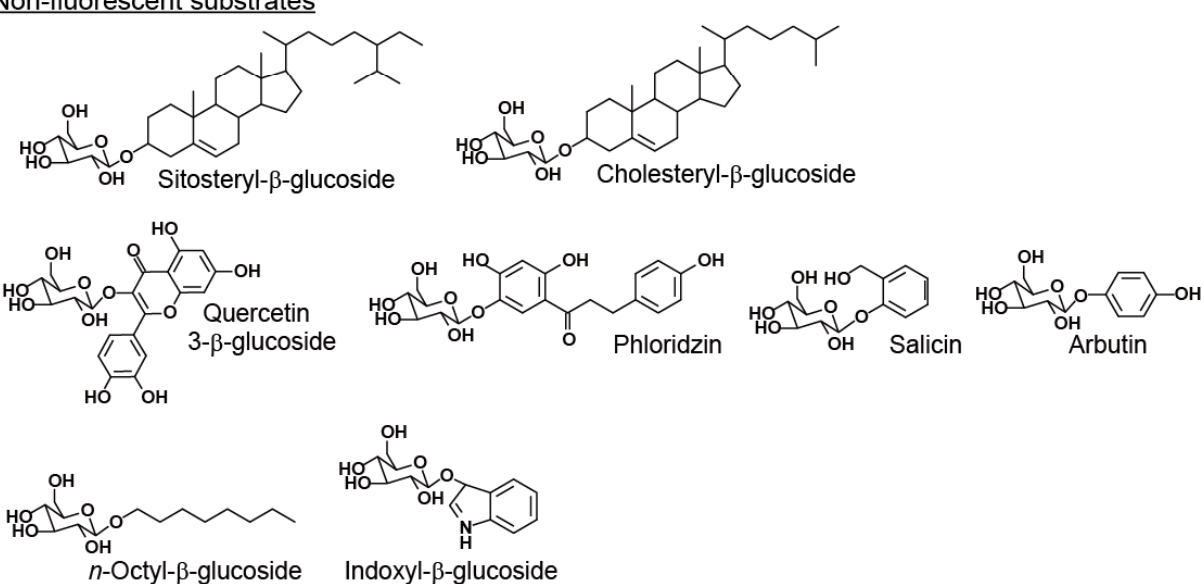


FIGURE 2-4. Structures of β-glucosides used to analyze the specificity of rEGCrP2.

The specificity of EGCrP2 was examined using various β-glucosides as indicated.

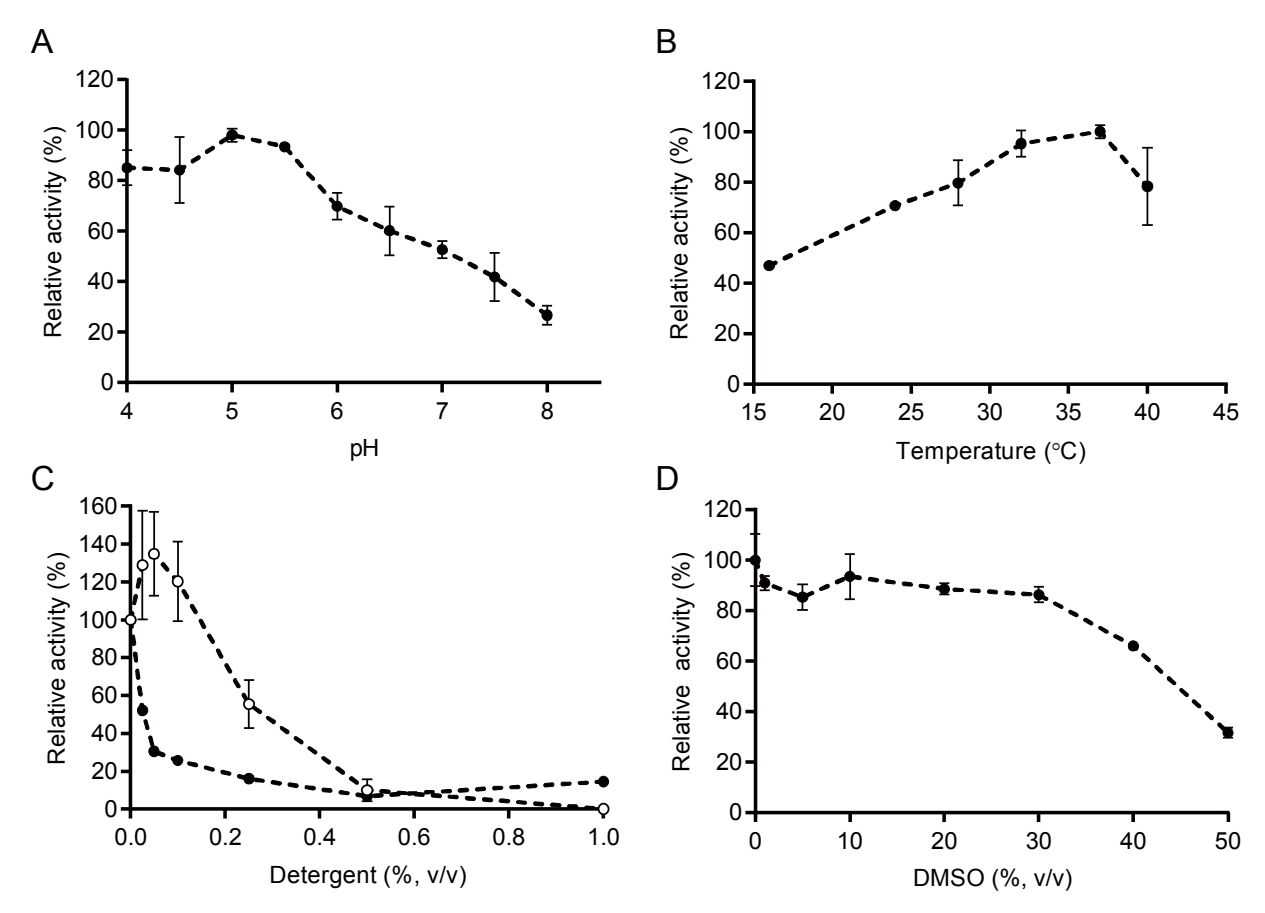


FIGURE 2-5. General properties of rEGCrP2.

A, pH dependency of C. neoformans rEGCrP2. 150 mM of GTA buffer was used for the assay. B, Effects of temperature on EGCrP2 activity. C, Effects of detergents on EGCrP2 activity. Closed circles, Triton X-100; open circles, sodium cholate. D, Effects of DMSO on EGCrP2 activity. Data represent the mean  $\pm$  S.D. of three experiments. The assay was conducted using C6-NBD-ClcCer as the substrate.

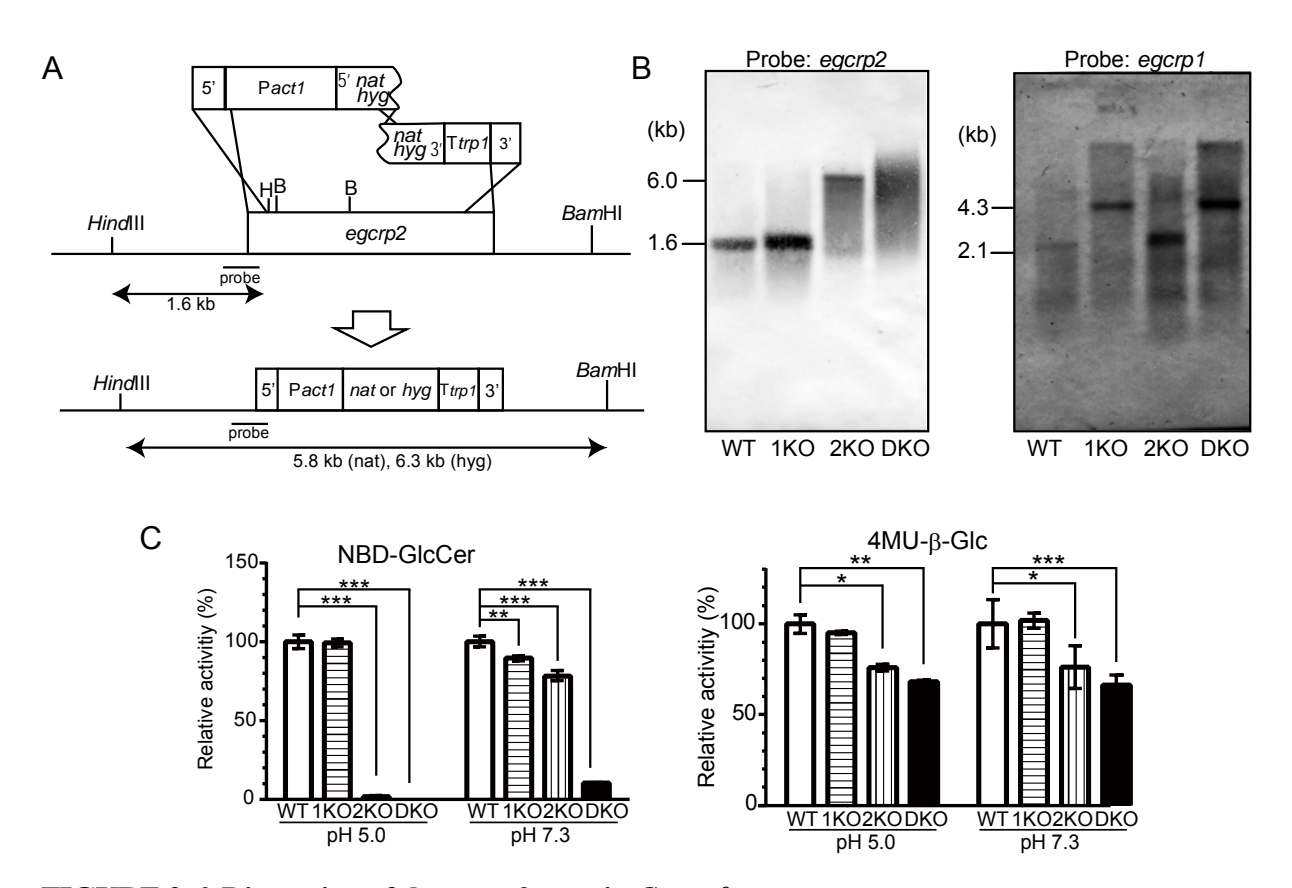


FIGURE 2-6. Disruption of the egcrp2 gene in C. neoformans.

A, Strategy for the disruption of *C. neoformans egcrp2* using the split marker method. *B*, Southern blot analysis of *BamHI-Hind*III-digested genomic DNA for *egcrp2* (left panel) and *Hind*III-digested genomic DNA for *egcrp1* (right panel). The disruption of *egcrp1* and Southern blot analysis of *Hind*III digested-genomic DNA were performed by the method described in (40). *C*, the activity of β-glucosidase was measured using C6-NBD-GlcCer (left) and 4MU-β-Glc (right). Activities were measured at 37°C for 18 h using C6-NBD-GlcCer and 2 μg of protein for pH 5.0 or 10 μg of protein for pH 7.3. When 4MU-β-Glc was the substrates, 1 μg of protein was incubated at 37°C for 18 h for both pHs. The activity was expressed as a percentage of that of WT. \*, \*\*, and \*\*\* represent p<0.01, p<0.001, and p<0.0001, respectively.

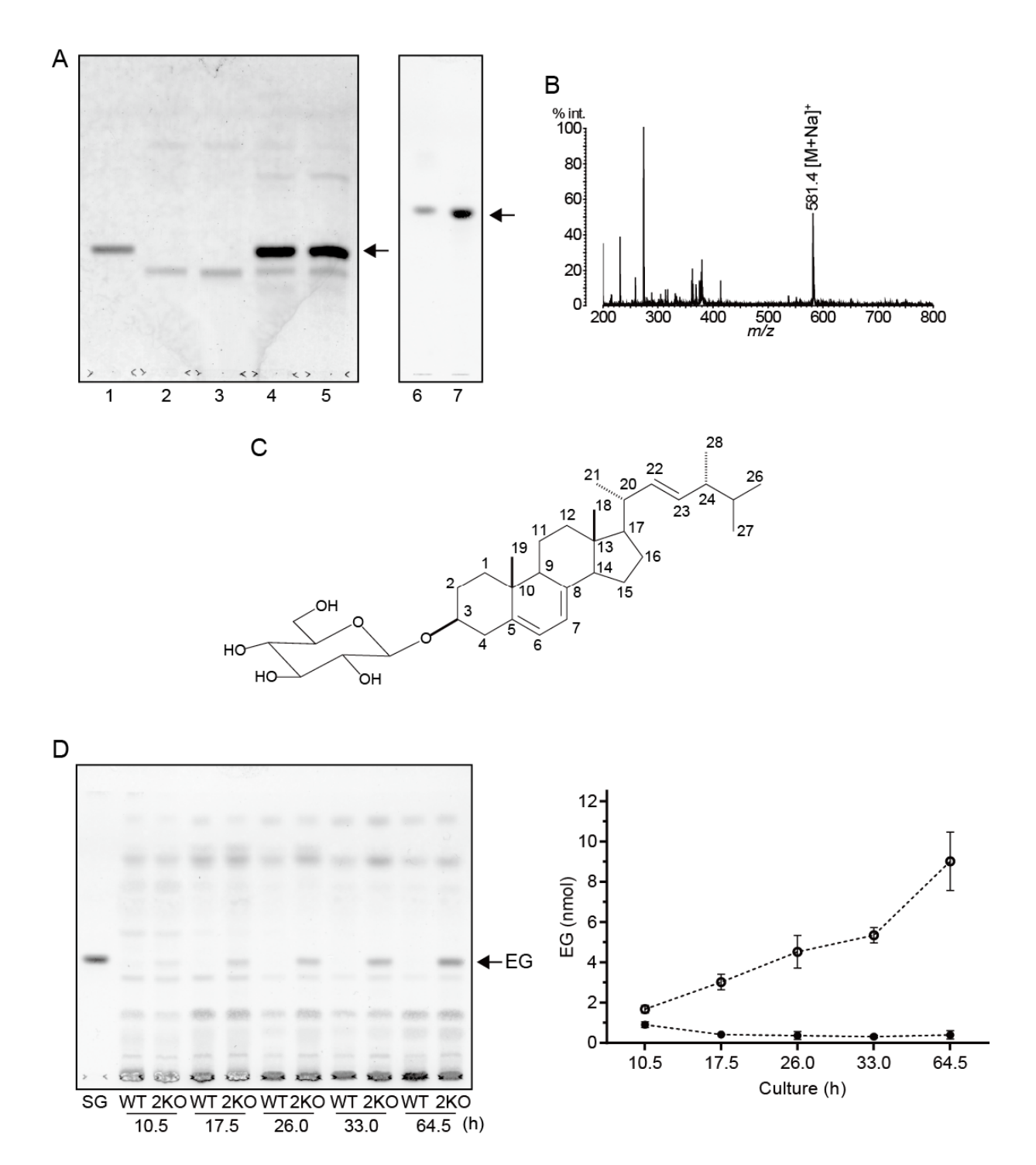


FIGURE 2-7. Identification of the lipid that accumulated in *egcrp2*-disrupted mutant (2KO) of *C. neoformans*.

A, TLC showing the glycolipid that accumulated in the mutants. Glycolipids were extracted by chloroform/methanol (1:2, v/v) from the cells after cultivation at 25°C for 3 days, and purified using a Sep-Pak plus silica column. Lipids corresponding to 4-mg dry cells were loaded onto a TLC plate, which was devel-

oped with chloroform/methanol/water (65:16:2, v/v/v) for *lanes* 1-5 (left panel) and chloroform/methanol/water (65:25:4, v/v/v) for *lanes* 6-7 (right panel). Glycolipids were visualized by orcinol sulfate reagent. *Lane* 1, sitosteryl  $\beta$ -glucoside standard (5 nmol); *lane* 2, WT; *lane* 3, 1KO; *lane* 4, 2KO; *lane* 5, DKO; *lane* 6, sitosteryl  $\beta$ -glucoside standard; 7, purified glycolipid from 2KO. Arrows are the lipid that accumulated in 2KO. B, MALDI-TOF-MS of the glycolipid that accumulated in 2KO. C, the proposed structure of the glycolipid that accumulated in 2KO. D, TLC showing the accumulation of EG in 2KO during the course of cultivation. Total lipids were extracted by chloroform/methanol (1:2, v/v) from cells cultivated at 25°C for the period indicated. SG, sitosteryl  $\beta$ -glucoside standard (10 nmol). EG contents on the TLC were calculated by a TLC chromatoscanner (right column). Open circle, 2KO; closed circle, WT. Data represent the mean  $\pm$  S.D of three experiment.

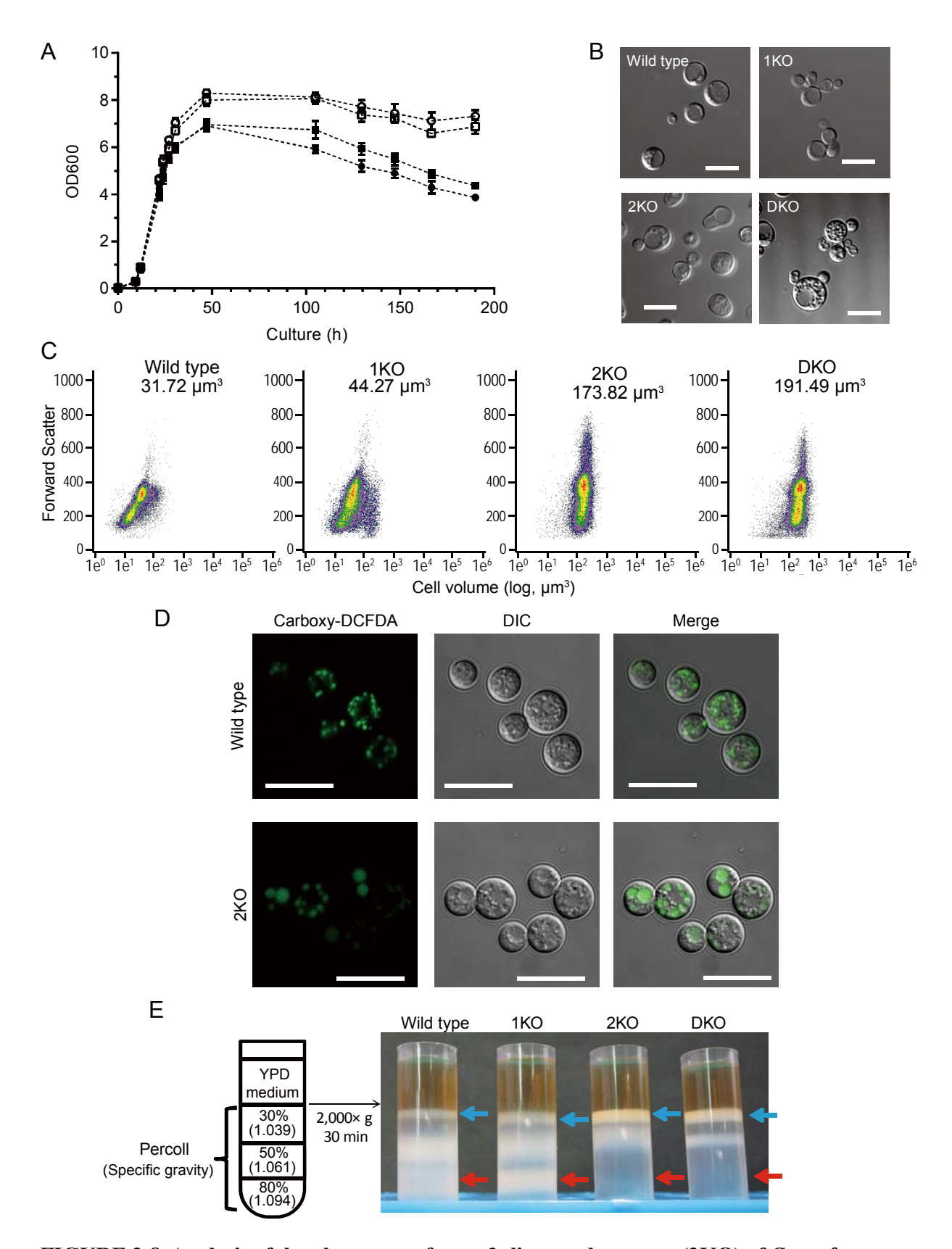


FIGURE 2-8. Analysis of the phenotype of egcrp2-disrupted mutants (2KO) of C. neoformans.

A, Growth curves of WT (open circles), 1KO (open squires), 2KO (close circles), and DKO (close squires). Data represent the mean  $\pm$  S.D of three experiments. B, Cells observed under a differential interference contrast microscope. 2KO and DKO cells exhibited cell-budding dysfunction, resulted in enlarged cells. Scale bar, 10  $\mu$ m. C, Flow cytometric analysis. The average cell volumes of WT, 1KO, 2KO and DKO were presented in each panel. D, Vacuoles stained with carboxy-DCFDA of WT and 2KO. Cells, cultured at 25°C for 1 day, were incubated with 100  $\mu$ M carboxy-DCFDA at 25°C for 20 min and observed with confocal microscopy. Scale bar, 10  $\mu$ m. E, Density gradient centrifugation of WT, 1KO, 2KO, and DKO cells by Percoll. Blue and red arrows indicate the layers including cells with the lightest and heaviest specific gravities, respectively.

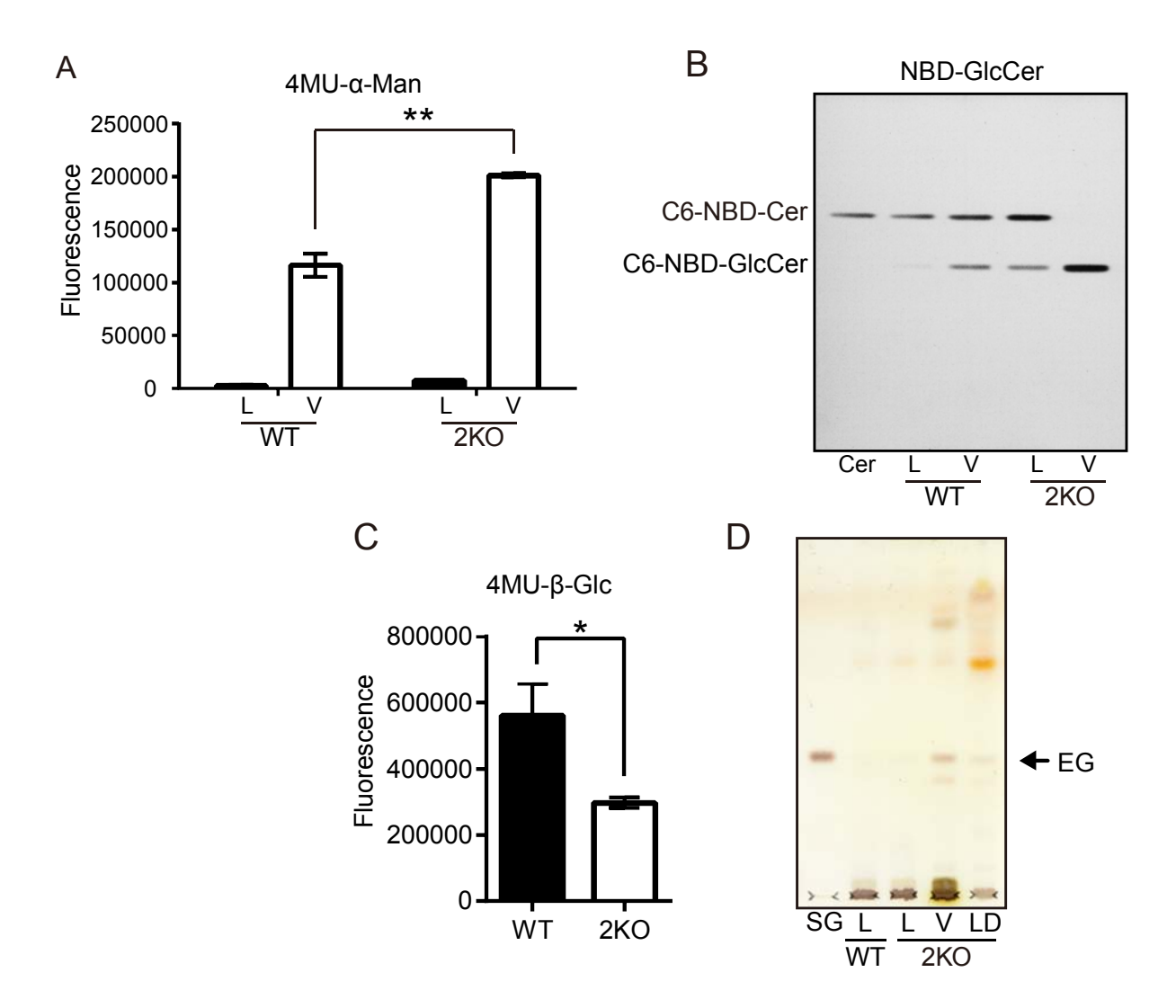


FIGURE 2-9. Cellular localization of EG that accumulated in *egcrp2*-disrupted mutants (2KO) of *C. neoformans*.

A, The α-mannosidase activity of the cell lysate and vacuole fractions. Activity was measured at 37°C for 1 h using 0.5 μg of protein from each fraction and 20 nmol 4MU-α-mannoside as a substrate in 100 μl of 50 mM phosphate buffer, pH 6.5. L, lysate; V, vacuole fraction. B, C, The β-glucosidase activity of the vacuole fraction of WT and 2KO. Activity was measured at 30°C for 18 h by using 0.25 μg of protein from vacuole fraction and 50 pmol C6-NBD-GlcCer (B) in 20 μl or 30 nmol 4MU-β-glucoside (C) as a substrate in 100 μl of 50 mM sodium acetate buffer, pH 5.0. C, TLC showing EG that accumulated in 2KO. Glycolipids were extracted from the lysate and vacuole fractions of WT and 2KO (each 50 μg as protein) and analyzed by TLC using the method described in the legend A of Fig. 2-5. L, lysate; V, vacuole fraction; LD, lipid droplet fraction. \* and \*\* represent p<0.05 and p<0.0001, respectively.

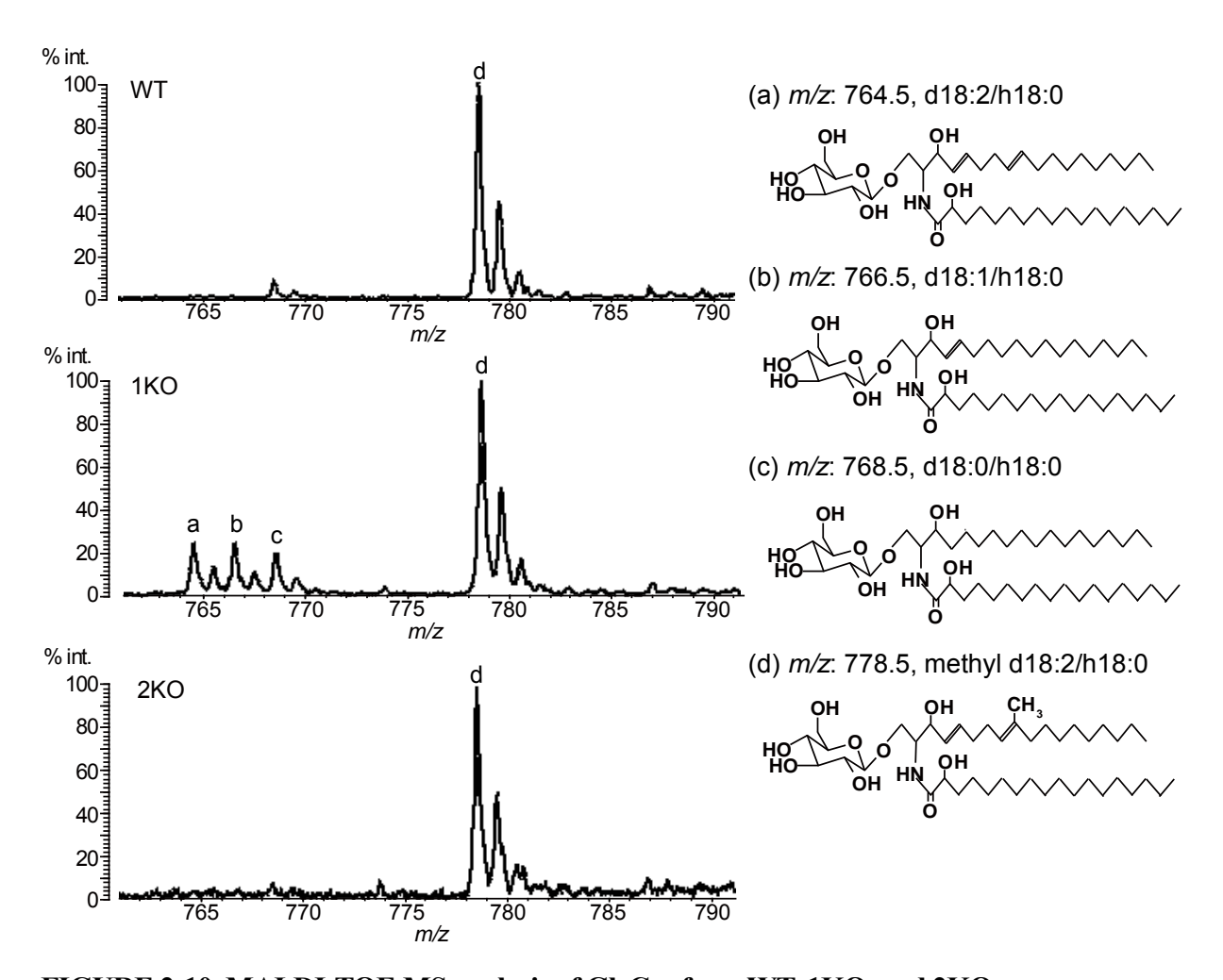


FIGURE 2-10. MALDI-TOF-MS analysis of GlcCer from WT, 1KO, and 2KO.

GlcCer, purified from WT, 1KO, and 2KO, were analyzed by MALDI-TOF-MS in a positive ion mode using 2,5-dihydroxybenzoic acid as a matrix. The major ion peak at m/z 778.5 (d), which corresponds to the molecular mass of mature GlcCer possessing Cer composed of methyl d18:2/h18:0, was detected in GlcCer from WT, 1KO, and 2KO. However, ion peaks at m/z 764.5 (a), 766.5 (b), and 768.5 (c), which correspond to the molecular mass of immature GlcCer possessing Cer composed of d18:2/h18:0, d18:1/h18:0, and d18:0/h18:0, respectively, were detected in GlcCer from 1KO but not WT or 2KO.

TABLE 2-1. Oligonucleotide primers used in this study.

Oligonucleotide	Sequence (5'-3')	Aim	
EGCrP-05607S-NotI	ATG <u>GCGGCCGC</u> ATGCCTCCTCCACCAGAAGTCTCTCCTGTCA	E	
EGCrP-05607AS-XhoI	ATG <u>CTCGCG</u> AGCAATAACGCATTCAGGACATC	Expression	
13CN005607seq-U	GACGGCAAGAACATTCAAGACT	G	
14CN005607seq-D	CGTGAGGGTAGCTGAGGAGTT	Sequencing	
CN05607N-U	ATGCCTCCTCCACCAGAAGTCT		
CN05607N-AP-D	AATAGCGAGTCCATCGTCGAGATTCAAAGGT		
ActinP-U	ACTCGCTATTGTCCAGGCTGC		
Act-Nat-Down	CTTCTTCCATAGACATGTTGGGCGAG		
Actin-HygroR-D	CTCGACAGACGTCGCGGTGAGCATAGACATGTTGGGCGAGT		
Nat-Up	ATGGAAGAAGAAGTCACTCTTGACGACACGGCTTACC		
Hygro-U	CTCACCGCGACGTCTGTCGAG		
NSL-2	AAGGTGTTCCCCGACGACGAATCG		
NSR-2	AACTCCGTCGCGAGCCCCATCAAC		
HSL	GGATGCCTCCGCTCGAAGTA	Gene disruption	
HSR	CGTTGCAAGACCTGCCTGAA		
Nat-Ttrp-Down	TAACCCCTTACCGCCTTGGGGCAGGGCATGCTCA		
	GTATATATACACCCTCTAAGGAAAACTATTCCTTTGCCCTCGGA		
Hygro-TrpT-D	CG		
Ttrp-Up	AAGGCGGTAAGGGGTTAATTTTCCTTAGAGGGTG		
Trp-U(hyg)	TTTTCCTTAGAGGGTGTATATATAC		
TrpT-CN05607C-D	GGATCGATACAGATGAGGGGTGCGACAGAAGAGA		
CN05607C-U	ACCCCTCATCTGTATCGATCC		
CN05607C-D	CTAAGCAATAACGCATTCAGG		
E2-5SENSE	CGGTGACTTAATTAGAACGCTG		
E2-5ANTISENSE	CCATCGTCGAGATTCAAAGGT	Southern blot	
3Probe-S	TCCGAAAAGAGTCCACAGAG	Souncill Diol	
3Probe-A	TTGTTCCTGCCCTGGTTG		

Restriction enzyme sites are underlined.

TABLE 2-2. Kinetic parameters of recombinant EGCrP2 and EGCrP1.

Substrate	Enzyme	Km	Kcat	K <sub>cat</sub> /K <sub>m</sub>
		$\mu M$	s <sup>-1</sup>	$M^{-1}s^{-1}$
C6-NBD-GlcCer	EGCrP2	$38.4 \pm 2.6$	$0.53 \pm 0.03$	$(13.8 \pm 0.05) \times 10^3$
4MU-β-Glc	EGCrP2	$340 \pm 13.4$	$8.8 \pm 0.18$	$(25.7 \pm 1.4) \times 10^3$
Resorufin-β-Glc	EGCrP2	$43.6 \pm 2.4$	$21.9 \pm 0.36$	$(504 \pm 24.2) \times 10^3$
pNP-β-Glc	EGCrP2	$817 \pm 37.4$	$13.8 \pm 0.15$	$(16.9 \pm 0.16) \times 10^3$
C6-NBD-GlcCer	EGCrP1	$5.80 \pm 0.3$	$(38.3 \pm 0.20) \times 10^{-3}$	$(6.6 \pm 0.40) \times 10^3$

Values are the mean  $\pm$  S.D. of three experiments. The values for EGCrP1 are from Ref. 40.

TABLE 2-3. <sup>13</sup>C and <sup>1</sup>H NMR spectral data of EG and ergosterol.

<sup>13</sup> C NMR data			<sup>1</sup> H-NMR data			
Carbon	EG	Ergosterol	Multiplicity	Proton	EG	Ergosterol
1	39.0	39.0	CH <sub>2</sub>	1α	1.32	1.30
				1β	1.93	1.90
2	30.5	32.0	$CH_2$	$2\alpha$	2.00	1.86
				2β	1.67	1.50
3	78.2	70.4	CH	3	3.72(m)	3.54(m)
4	37.8	40.9	$CH_2$	$4\alpha$	2.60(brd,14.7)	2.44
				4β	2.33(brt,13.0)	2.27
5	140.1	140.6	C=	-		
6 7	120.5	120.1	CH=	6	5.57(brs)	5.55
7	116.9	116.9	CH=	7	5.38(brs)	5.38
8	141.8	141.6	C=	_		
9	46.9	46.9	СН	9	1.99	1.97
10	37.8	37.6	C	-		
11	21.6	21.7	$CH_2$	11α	1.74	1.74
				11β	1.62	1.62
12	39.7	39.7	$CH_2$	$12\alpha$	1.30	1.28
				12β	2.09	2.09
13	43.4	43.4	C			
14	55.1	55.1	CH	14	1.92	1.90
15	23.5	23.5	$CH_2$	$15\alpha$	1.69	1.67
	• • • •		~~~	15β	1.32	1.38
16	28.8	28.8	$CH_2$	16α	1.79	1.78
1.5	<b>7</b>	5 C A	CIT	16β	1.36	1.34
17	56.4	56.4	CH	17	1.30	1.28
18	12.4	12.4	CH <sub>3</sub>	18	0.65(3H,s)	0.65
19	16.5	16.5	CH <sub>3</sub>	19	0.96(3H,s)	0.95
20	41.1	41.0	CH	20	2.06	2.06
21	21.4	21.4	CH <sub>3</sub>	21	1.05(3H,d,6.7)	1.05
22	136.3	136.2	CH=	22	5.20(dd,7.8,15.3)	5.19
23	132.6	132.6	CH=	23	5.24(dd,7.3,15.3)	5.24
24	43.6	43.5	CH	24	1.87	1.86
25	33.7	33.7	CH	25	1.48	1.48
26	19.9	19.9	CH <sub>3</sub>	26	0.84(3H,d,6.9)	0.84
27	20.2	20.2	CH <sub>3</sub>	27	0.85(3H,d,6.9)	0.85
28	17.9	18.0	CH <sub>3</sub>	28	0.93(3H,d,6.7)	0.93
β-Glc						
C-1'	101.9		СН	H-1'	4.43(d,7.8)	
C-1,	74.3		CH	H-2'	3.22(t,8.4)	
C-2,	74.3 77.3		CH	H-3'	3.41(t,8.8)	
C-4'	80.0		CH	H-4'	3.38(t,9.0)	
C-5'	76.9		CH	H-5'	3.30(m)	
C-6'	62.3		CH <sub>2</sub>	H-6a'	3.73(dd,5.2,11.9)	
~ 0	02.5		J11 <sub>2</sub>	H-6b'	3.87(dd,2.7,11.9)	

NMR chemical shifts of standard ergosterol were assigned by MQ-COSY, TOCSY, HSQC and HMBC experimental data, which measured at the same condition of EG.

## **CHAPTER 3**

# An ergosteryl-β-glucosidase (Egh1) involved in vacuole formation in Saccharomyces cerevisiae

#### 3-1. INTRODUCTION

Sterylglucosides (SGs), a class of glycolipid composed of a glucose (Glc) and sterol derivatives, are distributed in bacteria, fungi, plants, and mammals (49). The structures of SGs show diversity in the sterol moiety and anomeric linkage of glucose bound to sterols. The main sterol in fungi is ergosterol (126), whereas that in plants and mammals is sitosterol and cholesterol, respectively (127). Although most SGs possess β-Glc, the SG of *Helicobacter pylori* is composed of cholesterol and α-Glc. *H. pylori* SG was previously reported to be involved in the suppression of phagocytosis by macrophages (71). The amount of SG is known to increase under stress conditions, e.g., SG levels in the rat stomach were increased by cold shock (65), while those of slim mold (64), *Pichia pastoris* (52), and human fibroblasts (50) were increased by heat shock. Although SG has been shown to induce the expression of heat shock protein 70 (HSP70) in human fibroblasts (63), the physiological relevance of SGs under stress conditions remains unclear.

Fungal and yeast SGs are synthesized by Ugt51(Atg26), a sterol 3-β-glucosyltransferase (EC 2.4.1.173) (54); however, the *in vivo* catabolism of SGs has yet to be identified because a SG-degrading enzyme had not been identified until the discovery of EGCrP2 (endoglycoceramidase-related protein 2) in *Cryptococcus neoformans*. EGCrP2 was detected in *C. neoformans* as a paralogue of EGCrP1 (en-

doglycoceramidase-related protein 1), which is a glucocerebrosidase that is capable of degrading glucosylceramide (GlcCer), but not SGs. In contrast to EGCrP1, EGCrP2 hydrolyzed the  $\beta$ -glucosidic linkage in various SGs as well as GlcCer. Furthermore, EGCrP2-disrupted mutants (egcrp2 $\Delta$ ) of *C. neoformans* were found to accumulate ergosteryl  $\beta$ -glucoside (EG) in vacuoles. These finding clearly indicated which EGCrP2 was the steryl- $\beta$ -glucosidase that was missing in the catabolism of EG in *C. neoformans*.

The author found the EGCrP2 homologue (Egh1; ORF name, Yir007w) in the genomic database of budding yeast S. cerevisiae, and, thus, characterized the enzyme in vivo as well as in vitro in the present study. The author herein demonstrated that recombinant Egh1 hydrolyzed various  $\beta$ -glucosides including SGs and the EGH1-desrupted mutants  $(egh1\Delta)$  of S. cerevisiae accumulated EG in vivo, indicating that the enzyme is responsible for the catabolism of EG in S. cerevisiae. The author also observed the fragmentation of vacuoles in  $egh1\Delta$ , suggesting that a dysfunction in the catabolism of EG affected the process of vacuole fusion in S. cerevisiae.

## 3-2. MATERIALS AND METHODS

#### **Materials**

C6-7-nitro-2,1,3-benzoxadiazole (NBD)-ceramide (Cer), C6-NBD-GlcCer, C6-NBD-GalCer, and C12-NBD-Gb3Cer were purchased from Matreya, and C6-NBD-LacCer, C12-NBD-sphingomyelin (SM), and *para*-nitrophenyl (*p*NP) glycosides were from Sigma-Aldrich. C12-NBD-GM1 and C12-NBD-GM4 were prepared using the sphingolipid Cer *N*-deacylase by a previously described method (104). Protease inhibitor cocktail (Complete mini EDTA-free) was purchased from Roche Diagnostics.

#### Generation of mutant strains

The mutant strains of *S. cerevisiae* used in the present study were prepared from the strain BY4741 (wild type, WT) and listed in Table 3-1. The oligonucleotide primers used in this study are shown in Table 3-2. Mutants were prepared by gene-specific disruption constructs generated by PCR using delYIR007W-S1 and delYIR007W-S2 primers, and pFA6a-kanMX4 (128) as a template for  $egh1\Delta$ , and delUGT51-S1 and delUGT51-S2 primers for ugt51 $\Delta$ , respectively. In order to generate  $egh1\Delta ugt51\Delta$ , hphMX4-S and hphMX4-A primers, and pFA6-hphNT1 (128) as a template were used to switch the selective marker of the gene replacement cassette in  $egh1\Delta$  from kanMX4 to hphMX4, and  $ugt51\Delta$  was disrupted by homologous recombination. Yeast cells, transformed by lithium acetate and heat shock methods, were cultured on YPD medium with 200 mg/l of geneticin (G418) for kanMX4, 200 mg/l of hygromycin B for hphMX4, and 100 mg/l of nouseothricin (clonNAT) for natNT2, respectively.

PCR was carried out using pRS416/yir007w-IF-S and pRS416/yir007w-IF-A primers, and genomic DNA as a template, to generate revertants of EGH1 from  $egh1\Delta$ . The amplified products were inserted into the EcoRI digestive pRS416 vector using the In-Fusion HD cloning kit (Takara Bio Inc.). Transformed yeast cells were cultured in SD medium (FORMEDIUM) lacking uracil.

Green fluorescence protein (GFP)-fused Egh1 was created as described in Ref. 129 and 130. Briefly, DNA fragments were generated by PCR using delYIR007W-S1 and YIR007W-S4 primers, and pKT127 (129) as a template for carboxy-terminal GFP-fused Egh1. To express amino-terminal GFP-fused Egh1 with TEF promoter, DNA fragments were amplified using YIR007W-GFP127-S and YIR007W-GFP127-A primers, and pYM-N21 (128) as a template. To exchange the natural *EGH1* promoter with the TEF promoter, DNA fragments were amplified using the delYIR007W-S1 and YIR007W-S4 primers, and pYM-N19 (128) as a template.

# **Construction of the expression vector**

Total RNA was obtained from yeast cells using the SV Total RNA Isolation System (Promega). First strand cDNA was synthesized from 1 µg of total RNA using the PrimeScript 1st strand cDNA synthesis kit (Takara Bio Inc.). To insert the overlap region, PCR was carried out using first strand cDNA as a template and the expression primers listed in Table 3-2. Amplification was performed using PrimeSTAR GXL DNA polymerase (Takara Bio Inc.). The amplified product was inserted into the NdeI and PstI double digestive pCold TF (Takara Bio Inc.) vector using the In-Fusion HD cloning kit.

## Expression and purification of recombinant Egh1

The S. cerevisiae EGH1 gene was expressed in Escherichia coli BL21 (DE3) using a pCold TF vector containing EGH1. After incubating transformants at 37°C in Luria-Bertani (LB) medium containing 100 µg/ml of ampicillin until the  $A_{600nm}$  reached ~0.6, the culture was kept at 15°C for 30 min. Isopropyl β-D-thiogalactopyranoside was then added to the culture at a final concentration of 1 mM. After being kept at 15°C for 24 h, the cells were harvested by centrifugation (8000 × g for 15 min), and suspended in 50 mM Tris-HCl buffer, pH 7.5, containing 150 mM NaCl and 20 mM imidazole. The suspension was kept in a sonic bath for 30 sec, this procedure was repeated 4 times to crush the cells, and the cell debris was removed by centrifugation (18,000 x g for 15 min). The supernatant was applied to Ni Sepharose 6 Fast Flow (GE Healthcare) packed in Muromac mini column M (Muromachi Technos), and the column was then washed with 50 mM Tris-HCl, pH 7.5, containing 150 mM NaCl and 40 mM imidazole. Recombinant Egh1 was eluted with 50 mM Tris-HCl, pH 7.5, containing 150 mM NaCl and 200 mM imidazole. The purified enzyme was dialyzed against 50 mM Tris-HCl, pH 7.5, containing 150 mM NaCl using Amicon Ultra-4 30k unit (Merck Millipore), and subjected to a Superdex 200 10/300 GL (GE Healthcare) gel filtration column equilibrated with 25 mM MES, pH 6.0, and containing 100 mM NaCl. EGCrP2 was eluted from the column with the same buffer at a flow rate of 0.5 ml/min, and each 0.5 ml fraction was collected using a fraction collector (GE Healthcare).

#### Protein assay

Protein content was determined by the Pierce 660 nm Protein Assay Reagent

(Thermo Fisher Scientific) with bovine serum albumin as a standard. SDS-PAGE was carried out according to the method of Laemmli (105) with the Spectra Multicolor Broad Range Protein Ladder (Thermo Fisher Scientific) as a marker. Proteins were stained with CBB Stain One (Nacalai Tesque).

## Enzyme assay

An aliquot of each substrate (NBD-labeled GSLs, *p*NP glycosides, and sitosteryl β-glucoside) was incubated at 30°C for an appropriate period with the enzyme in 20 μl of 50 mM phosphate buffer, pH 5.5, containing 0.025% sodium cholate. The reaction mixture, dried using a SpeedVac concentrator, was dissolved in 10 μl of chloroform/methanol (1:2, v/v) and applied to a Silica Gel 60 TLC plate (Merck Millipore), which was developed with chloroform/methanol/water (60:35:8, 65:25:4 or 65:16:2, v/v/v). NBD-labeled GSLs were visualized using AE-6935B VISIRAYS-B (ATTO). The C6-NBD-Cer generated by the enzyme reaction was separated from C6-NBD-GlcCer on a normal phase HPLC column (Inertsil SIL 150A-5, GL Science) and quantified according to the method described by Hayashi *et al* (106). Sitotesryl-β-glucoside and glucose were visualized by spraying the TLC plate with Orcinol sulfate reagent. *p*-Nitrophenol released from *p*NP glycosides by the action of the enzyme was measured at 405 nm with a Multiskan FC microplate reader (Thermo Fisher Scientific).

## **Crude enzyme preparation**

Yeast cells were harvested at  $A_{600\text{nm}}$  0.8-1.0 by centrifugation at 4,400 × g for 2

min at 4°C and washed twice with PBS. Ten microliters of the cell suspension ( $A_{600nm}$  1.0) was added to lysis buffer (50 mM phosphate buffer, pH 7.3) and crushed at 3,200 rpm for 30 sec on ice with a bead crusher  $\mu$ T-12 (Taitech) using approximately 0.2 cm<sup>3</sup> of 0.6-mm diameter glass beads in a 1.5-ml tube. This procedure was repeated three times. The supernatant was obtained by centrifugation at 800 x g for 15 min at 4°C.

## Extraction and purification of glycolipids

Total lipids were extracted from *S. cerevisiae* with chloroform/methanol (1:2, v/v), and applied to a TLC plate (corresponding to 30 mg dry cells per lane), which was developed with chloroform/methanol/water (65:16:2, v/v/v) as a developing solvent, and stained with Orcinol sulfate reagent. The glycolipid that accumulated in  $egh1\Delta$  was extracted with chloroform/methanol (1:2, v/v) and treated with 0.1 M NaOH. Alkaline-resistant lipids were dissolved in chloroform and loaded onto a Sep-Pak plus silica column cartridge equilibrated with chloroform. The lipids were eluted from the cartridge by a stepwise elution with chloroform, chloroform/methanol (98:2, v/v), chloroform/methanol (95:5, v/v), and chloroform/methanol (90:10, v/v). The glycolipid was mainly recovered in the chloroform/methanol (95:5, v/v) fraction.

## **HPLC** and MS analyses

A reverse phase HPLC analysis was conducted using an EZChromate light HPLC system (Hitachi) with a diode-array detector and COSMOSIL 5C22-AR-II column ( $4.6 \times 250$  mm, 5  $\mu$ m, Nacalai Tesque) using methanol as an isocratic mobile phase, which was operated at a flow rate of 1 ml/min at 40°C in a column oven. LC-MS was performed using a HPLC system (Agilent Technologies) coupled to a mass spectrometry

apparatus (3200 QTRAP/MS/MS, AB SCIEX). LC was conducted using an Inertsustain C18 column ( $2.1 \times 150$  mm, GL Science) with methanol/1M ammonium formate = 99:1 (v/v) as the eluent at a flow rate of 200  $\mu$ l/min at 25°C in a column oven. An MS analysis was performed under the following conditions: ion spray voltage, 5,500 V; gas pressure, 0.3 psi; scan speed, 1,000 atomic mass units/s; scan range, m/z 500–700; trap fill time, 5 ms; declustering potential, 35V; collision energy, 10 eV; resolution of Q1/Q3 unit.

## Vacuole staining

Vacuoles were observed under fluorescent microscopy after the incorporation of 5-(and-6)-carboxy-2',7'-dichlorofluorescein diacetate (carboxy-DCFDA, Molecular Probes) or N-(3-Triethylammoniumpropyl)-4-(6-(4-(Diethylamino)phenyl)hexatrienyl) Pyridinium Dibromide (FM4-64, Molecular Probes). To verify vacuole formation, the number of vacuoles per 100 cells was counted according to the method described by Baars *et al* (92). At least three independent experiments were carried out, and categorized into four groups: 1-2, 3-4, 5-8, and >9 vacuoles/cell.

#### 3-3. RESULTS

# Molecular cloning and characterization of recombinant Egh1

Egh1 showed 54% and 36% identities caluculated by Protein BLAST to *C. neoformans* EGCrP2 and rhodococcal endoglycoceramidase II (EGCase II), respectively. The alignment of the deduced amino acid sequence of Egh1 with those of EGCrP2 and EGCase II revealed that eight amino acid residues, essential for the catalytic activity of glycoside hydrolase (GH) family 5 glycosidases (115), were completely conserved in these enzymes (Fig. 3-1, circles). Of the 8 residues of Egh1, two catalytic glutamates, Glu265 and Glu516, at the end of β-strands 5 and 8, respectively, were thought to be an acid/base catalyst and nucleophile, respectively (Fig. 3-1, closed circles).

To characterize the enzymatic properties of the Egh1, *EGH1* gene encoding 764 residues was cloned from the complementary DNA of *S. cerevisiae* and expressed in *E. coli* BL21 (DE3) as a Trigger factor-fused protein. The recombinant Egh1 (rEgh1) was purified by a Nickel-conjugated Sepharose column, followed by gel filtration using a Superdex 200 column. The purified rEgh1 showed a protein band with a molecular mass of approximately 138 kDa on SDS-PAGE after staining with Coomassie Brilliant Blue (Fig. 3-2A). This molecular mass coincided with the deduced molecular mass of Trigger factor-conjugated Egh1.

Purified rEgh1 hydrolyzed sitosteryl β-glucoside and cholesteryl β-glucoside to generate Glc (Fig. 3-2B). The enzyme also hydrolyzed C6-NBD-GlcCer to generate C6-NBD-Cer; however, it did not degrade any of the other NBD-glycosphingolipids tested or NBD-sphingomyelin (Fig. 3-2C). The specificity of rEgh1 was to the β-glucosidic linkage because it hydrolyzed pNP-β-Glc, but not other pNP-glycosides

including pNP- $\beta$ -galactoside and pNP- $\alpha$ -Glc (Fig. 3-2D). These results clearly indicated that Egh1 was a  $\beta$ -glucosidase with broad aglycone specificity similar to EGCrP2. In contrast to EGCrP2, the EGCrP1 of *C. neoformans* was specific to GlcCer and was not able to hydrolyze any SGs including EG. An EGCrP1 homologue was not found in the *S. cerevisiae* genome database, and this was consistent with *S. cerevisiae* not possessing any GlcCer (48).

# Identification of the glycolipid that accumulated in $egh1\Delta$

To determine the physiological functions of Egh1,  $egh1\Delta$  were generated from S. cerevisiae BY4741 (WT). \(\beta\)-Glucosidase activity was markedly greatly reduced at acidic as well as neutral pH in egh1 $\Delta$  when C6-NBD-GlcCer was used as a substrate (Fig. 3-3A). The glycolipid, whose Rf corresponded to that of SG, was detected in the total lipid fraction of  $egh1\Delta$ , but not in that of WT (Fig. 3-3B lanes 2, 3). The glycolipid fraction was prepared from  $eghl\Delta$  by a silica-based cartridge and subjected to reverse-phase HPLC with diode array detection. The UV spectra of the glycolipid eluted at 6.3 min (peak indicated by the arrow, Fig. 3-3C, upper panel) showed four absorbance peaks at 262, 271, 282, 293 nm (Fig. 3-3C, lower panel), which are typical UV spectra for ergosterol (130). The main molecular ion peak, [M+NH<sub>4</sub>]<sup>+</sup>, was observed at m/z 576 for the glycolipid with LC-MS, which is consistent with that of EG (Fig. 3-3D, upper panel). The MS/MS spectra showed the typical fragment ion of EG at m/z379 (Fig. 3-3D, lower panel). Furthermore, the purified glycolipid was hydrolyzed by C. neoformans EGCrP2 to generate Glc, indicating that Glc was linked to ergosterol via the β-glycosidic linkage (Fig. 3-3E). Collectively, these results clearly demonstrated that the glycolipid that accumulated in egh1 $\Delta$  was EG, indicating that Egh1 was responsible for the degradation of EG in *S. cerevisiae*. EG was not detected in EGHI/UGT51-double knockout mutants  $(egh1\Delta ugt51\Delta)$  (Fig. 3-3B, lane 5), which indicated that EG was synthesized by Ugt51(Atg26) and degraded by Egh1 *in vivo*.

## Intercellular localization of Egh1

To clarify the intracellular localization of Egh1, GFP-fused Egh1 was expressed in S. cerevisiae BY4741 (WT). In the present study, two types of Egh1 overexpressors driven with the TEF promoter were generated; one was fused with GFP at the carboxyl terminal of Egh1, while the other was fused at the amino terminal of Egh1. Both GFP-fused Egh1 were detected as a 138-kDa band on Western blotting using an anti-GFP antibody (Fig. 3-4A, lanes 2 and 4). However, the expression of GFP-fused Egh1 was too low to detect under the conditions used whether GFP-fused protein was expressed with a natural EGH1 promoter (Fig. 3-4A, lane 3). The author confirmed that the enzyme activities of the two Egh1 overexpressors were higher than that of WT, even though GFP was conjugated at either the amino terminal or carboxyl terminal (Fig. 3-4B). The intracellular distribution of two GFP-fused Egh1 differed depending on the site of GFP conjugated to Egh1, i.e., both were mainly localized at the cytosol, whereas one with the amino terminal GFP was also localized at an intracellular organelle with a granular structure (Fig. 3-4C), suggesting that a putative targeting signal was located at the C-terminal. However, the organelle to which amino terminal GFP-fused Egh1 was delivered has not yet been identified.

# Effects of the disruption of EGH1 on vacuole morphology

The author previously reported that the EGCrP2-deficient mutants ( $egcrp2\Delta$ ) of C. neoformans showed distinct growth arrest, a dysfunction in cell budding, and an abnormal vacuole morphology (131). However, no apparent difference was observed in cell growth and cell budding between WT and  $egh1\Delta$  in under the conditions used. On the other hand, a marked difference was detected in vacuole morphology. The  $egcrp2\Delta$  of C. neoformans exhibited the hypertrophy of vacuoles, while the  $egh1\Delta$  of S. cerevisiae showed the fragmentation of vacuoles when cells were observed under fluorescent microscopy after staining with carboxy-DCFDA (Fig. 3-5B). To quantify the fragmentation of vacuoles, cells were stained with FM4-64 and the number of vacuoles/cell was counted (Fig. 3-5C). The results revealed that the number of cells exhibiting 1-2 vacuoles/cell decreased while those exhibiting 5-8 vacuoles/cell increased in  $egh1\Delta$  (Fig. 3-5D). Furthermore, the size of vacuoles decreased with the disruption of EGH1 (Fig. 3-5C). The abnormal vacuole morphology observed in  $egh1\Delta$  was restored by the expression of EGH1 in  $egh1\Delta$  (revertants) (Fig. 3-5C, D).

#### 3-4. DISCUSSION

Endoglycoceramidase (EGCase, EC3.2.1.123; ceramide glycanase) is an enzyme that is capable of hydrolyzing the O-glycosidic linkage between an oligosaccharaide and ceramide of various glycosphingolipids (GSLs). However, EGCase hardly hydrolyzed GlcCer, and the minimum sugar structure required for the hydrolysis of GSLs is lactose (101,102). EGCrP1 and EGCrP2 are homologues of EGCase; however, neither can hydrolyze GSLs, except for GlcCer, and, thus, the specificities of EGCrP1/EGCrP2 are completely different from that of EGCase. EGCase is distributed from procaryotes to invertebrates, but not in fungi and yeasts, while EGCrP1/EGCrP2 are distributed in fungi and yeasts.

EGCase is a glycohydrolase that belongs to Glycoside Hydrolase (GH) family 5, which is one of the largest of all CAZy glycoside hydrolase families and includes endoglucanase (cellulase), endomannanase, β-glucosidase, and β-mannnosidase. EGCase was clarified the sole enzyme capable of hydrolyzing GSLs in GH family 5; however, EGCrP1/EGCrP2 emerged as other enzymes capable of hydrolyzing GSLs in GH family 5. The aglycone specificities of EGCase and EGCrP1 are strict (narrow) because they are specific to GSLs that are glycolipids containing a ceramide (sphingoid bases). In contrast, the aglycone specificity of EGCrP2/Egh1 was previously shown to be very broad (131), which was consistent with our results, i.e., they were able to hydrolyze various β-glucosides, not only GlcCer, but also various SGs and other artificial β-glucosides such as pNP-β-Glc. However, it was important to determine how EGCrP2/Egh1 functioned *in vivo*, and the author demonstrated that EG accumulated in the egcrp2 $\Delta$  of *C. neoformans* (131) and *egh1* $\Delta$  of *S. cerevisiae* (this study), thereby in-

dicating that EGCrP2/Egh1 physiologically functioned as an EG-degrading enzyme (ergosteryl  $\beta$ -glucosidase), which is involved in the EG catabolic pathway in fungi and yeasts. EGCrP2 was distributed widely in fungi, which possess SGs including EG, and, thus, EGCrP2 may be a universal ergosteryl  $\beta$ -glycosidase involved in the catabolism of SG in fungi.

Fungal SGs are synthesized by Ugt51(Atg26) and this enzyme appears to be responsible for the synthesis of EG in *S. cerevisiae* (54). However, EG was undetectable not only in  $ugt51\Delta$ , but also in WT of *S. cerevisiae*; thus, it remains ambiguous whether Ugt51(Atg26) can synthesize EG *in vivo* of the budding yeast. The reason why EG was undetectable in *S. cerevisiae* regardless of the presence of Ugt51(Atg26) may have been due to the active catabolism of EG (54), although the enzyme responsible for the degradation of EG had not been identified until this study. EG was detected in  $egh1\Delta$  as expected (Fig. 3-3B), indicating that Ugt51(Atg26) synthesized EG *in vivo*. However, the EG content in the WT of *S. cerevisiae* appears to be 10-fold less than that of *C. neoformans* when estimated by the HPLC-based assay (data not shown).

SG levels are known to increase in human fibroblasts with heat shock (50,64). Since SG can induce the expression of heat shock protein 70 (HSP70) in fibroblasts (63), it is considered to be a HSP-inducible as well as stress-induced glycolipid in mammals. Heat shock also induced the accumulation of EG, a major SG in lower eucaryotes, in slime mold and fungi. However, the mechanism underlying the EG-mediated stress response may differ between mammals and lower eukaryotes because the enzymes responsible for the synthesis and degradation of SG (EG) are completely different, i.e., homologues of Ugt51(Atg26) and EGCrP2/Egh1 have not been found in mammals; alternatively, the synthesis of SG appeared to be catalyzed by glucocerebrosidase GBA1,

which transfers Glc from GlcCer to sterols (132). The enzyme responsible for the degradation of SG remains unknown in mammals.

The physiological significance of SGs remains to be elucidated; however, a study on the relationship between EG and pexophagy is of particular interest. Pexophagy, which is a kind of autophagy characterized by the degradation of peroxisomes in vacuoles, is frequently observed in the methylotrophic yeast *P. pastoris*, in which EG is a major glycolipid and inducible by heat shock. The *UGT51*-disrupted mutants of *P. pastoris*, which lacks EG, lost the ability to undergo pexophagy, suggesting that EG and Ugt51 are involved in the process of pexophagy. This phenomenon was not observed in *S. cerevisiae*, and was attributed to the low quantities of EG.

In the present study, the author showed that the disruption of EGHI resulted in vacuole fragmentation, as well as the accumulation of EG, in S. cerevisiae (Fig. 3-4B-D), and these phenotypes were restored by the expression of EGHI in  $eghI\Delta$ . This result suggests that the content of EG is closely related to vacuole formation, especially the vacuole fusion process. Several S. cerevisiae genes have been identified in relation to the formation of vacuoles, i.e, disruption of the genes responsible for the synthesis of ergosterol, phosphoinositide-3-phosphate, phosphoinositide-4,5-diphosphate, phosphatidic acid, and phosphatidyl ethanolamine led to abnormal vacuole phenotypes (93,133-135). The morphology of vacuoles in  $eghI\Delta$  was similar to that in ergosterol-deficient mutants. One possible interpretation is that EG is a reservoir that regulates the content of ergosterol  $in\ vivo$ .

Abnormal vacuole phenotypes were observed not only in  $egh1\Delta$  but also in egcrp2 $\Delta$ ; however, these phenotypes appeared to be reversed, i.e., the former (exhibiting fragmented vacuoles) stemmed from a dysfunction in the fusion process, while the latter

(exhibiting enlarged vacuoles), from a fission process during vacuole formation. The reason for the discrepancy is currently ambiguous; however, variations in the quantity of EG in *C. neoformans* and *S. cerevisiae* cells (the EG content of *C. neoformans* is  $\geq 10$  times higher than that of *S. cerevisiae*) may explain these different phenotypes.

The results obtained herein on of Egh1 will shed light on the relationship between EG catabolism and vacuole formation in *S. cerevisiae*.

#### 3-5. SUMMARY

Sterylglucosides (SGs) are composed of a glucose and sterol derivatives, and are distributed in fungi, plants, and mammals. The author recently identified EGCrP1 and EGCrP2 (endoglycoceramidase-related proteins 1 and 2) as a  $\beta$ -glucocerebrosidase and steryl- $\beta$ -glucosidase, respectively, in *Cryptococcus neoformans*. The author herein described an EGCrP2 homologue (Egh1; ORF name, Yir007w) involved in SG catabolism in *Saccharomyces cerevisiae*. The purified recombinant Egh1 hydrolyzed various  $\beta$ -glucosides including ergosteryl  $\beta$ -glucoside (EG), sitosteryl  $\beta$ -glucoside, cholesteryl  $\beta$ -glucoside, *para*-nitrophenyl  $\beta$ -glucoside, and glucosylceramide. The disruption of *EGH1* in *S. cerevisiae* BY4741 (*egh1* $\Delta$ ) resulted in the accumulation of EG and fragmentation of vacuoles. The expression of *EGH1* in *egh1* $\Delta$  (revertant) reduced the accumulation of EG, and restored the morphology of vacuoles. The accumulation of EG was not detected in *EGH1* or *UGT51*(*ATG26*) double-disrupted mutants (*ugt51* $\Delta$  *egh1* $\Delta$ ), indicating that EG was synthesized by Ugt51(Atg26) and degraded by Egh1 *in vivo*. These results clearly demonstrated that Egh1 is an ergosteryl- $\beta$ -glucosidase that is functionally involved in the EG catabolic pathway and vacuole formation in *S. cerevisiae*.

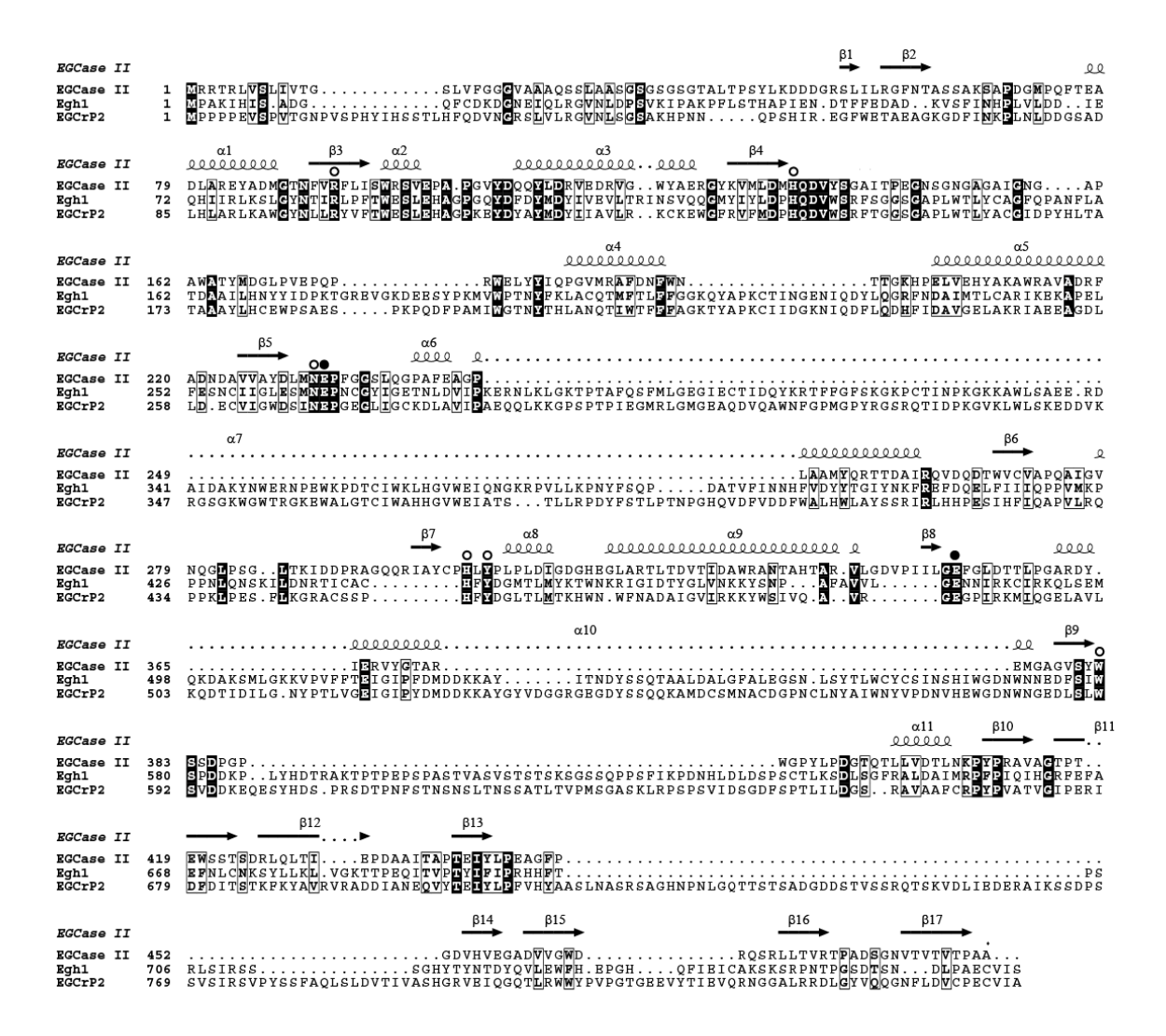


### FIGURE 3-1. Alignment of EGCrP2 and Egh1 with EGCase II.

The amino acid sequences of *Rhodococcus* EGCase II (accession: AAB67050.1), *C. neoformans* EGCrP2, and *S. cerevisiae* Egh1 were aligned using ClustalW (123) and ESPript (124). White letters on a black background and black letters in an open box show identical and similar residues, respectively. Open circles indicate amino acid residues conserved in GH family 5 glycosidase. Two glutamates, the Glu270 and Glu520 of EGCrP2 and Glu265 and Glu483 of Egh1, are indicated by closed circles as a possible acid/base catalyst and nucleophile, respectively. The secondary structural elements are shown above the amino acid sequence of EGCase II (125).

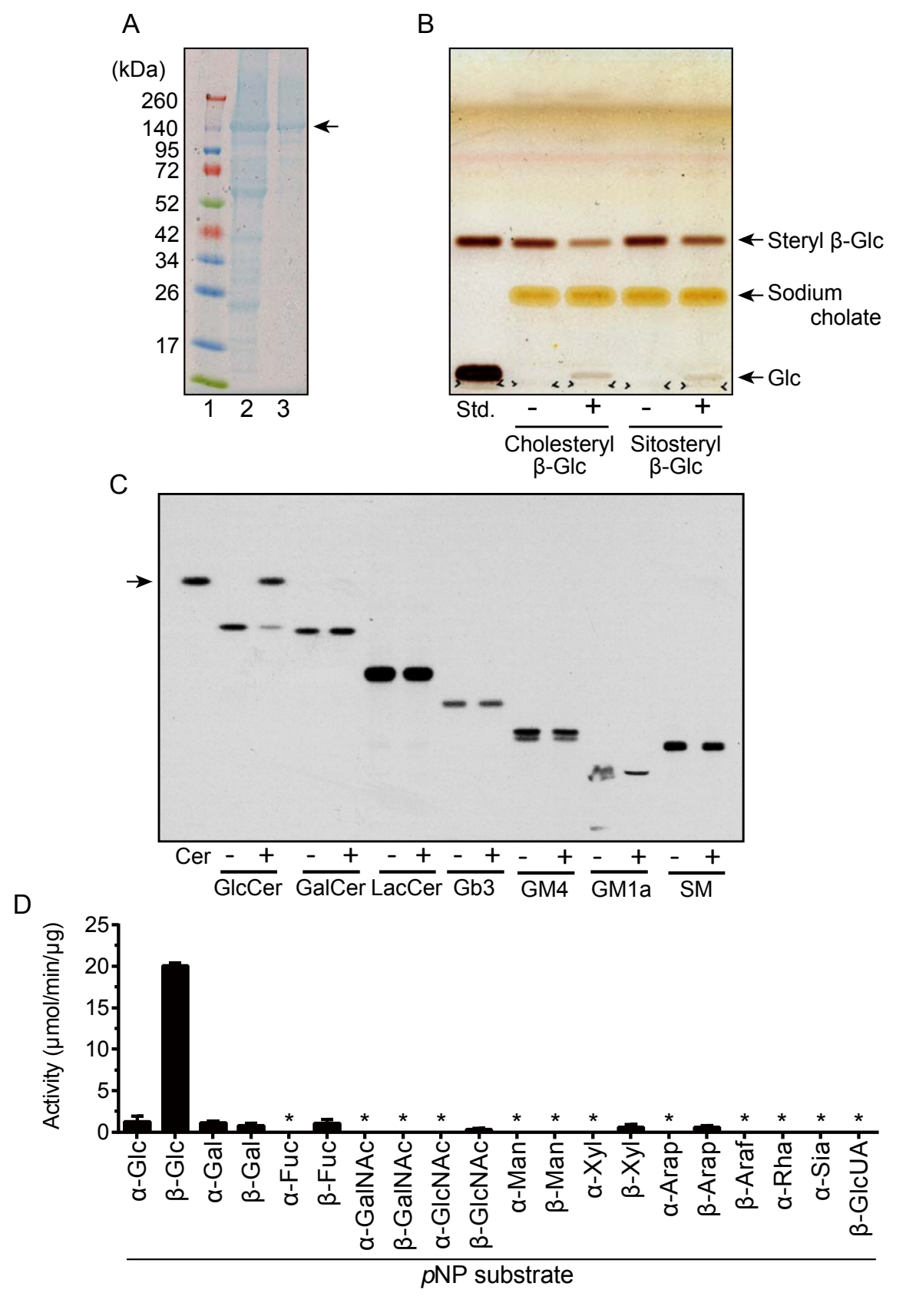


FIGURE 3-2. Purification and characterization of recombinant Egh1.

A, Final preparation of recombinant Egh1 on 10% SDS-PAGE. The protein eluted from the Ni-Sepharose column was purified using Superdex 200 10/300 GL. *Lane* 1, protein marker; *lane* 2, proteins eluted from the Ni-sepharose column; *lane* 3, final preparation of Egh1. B, TLC showing the specificity of recombinant Egh1 (rEgh1) toward cholesteryl β-Glc and sitosteryl β-Glc. Each substrate was incubated in 20 μl of 50 mM phosphate buffer, pH 5.5, at  $30^{\circ}$ C for 18 h with 2 μg of rEgh1 (+) or heat-inactivated enzyme (-). TLC was developed with chloroform/methanol/water (65:16:2, v/v/v), and stained with orcinol sulfate reagent. *C*, TLC showing the specificity of rEgh1 toward various NBD-GSLs and NBD-sphingomyelin (SM). Each NBD-GSL or NBD-SM (50 pmol) was incubated in 20 μl of 50 mM phosphate buffer, pH 5.5, with 1 μg of rEgh1 (+) or heat-inactivated enzyme (-) at  $30^{\circ}$ C for 18 h. Samples were loaded onto a TLC plate, which was developed with chloroform/methanol/water (60:35:8, v/v/v). *D*, Hydrolysis of *p*NP substrates by rEgh1. Error bars represent the mean ± S.D. of three experiments. An asterisk indicates no hydrolysis of *p*NP substrates.

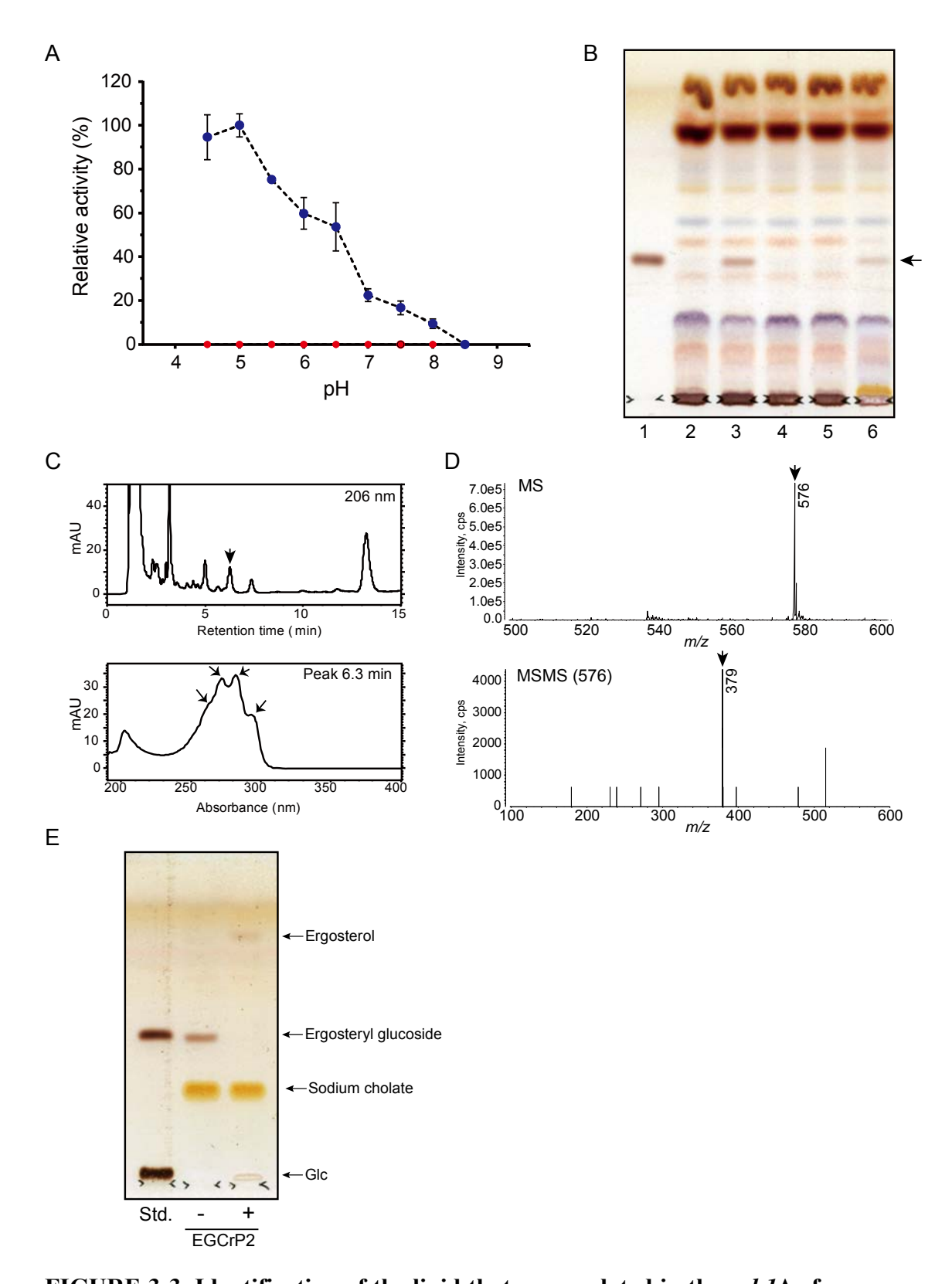


FIGURE 3-3. Identification of the lipid that accumulated in the  $egh1\Delta$  of

#### S. cerevisiae.

A, Activity of cell lysates from wild type (WT) and  $eghl\Delta$  at different pHs. Blue circles, WT; red circles,  $egh1\Delta$ . In this assay, C6-NBD-GlcCer was used as a substrate in 150 mM of GTA buffer at different pHs. Relative activity was expressed as a percentage of the activity of WT at pH 5.0. B, TLC showing the glycolipid that accumulated in egh  $l\Delta$ . Glycolipids were extracted by chloroform/methanol (1:2, v/v) from cells after cultivation at 30°C for 36 h. Lipids corresponding to 30 mg dry cells were loaded onto a TLC plate, which was developed with chloroform/methanol/water (65:16:2, v/v/v). Glycolipids were visualized by an orcinol sulfate reagent. The arrow indicates the accumulated lipid. Lane 1, sitosteryl glucoside; lane 2, WT; lane 3, egh $1\Delta$ ; lane 4, ugt $51\Delta$ ; lane 5, ugt $51\Delta$  egh $1\Delta$ ; lane 6, revertant of  $eghl\Delta$  with EGH1. C, UV spectra of the glycolipid that accumulated in  $eghl\Delta$ . Lipids were subjected to a mild alkaline treatment and then purified by Sep-Pak plus silica cartridge, followed by HPLC equipped with a COSMOSIL 5C22-AR-II column and diode array detector. The upper panel shows the elution profile of glycolipids from HPLC monitored at 206 nm, while the lower panel shows the UV spectra of glycolipids eluted from HPLC at 6.3 min (arrow in upper panel). The four arrows in the lower panel show specific UV absorbance at 262, 271, 282, 293 nm, which are typical characteristic UV absorbances for ergosterol. D, An LC-MS analysis of the glycolipid that accumulated in  $eghl\Delta$ . The upper and lower panels show MS and MS/MS analyses of the glycolipid, respectively. The arrow in the upper panel indicated the  $[M+NH_4]^+$  of EG (m/z 576). MS/MS was conducted using the peak at m/z 576 as a precursor ion. The arrow in lower panel indicated the typical fragment ion of EG at m/z 379. E, The glycolipid eluted by HPLC at 5-10 min was pooled and digested by 1 µg of EGCrP2 (+) or heat-inactivated EGCrP2 (-) for 18 h at 30°C. Std., sitosterylglucoside (upper) and glucose (lower) standards.

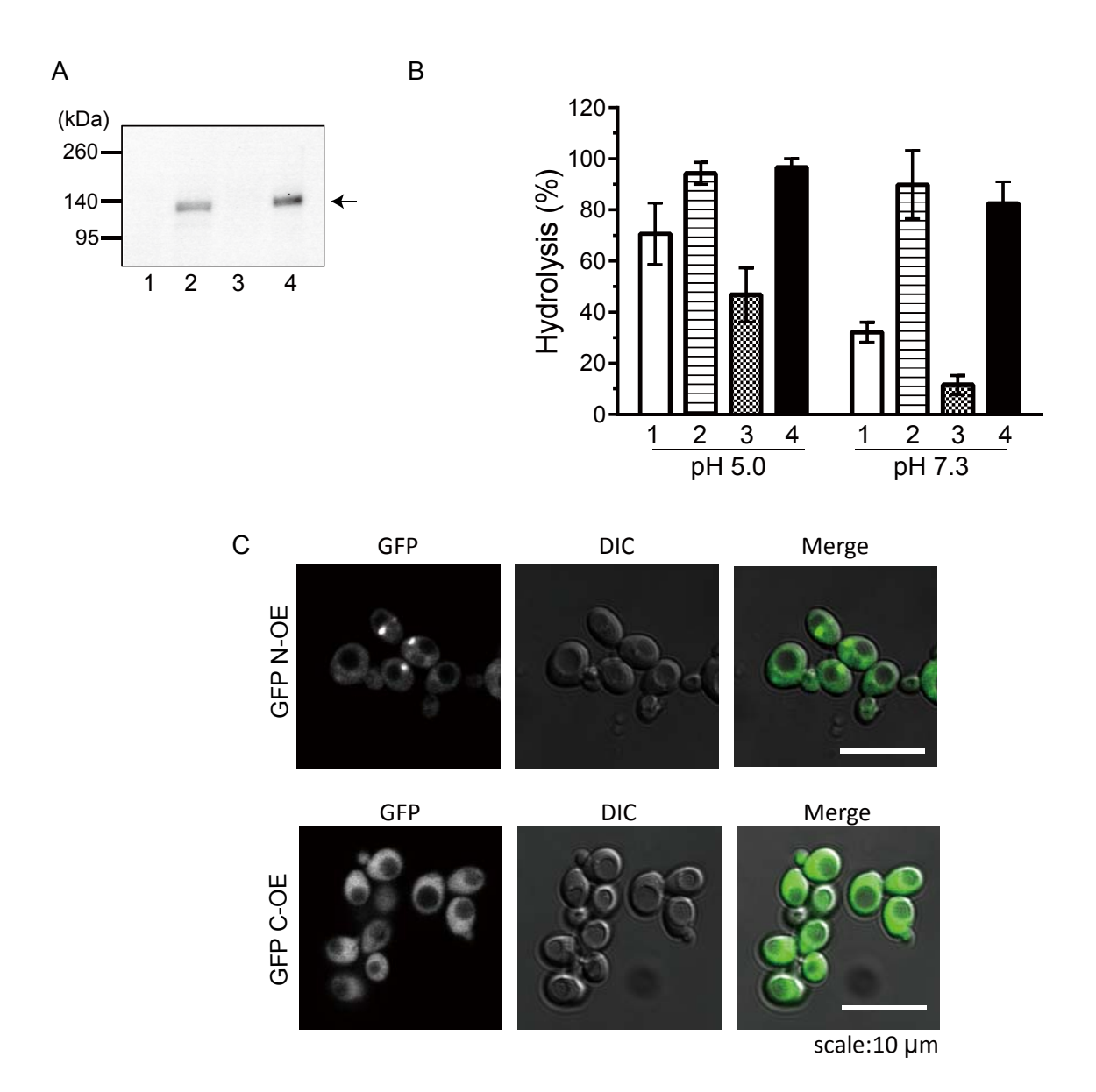


FIGURE 3-4. Localization of Egh1 in S. cerevisiae.

A, Western blotting of GFP-fused Egh1 using an anti-GFP antibody. B, β-glucosidase activity of Egh1 as measured by C6-NBD-GlcCer as a substrate. Activities were measured at 30°C for 18 h using 50 μg of protein. Lane 1, WT; lane 2, overexpression of Egh1 fused with GFP at the N-terminal (GFP N-OE); lane 3, normal expression of Egh1 fused with GFP at the C-terminal; lane 4, overexpression of Egh1 fused with GFP at the C-terminal (GFP C-OE). C, intracellular distribution of GFP-fused Egh1 observed under fluorescence and differential interference contrast (DIC) microscopy.

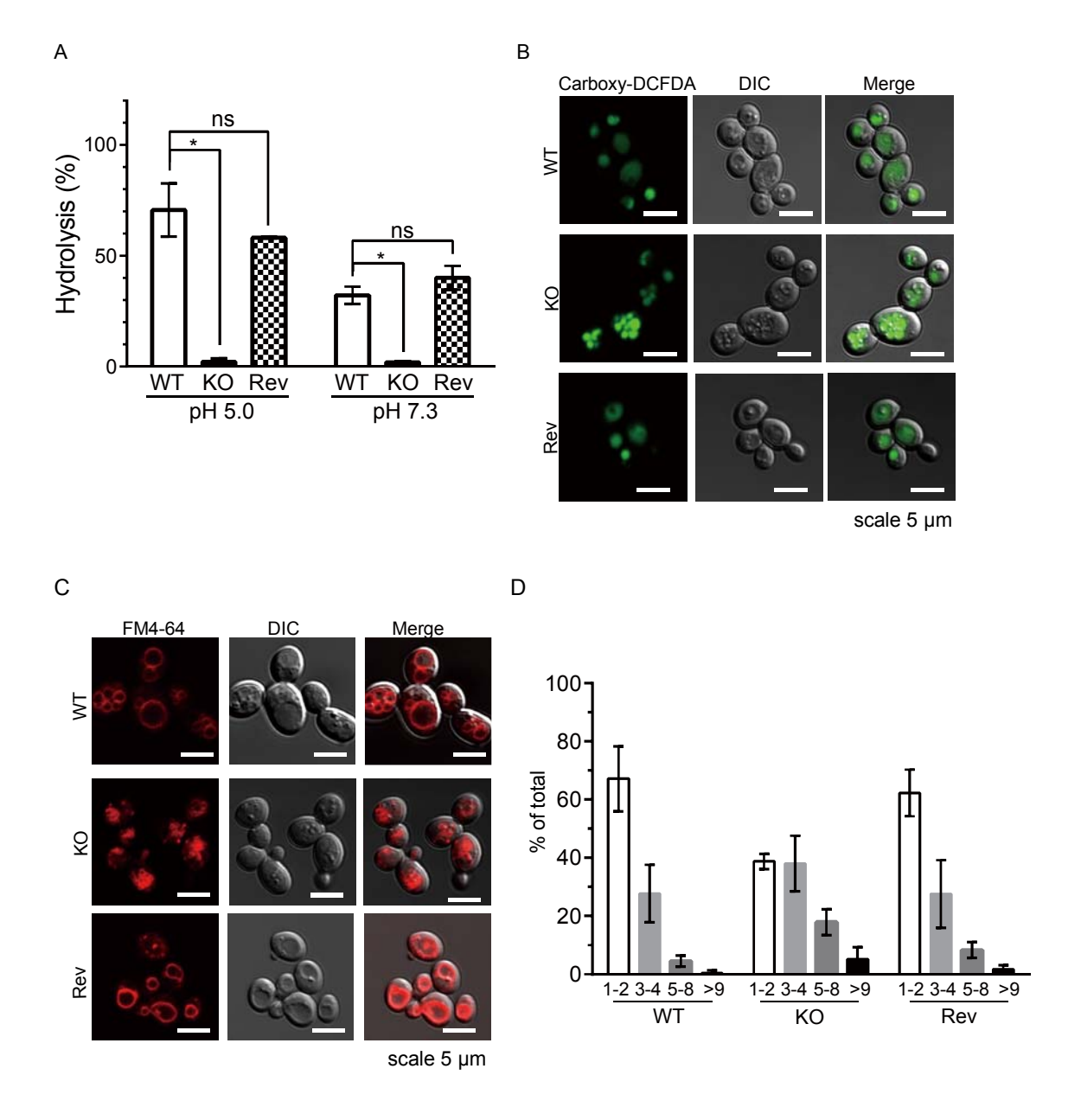


FIGURE 3-5. Vacuole morphology of WT,  $egh1\Delta$ , and revertant with EGH1.

A,  $\beta$ -glucosidase activity of cell lysates as measured by C6-NBD-GlcCer as a substrate. WT, KO, and Rev represent wild type,  $egh1\Delta$ , and revertant with EGH1, respectively. Activities were measured at 30°C for 18 h using 50 µg of cell lysate at pH 5.5. \*, p<0.0001; ns, not significant. Error bars represent the mean  $\pm$  S.D. of three experiments. B, C, Vacuole morphology after staining with carboxy-DCFDA (B) and FM4-64 (C). D, Extent of fragmentation of vacuoles. The number of vacuoles/cell were counted using at least 100 cells after staining with FM4-64, and categorized into 4 groups: 1-2, 3-4, 5-8, >9 vacuoles/cell, respectively.

TABLE 3-1. Yeast strains used in this study.

Strain	Genotype	Source
BY4741 (WT)	MAT1a his2Δ1 leu2Δ0 met15Δ0 ura3Δ0	
$eghl\Delta$	BY4741; egh1\Delta::kanMX4	This study
Revertant	egh1Δ, pRS416-EGH1	This study
GFP N-OE	BY4741; TEFp-yeGFP-EGH1::natNT2	This study
GFP C	BY4741; EGH1-yeGFP::kanMX4	This study
GFP C-OE	BY4741; TEFp-EGH1-yeGFP::natNT2,kanMX4	This study
ugt51∆	BY4741; <i>ugt51</i> Δ:: <i>kanMX4</i>	This study
ugt $51\Delta$ egh $1\Delta$	BY4741; ugt51Δ::kanMX4, egh1Δ::hphMX4	This study

TABLE 3-2. Oligonucleotide primers used in this study.

Oligonucleotide	Sequence (5'-3')	Purpose	
YIR007W-IF-S	TCGAAGGTAGGCATATGCCTGCCAAAATACACATT		
	TC	Ei	
YIR007W-IF-A2	GATTACCTATCTAGACTGCAGTTAGCTGATAACGC	Expression	
	ATTCCG		
delYIR007W-S1	TTTTTCTTTCGTACCTAAATTGTTTGAATTTAATAA		
	GAACAGATCATATGCGTACGCTGCAGGTCGAC		
delYIR007W-S2	TGTATATATATATATGACTACTATAGCTTTTGGT		
	TCAATTTTGTTTAATCGATGAATTCGAGCTCG	Disruption &	
YIR007W-S4	CCATCTTTATCGCAAAACTGACCGTCTGCAGAAATG	GFP fusion	
1 IK00 / W - 54	TGTATTTTGGCAGGCATCGATGAATTCTCTGTCG	for EGH1	
YIR007W-GFP127-S	CCCCTGGAAGTGACACTTCGAATGACTTACCAGCG	101 <i>L</i> 0111	
11K00/W-GFF12/-S	GAATGCGTTATCAGCGGTGACGGTGCTGGTTTA		
YIR007W-GFP127-A	TGTATATATATATATGACTACTATAGCTTTTGGT		
11K007W-GI1127-A	TCAATTTTTGTTTATCGATGAATTCGAGCTCG		
pRS416/yir007w-IF-S	GCTTGATATCGAATTCAATCGGTTATCGTGAGCA	Revertant	
pRS416/yir007w-IF-A	CGGGCTGCAGGAATTATTGGCTGGACAATCCAAG		
delUGT51-S1	TTCAGTTGCACTTTATGCTTTGGTGAAAATCCGTAT		
de100131-31	AACTTAAAAGAATGCGTACGCTGCAGGTCGAC		
delUGT51-S2	ATGATTAGATGTTACGCTTTTTTATAAAAGTGAGA		
de10G131-82	GTGATACTCGGTTTAATCGATGAATTCGAGCTCG	Disruption	
hnhMV4 S	TGCTAGGATACAGTTCTCACATCACATCCGAACAT	for UGT51	
hphMX4-S	AAACAACCATGGGTAAAAAGCCTGAACTCA		
hphMX4-A	GACAAGTTCTTGAAAACAAGAATCTTTTTATTGTC		
пршугд4-А	AGTACTGATTATTCCTTTGCCCTCGGACGA		

### **CHAPTER 4. GENERAL DISCUSSION**

### GlcCer degrading enzyme in fungi

GlcCer, which is the simplest GSL, comprising ceramide and β-glucose, is hydrolyzed by glucocerebrosidase (136). Four types of glucocerebrosidase have been found in humans and mice: GBA1, a lysosomal acid glucocerebrosidase assigned to GH family 30 (137); GBA2, a bile acid β-glucosidase assigned to GH family 116 (138); GBA3, a non-lysosomal neutral glucocerebrosidase (Klotho-related protein, KLrP) assigned to GH family 1 (139); and lactase phlorizin hydrolase (140). non-mammalian glucocerebrosidases, Paenibacillus sp. β-glucosidase, assigned to GH family 30, and C. neoformans EGCrP1 and EGCrP2, both assigned to GH family 5, were identified (40,141). Paenibacillus sp. appears to possess no GlcCer; thus, the enzyme is likely to participate in the digestion of extracellular GSLs for nutrition. As described in Chapter 1, C. neoformans EGCrP1 is the first glucocerebrosidase to be identified in fungi and is involved in GlcCer quality control, which is related to polysaccharide capsule production (40). In contrast to the strict specificity of EGCrP1, EGCrP2 is a β-glucosidase with a broad specificity for a glycon moieties. However, EG was shown to be an in vivo substrate for EGCrP2 because EG but not GlcCer specifically accumulated in C. neoformans EGCrP2-deletion mutants. Notably, the distribution of the EGCrP1 homologue is restricted in some fungi such as Cryptococcus and Rhizopus, whereas that of EGCrP2 is broad, as shown in Fig. 2-1 in Chapter 2. The author generated egcrp1/egcrp2-double-knockout mutants in this study. However, glucocerebrosidase activity was maintained at neutral pH (Fig. 2-6, Chapter 2), and GlcCer accumulation was not significant even in the double-knockout mutants, indicating the presence of other glucocerebrosidases that are involved in GlcCer catabolism in *C. neoformans*.

# SG-degrading enzyme in fungi and other organisms

SG is the most abundant sterol derivative in many organisms. The SG-degrading enzyme remained unknown for a long time; however, the author and co-workers identified EGCrP2 as the SG-degrading enzyme in *C. neoformans*. This enzyme was likely to be conserved in fungi, including the four popular deep-seated mycoses *Candida albicans*, *Aspergillus fumigatus*, *Rhizopus oryzae*, and *C. neoformans*. However, the SG-degrading enzymes of plants and mammals remain unknown because EGCrP2 homologues have not yet been identified in plant and mammalian genome databases.

The discovery of EGCrP2, a missing link in SG metabolism, reveals the whole picture of SG metabolism in fungi (Fig. GD-1).

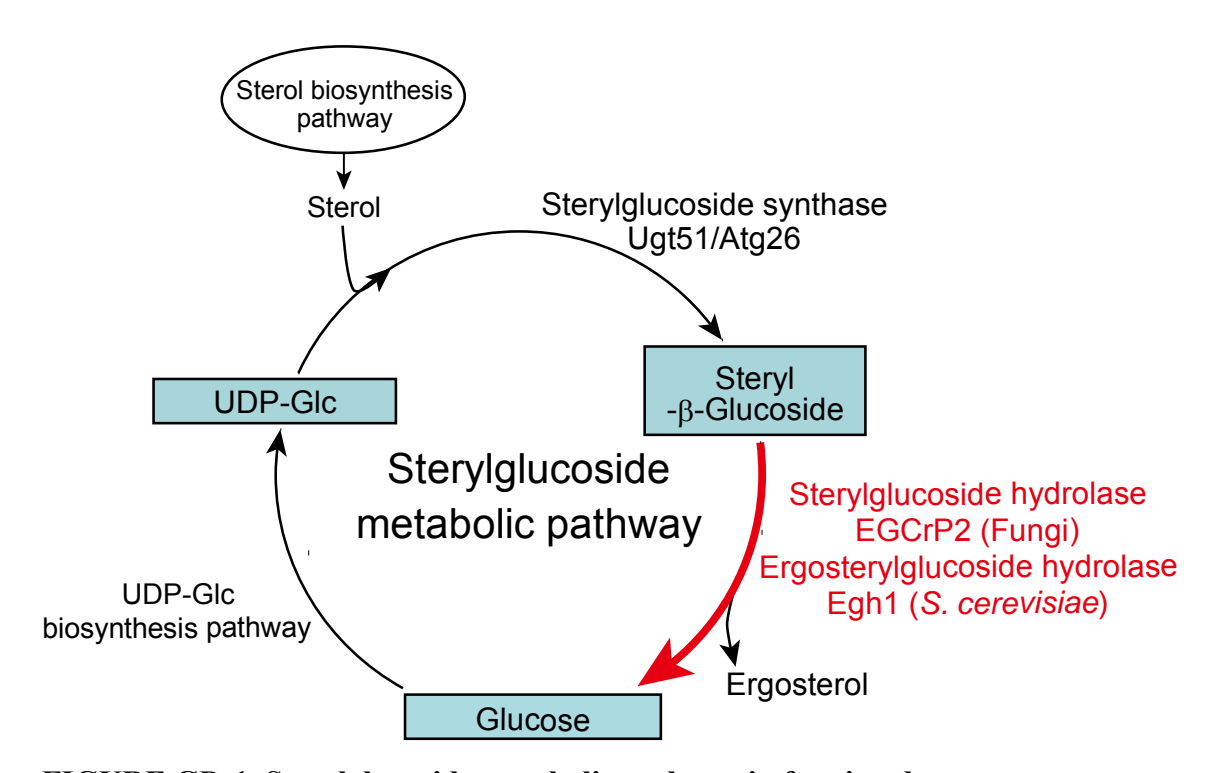


FIGURE GD-1. Sterylglucoside metabolic pathway in fungi and yeast.

# The localization and biological functions of SG

The localization of SG, a stress-inducible biological lipid, remains ambiguous in fungi. One potential reason is the lower amount of SG compared with that of sterols and phosphoglycerolipids. In addition, no good tools such as specific monoclonal antibody or toxins specific to SG are available at present to detect SG in vivo. However, biochemical analysis after the extraction of SG from cells revealed that SG is present in lipid rafts (a Triton X-100 insoluble membrane fraction) in plants, whereas fungal SG is not present in the raft fraction (142,143). This suggests that the localization of SG may differ depending on the organism as well as on the cell type. In this study, the author showed that EG accumulated in the vacuole fractions in *C. neoformans* EGCrP2-deletion mutants (See Chapter 2). This may indicate that EG catabolism occurs in vacuoles in the mutants; however, this does not rule out the possibility that EG is catabolized in a different organelle in wild type *C. neoformans*.

In *A. thaliana*, SG was reported to function in the trafficking of lipid precursors such as suberin and cutin and as a glucose acceptor for cellulose (66,144). SG is required for pexophagy in *P. pastoris* and *C. orbiculare* but not in *S. cerevisiae* (59,69). Interestingly, however, SG is commonly induced in mammals, plants and fungi by stress such as heat shock stress (50,64,65). Identifying the intracellular localization of SG is necessary to understand the physiological functions of SG *in vivo*.

The morphology of vacuoles was completely different in *C. neoformans and S. cerevisiae* upon disrupting the gene encoding the SG-degrading enzyme (Table. GD-1); vacuoles were enlarged in the *C. neoformans* mutants and fragmented in the *S. cerevisiae* mutants. This result suggests that the lack of the SG-degrading enzyme leads to

dysfunction of the vacuolar fission and fusion processes in C. neoformans and S. cerevisiae, respectively. In addition, severe effects on cell growth and cell budding were observed in the C. neoformans mutants; however, these abnormalities were not detected in the S. cerevisiae mutants. The author considered that this difference could stem from the difference in the SG content in these organisms. The SG content of C. neoformans is  $\geq 10$  times higher than that of S. cerevisiae under normal cultivation conditions.

TABLE GD-1. Vacuole morphology of C. neoformans and S. cerevisiae.

4	C. neoformans	S. cerevisiae	
SG degrading enzyme	EGCrP2	Egh1	
Substrate specificity	various β-glusodies		
Vacuole morphology	(middle log phase) enlargement	WT KO  (Stationary phase) fragmentation	
Vacuole formation	Fusion ←→ Fission	Fusion $\longrightarrow$ Fission	
Growth of KO	growth defect at late log phase	unchanged	
SG accumulation	very high	low	

# New target of antifungal drugs

The drugs that are commonly used to treat deep-seated mycoses are categorized into 4 groups: polyene antibiotics (e.g., amphotericin B), azole antibiotics (e.g., imidazoles and triazoles), fluoropyrimidines (e.g., flucytosine), and candins (e.g., caspofungin and micafungin). Each of these drugs has merits and demerits. The action of amphotericin B against pathogenic fungi is very strong but is also associated with a relatively high number of side effects. Azole antibiotics inhibit the ergosterol biosynthesis of fungi. Flucytosine is effective for both *Cryptococcus* and *Candida*; however, it cannot be used to treat other deep-seated mycoses. Furthermore, antibiotic-resistant fungi have appeared (145). Candins, which are drugs that inhibit  $\beta$ -1,3-glucan synthase, are widely used to treat systemic infections caused by *Candida* and *Aspergillus* because of their high potency and low toxicity to humans; however, these drugs are not effective against *Cryptococcus*.

Recently, new targets for the development of anti-cryptococcal drugs have been proposed. For example, Do *et al* and Kretschmer *et al* indicated the usefulness of targeting fungal-specific amino acid synthase (146) and fungal fatty acid/lipid metabolism (147), respectively. To develop specific anti-fungal drugs with wide spectra, the identification of new drug targets is still required. In this context, EGCrP2 could be a potent and promising target of anti-fungal drugs because EGCrP2 is widely distributed in fungi, including four major deep-seated mycoses, but not in humans (Fig. GD-2). However, the physiological effects of disrupting EGCrP2 in pathogenic fungi other than *C. neoformans* remain to be assessed.

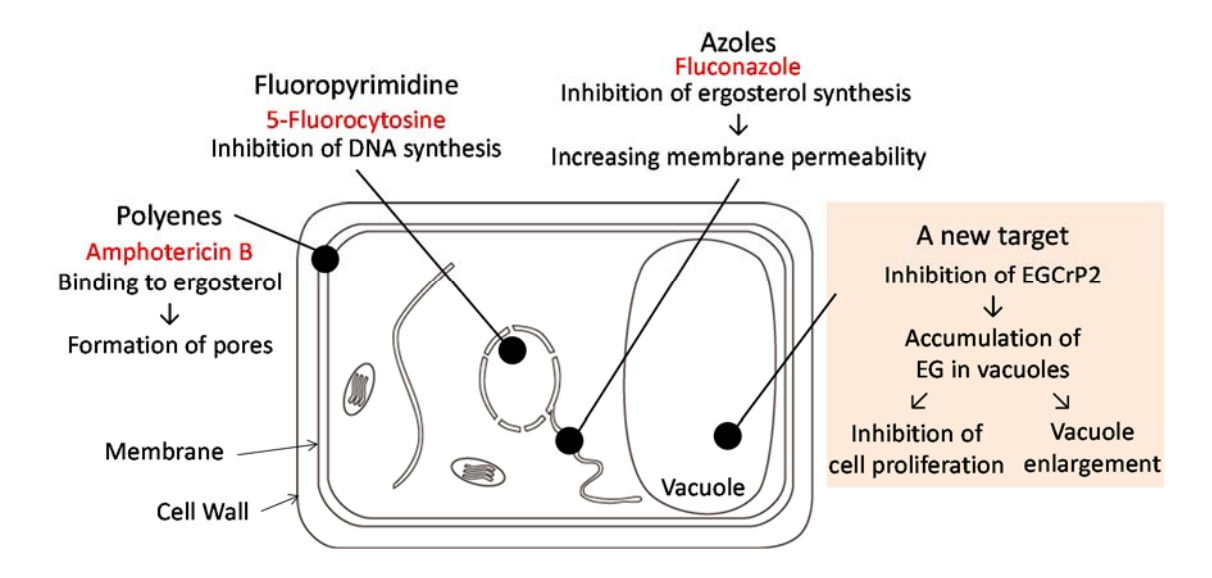


FIGURE GD-2. New targets of antifungal drug.

## **REFERENCES**

- 1. Park, B. J., Wannemuehler, K. A., Marston, B. J., Govender, N., Pappas, P. G., and Chiller, T. A. (2009) Estimation of the current global burden of cryptococcal meningitis among persons living with HIV/AIDS. *Aids* **23**, 525-530
- 2. Srikanta, D., Santiago-Tirado, F. H., and Doering, T. L. (2014) *Cryptococcus neoformans*: historical curiosity to modern pathogen. *Yeast* 31, 47-60
- 3. Astronomo, R. D., and Burton, D. R. (2010) Carbohydrate vaccines: developing sweet solutions to sticky situations? *Nat. Rev. Drug Discov.* **9**, 308-324
- 4. Doering, T. L. (2009) How sweet it is! Cell wall biogenesis and polysaccharide capsule formation in *Cryptococcus neoformans*. *Annu. Rev. Microbiol.* **63**, 223-247
- 5. Kozel, T. R., and Gotschlich, E. C. (1982) The capsule of *cryptococcus neoformans* passively inhibits phagocytosis of the yeast by macrophages. *J. Immunol.* **129**, 1675-1680
- 6. Feldmesser, M., Kress, Y., Novikoff, P., and Casadevall, A. (2000) *Cryptococcus neoformans* is a facultative intracellular pathogen in murine pulmonary infection. *Infect. Immun.* **68**, 4225-4237
- 7. Lee, S. C., Kress, Y., Zhao, M. L., Dickson, D. W., and Casadevall, A. (1995) Cryptococcus neoformans survive and replicate in human microglia. Lab. Invest. 73, 871-879
- 8. Alvarez, M., and Casadevall, A. (2007) Cell-to-cell spread and massive vacuole formation after *Cryptococcus neoformans* infection of murine macrophages. *BMC Immunol.* **8**, 16
- 9. Ma, H., Croudace, J. E., Lammas, D. A., and May, R. C. (2006) Expulsion of live pathogenic yeast by macrophages. *Curr. Biol.* **16**, 2156-2160
- 10. Kwon-Chung, K. J., and Varma, A. (2006) Do major species concepts support one, two or more species within *Cryptococcus neoformans? FEMS Yeast Res.* **6**, 574-587
- 11. Litvintseva, A. P., Thakur, R., Reller, L. B., and Mitchell, T. G. (2005) Prevalence of clinical isolates of *Cryptococcus gattii* serotype C among patients with AIDS in Sub-Saharan Africa. *J. Infect. Dis.* **192**, 888-892
- Morgan, J., McCarthy, K. M., Gould, S., Fan, K., Arthington-Skaggs, B., Iqbal, N., Stamey, K., Hajjeh, R. A., and Brandt, M. E. (2006) *Cryptococcus gattii* infection: characteristics and epidemiology of cases identified in a South African province with high HIV seroprevalence, 2002-2004. *Clin. Infect. Dis.* 43, 1077-1080
- 13. Sorrell, T. C. (2001) Cryptococcus neoformans variety gattii. Med. Mycol. 39, 155-168
- 14. Fraser, J. A., Giles, S. S., Wenink, E. C., Geunes-Boyer, S. G., Wright, J. R., Diezmann,

- S., Allen, A., Stajich, J. E., Dietrich, F. S., Perfect, J. R., and Heitman, J. (2005) Same-sex mating and the origin of the Vancouver Island *Cryptococcus gattii* outbreak. *Nature* **437**, 1360-1364
- 15. Fyfe, M., MacDougall, L., Romney, M., Starr, M., Pearce, M., Mak, S., Mithani, S., and Kibsey, P. (2008) *Cryptococcus gattii* infections on Vancouver Island, British Columbia, Canada: emergence of a tropical fungus in a temperate environment. *Can. Commun. Dis. Rep.* **34**. 1-12
- Hoang, L. M., Maguire, J. A., Doyle, P., Fyfe, M., and Roscoe, D. L. (2004)
   Cryptococcus neoformans infections at Vancouver Hospital and Health Sciences Centre (1997-2002): epidemiology, microbiology and histopathology. J. Med. Microbiol. 53, 935-940
- 17. Ngamskulrungroj, P., Price, J., Sorrell, T., Perfect, J. R., and Meyer, W. (2011) Cryptococcus gattii virulence composite: candidate genes revealed by microarray analysis of high and less virulent Vancouver island outbreak strains. PLoS One 6, e16076
- 18. Balkis, M. M., Leidich, S. D., Mukherjee, P. K., and Ghannoum, M. A. (2002) Mechanisms of fungal resistance: an overview. *Drugs* **62**, 1025-1040
- 19. Lingwood, D., and Simons, K. (2010) Lipid rafts as a membrane-organizing principle. *Science* **327**, 46-50
- 20. Furukawa, K., Tokuda, N., Okuda, T., Tajima, O., and Furukawa, K. (2004) Glycosphingolipids in engineered mice: insights into function. *Semin. Cell Dev. Biol.* **15**, 389-396
- 21. Pettus, B. J., Chalfant, C. E., and Hannun, Y. A. (2002) Ceramide in apoptosis: an overview and current perspectives. *Biochim. Biophys. Acta* **1585**, 114-125
- 22. Proia, R. L. (2003) Glycosphingolipid functions: insights from engineered mouse models. *Philos. Trans. R. Soc. Lond. B Biol. Sci.* **358**, 879-883
- 23. Watterson, K. R., Ratz, P. H., and Spiegel, S. (2005) The role of sphingosine-1-phosphate in smooth muscle contraction. *Cell. Signal.* 17, 289-298
- Eierhoff, T., Bastian, B., Thuenauer, R., Madl, J., Audfray, A., Aigal, S., Juillot, S., Rydell, G. E., Muller, S., de Bentzmann, S., Imberty, A., Fleck, C., and Romer, W. (2014) A lipid zipper triggers bacterial invasion. *Proc. Natl. Acad. Sci. U. S. A.* 111, 12895-12900
- 25. Matmati, N., and Hannun, Y. A. (2008) Thematic review series: sphingolipids. ISC1 (inositol phosphosphingolipid-phospholipase C), the yeast homologue of neutral sphingomyelinases. *J. Lipid Res.* **49**, 922-928
- 26. Xu, X., Bittman, R., Duportail, G., Heissler, D., Vilcheze, C., and London, E. (2001)

- Effect of the structure of natural sterols and sphingolipids on the formation of ordered sphingolipid/sterol domains (rafts). Comparison of cholesterol to plant, fungal, and disease-associated sterols and comparison of sphingomyelin, cerebrosides, and ceramide. *J. Biol. Chem.* **276**, 33540-33546
- Kubler, E., Dohlman, H. G., and Lisanti, M. P. (1996) Identification of Triton X-100 insoluble membrane domains in the yeast *Saccharomyces cerevisiae*. Lipid requirements for targeting of heterotrimeric G-protein subunits. *J. Biol. Chem.* 271, 32975-32980
- 28. Bagnat, M., Keranen, S., Shevchenko, A., Shevchenko, A., and Simons, K. (2000) Lipid rafts function in biosynthetic delivery of proteins to the cell surface in yeast. *Proc. Natl. Acad. Sci. U. S. A.* **97**, 3254-3259
- 29. Dickson, R. C., Sumanasekera, C., and Lester, R. L. (2006) Functions and metabolism of sphingolipids in *Saccharomyces cerevisiae*. *Prog. Lipid Res.* **45**, 447-465
- 30. Simons, K., and Ikonen, E. (1997) Functional rafts in cell membranes. *Nature* **387**, 569-572
- 31. Rhome, R., McQuiston, T., Kechichian, T., Bielawska, A., Hennig, M., Drago, M., Morace, G., Luberto, C., and Del Poeta, M. (2007) Biosynthesis and immunogenicity of glucosylceramide in *Cryptococcus neoformans* and other human pathogens. *Eukaryot*. *Cell* 6, 1715-1726
- 32. Mitchell, A. G., and Martin, C. E. (1997) Fahlp, a *Saccharomyces cerevisiae* cytochrome *b5* fusion protein, and its *Arabidopsis thaliana* homolog that lacks the cytochrome *b5* domain both function in the alpha-hydroxylation of sphingolipid-associated very long chain fatty acids. *J. Biol. Chem.* **272**, 28281-28288
- 33. Hama, H. (2010) Fatty acid 2-hydroxylation in mammalian sphingolipid biology. *Biochim. Biophys. Acta* **1801**, 405-414
- Grilley, M. M., Stock, S. D., Dickson, R. C., Lester, R. L., and Takemoto, J. Y. (1998)
   Syringomycin action gene SYR2 is essential for sphingolipid 4-hydroxylation in Saccharomyces cerevisiae. J. Biol. Chem. 273, 11062-11068
- 35. Ternes, P., Franke, S., Zahringer, U., Sperling, P., and Heinz, E. (2002) Identification and characterization of a sphingolipid Δ4-desaturase family. *J. Biol. Chem.* **277**, 25512-25518
- 36. Oura, T., and Kajiwara, S. (2008) Disruption of the sphingolipid Δ8-desaturase gene causes a delay in morphological changes in *Candida albicans*. *Microbiology* **154**, 3795-3803
- 37. Ternes, P., Sperling, P., Albrecht, S., Franke, S., Cregg, J. M., Warnecke, D., and Heinz, E. (2006) Identification of fungal sphingolipid C9-methyltransferases by phylogenetic

- profiling. J. Biol. Chem. 281, 5582-5592
- 38. Singh, A., Wang, H., Silva, L. C., Na, C., Prieto, M., Futerman, A. H., Luberto, C., and Del Poeta, M. (2012) Methylation of glycosylated sphingolipid modulates membrane lipid topography and pathogenicity of *Cryptococcus neoformans*. *Cell. Microbiol.* **14**, 500-516
- 39. Oura, T., and Kajiwara, S. (2010) *Candida albicans* sphingolipid C9-methyltransferase is involved in hyphal elongation. *Microbiology* **156**, 1234-1243
- 40. Ishibashi, Y., Ikeda, K., Sakaguchi, K., Okino, N., Taguchi, R., and Ito, M. (2012) Quality Control of Fungus-specific Glucosylceramide in *Cryptococcus neoformans* by Endoglycoceramidase-related Protein 1 (EGCrP1). *J. Biol. Chem.* **287**, 368-381
- 41. Levery, S. B., Momany, M., Lindsey, R., Toledo, M. S., Shayman, J. A., Fuller, M., Brooks, K., Doong, R. L., Straus, A. H., and Takahashi, H. K. (2002) Disruption of the glucosylceramide biosynthetic pathway in *Aspergillus nidulans* and *Aspergillus fumigatus* by inhibitors of UDP-Glc: ceramide glucosyltransferase strongly affects spore germination, cell cycle, and hyphal growth. *FEBS Lett.* **525**, 59-64
- 42. Pinto, M. R., Rodrigues, M. L., Travassos, L. R., Haido, R. M., Wait, R., and Barreto-Bergter, E. (2002) Characterization of glucosylceramides in *Pseudallescheria boydii* and their involvement in fungal differentiation. *Glycobiology* **12**, 251-260
- 43. Rodrigues, M. L., Travassos, L. R., Miranda, K. R., Franzen, A. J., Rozental, S., de Souza, W., Alviano, C. S., and Barreto-Bergter, E. (2000) Human antibodies against a purified glucosylceramide from *Cryptococcus neoformans* inhibit cell budding and fungal growth. *Infect. Immun.* **68**, 7049-7060
- 44. Thevissen, K., Warnecke, D. C., Francois, I. E., Leipelt, M., Heinz, E., Ott, C., Zahringer, U., Thomma, B. P., Ferket, K. K., and Cammue, B. P. (2004) Defensins from insects and plants interact with fungal glucosylceramides. *J. Biol. Chem.* **279**, 3900-3905
- 45. Rittershaus, P. C., Kechichian, T. B., Allegood, J. C., Merrill, A. H., Hennig, M., Luberto, C., and Del Poeta, M. (2006) Glucosylceramide synthase is an essential regulator of pathogenicity of *Cryptococcus neoformans*. *J. Clin. Invest.* **116**, 1651-1659
- 46. Saito, K., Takakuwa, N., Ohnishi, M., and Oda, Y. (2006) Presence of glucosylceramide in yeast and its relation to alkali tolerance of yeast. *Appl. Microbiol. Biotechnol.* **71**, 515-521
- Rodrigues, M. L., Shi, L., Barreto-Bergter, E., Nimrichter, L., Farias, S. E., Rodrigues,
   E. G., Travassos, L. R., and Nosanchuk, J. D. (2007) Monoclonal antibody to fungal glucosylceramide protects mice against lethal *Cryptococcus neoformans* infection. *Clin. Vaccine Immunol.* 14, 1372-1376

- 48. Leipelt, M., Warnecke, D., Zahringer, U., Ott, C., Muller, F., Hube, B., and Heinz, E. (2001) Glucosylceramide synthases, a gene family responsible for the biosynthesis of glucosphingolipids in animals, plants, and fungi. *J. Biol. Chem.* **276**, 33621-33629
- 49. Grille, S., Zaslawski, A., Thiele, S., Plat, J., and Warnecke, D. (2010) The functions of steryl glycosides come to those who wait: Recent advances in plants, fungi, bacteria and animals. *Prog. Lipid Res.* **49**, 262-288
- 50. Kunimoto, S., Kobayashi, T., Kobayashi, S., and Murakami-Murofushi, K. (2000) Expression of cholesteryl glucoside by heat shock in human fibroblasts. *Cell Stress Chaperones* **5**, 3-7
- 51. Power, F. B., and Salway, A. H. (1913) The identification of ipuranol and some allied compounds as phytosterol glucosides. *J. Chem. Soc.* **103**, 399-406
- 52. Sakaki, T., Zahringer, U., Warnecke, D. C., Fahl, A., Knogge, W., and Heinz, E. (2001) Sterol glycosides and cerebrosides accumulate in *Pichia pastoris*, *Rhynchosporium secalis* and other fungi under normal conditions or under heat shock and ethanol stress. *Yeast* 18, 679-695
- 53. Hirai, Y., Haque, M., Yoshida, T., Yokota, K., Yasuda, T., and Oguma, K. (1995) Unique cholesteryl glucosides in *Helicobacter pylori*: composition and structural analysis. *J. Bacteriol.* **177**, 5327-5333
- 54. Warnecke, D., Erdmann, R., Fahl, A., Hube, B., Muller, F., Zank, T., Zahringer, U., and Heinz, E. (1999) Cloning and functional expression of UGT genes encoding sterol glucosyltransferases from *Saccharomyces cerevisiae*, *Candida albicans*, *Pichia pastoris*, and *Dictyostelium discoideum*. *J. Biol. Chem.* **274**, 13048-13059
- 55. Warnecke, D. C., and Heinz, E. (1994) Purification of a membrane-Bound UDP-glucose:sterol β-D-glucosyltransferase based on its solubility in diethyl ether. *Plant Physiol.* **105**, 1067-1073
- Warnecke, D. C., Baltrusch, M., Buck, F., Wolter, F. P., and Heinz, E. (1997) UDP-glucose:sterol glucosyltransferase: cloning and functional expression in *Escherichia coli. Plant Mol. Biol.* 35, 597-603
- 57. Ullmann, P., Ury, A., Rimmele, D., Benveniste, P., and Bouvier-Nave, P. (1993) UDP-glucose sterol β-D-glucosyltransferase, a plasma membrane-bound enzyme of plants: enzymatic properties and lipid dependence. *Biochimie* **75**, 713-723
- 58. Oku, M., Warnecke, D., Noda, T., Muller, F., Heinz, E., Mukaiyama, H., Kato, N., and Sakai, Y. (2003) Peroxisome degradation requires catalytically active sterol glucosyltransferase with a GRAM domain. *EMBO J.* **22**, 3231-3241
- 59. Sakai, Y., Oku, M., van der Klei, I. J., and Kiel, J. A. (2006) Pexophagy: autophagic degradation of peroxisomes. *Biochim. Biophys. Acta* **1763**, 1767-1775

- 60. Yamashita, S., Oku, M., Wasada, Y., Ano, Y., and Sakai, Y. (2006) PI4P-signaling pathway for the synthesis of a nascent membrane structure in selective autophagy. *J. Cell Biol.* **173**, 709-717
- 61. Cao, Y., and Klionsky, D. J. (2007) Atg26 is not involved in autophagy-related pathways in *Saccharomyces cerevisiae*. *Autophagy* **3**, 17-20
- Stasyk, O. V., Nazarko, T. Y., Stasyk, O. G., Krasovska, O. S., Warnecke, D., Nicaud, J. M., Cregg, J. M., and Sibirny, A. A. (2003) Sterol glucosyltransferases have different functional roles in *Pichia pastoris* and *Yarrowia lipolytica*. *Cell Biol. Int.* 27, 947-952
- 63. Kunimoto, S., Murofushi, W., Kai, H., Ishida, Y., Uchiyama, A., Kobayashi, T., Kobayashi, S., Murofushi, H., and Murakami-Murofushi, K. (2002) Steryl glucoside is a lipid mediator in stress-responsive signal transduction. *Cell Struct. Funct.* 27, 157-162
- 64. Murakami-Murofushi, K., Nishikawa, K., Hirakawa, E., and Murofushi, H. (1997) Heat stress induces a glycosylation of membrane sterol in myxoamoebae of a true slime mold, *Physarum polycephalum. J. Biol. Chem.* **272**, 486-489
- Kunimoto, S., Murofushi, W., Yamatsu, I., Hasegawa, Y., Sasaki, N., Kobayashi, S.,
   Kobayashi, T., Murofushi, H., and Murakami-Murofushi, K. (2003) Cholesteryl glucoside-induced protection against gastric ulcer. *Cell Struct. Funct.* 28, 179-186
- 66. DeBolt, S., Scheible, W. R., Schrick, K., Auer, M., Beisson, F., Bischoff, V., Bouvier-Nave, P., Carroll, A., Hematy, K., Li, Y., Milne, J., Nair, M., Schaller, H., Zemla, M., and Somerville, C. (2009) Mutations in UDP-glucose:sterol glucosyltransferase in *Arabidopsis* cause transparent testa phenotype and suberization defect in seeds. *Plant Physiol.* 151, 78-87
- 67. Stucky, D. F., Arpin, J. C., and Schrick, K. (2015) Functional diversification of two UGT80 enzymes required for steryl glucoside synthesis in *Arabidopsis. J. Exp. Bot.* **66**, 189-201
- 68. Kim, Y. K., Wang, Y. H., Liu, Z. M., and Kolattukudy, P. E. (2002) Identification of a hard surface contact-induced gene in *Colletotrichum gloeosporioides* conidia as a sterol glycosyl transferase, a novel fungal virulence factor. *Plant J.* **30**, 177-187
- 69. Asakura, M., Ninomiya, S., Sugimoto, M., Oku, M., Yamashita, S., Okuno, T., Sakai, Y., and Takano, Y. (2009) Atg26-mediated pexophagy is required for host invasion by the plant pathogenic fungus *Colletotrichum orbiculare*. *Plant Cell* 21, 1291-1304
- Kershaw, M. J., and Talbot, N. J. (2009) Genome-wide functional analysis reveals that infection-associated fungal autophagy is necessary for rice blast disease. *Proc. Natl. Acad. Sci. U. S. A.* 106, 15967-15972
- 71. Wunder, C., Churin, Y., Winau, F., Warnecke, D., Vieth, M., Lindner, B., Zahringer, U., Mollenkopf, H. J., Heinz, E., and Meyer, T. F. (2006) Cholesterol glucosylation

- promotes immune evasion by Helicobacter pylori. Nat. Med. 12, 1030-1038
- 72. Kalinowska, M., and Wojciechowski, Z. A. (1978) Purification and some properties of steryl β-D-glucoside hydrolase from *Sinapis alba* seedlings. *Phytochemistry* **17**, 1533-1537
- 73. Aguirre, A., Peiru, S., Eberhardt, F., Vetcher, L., Cabrera, R., and Menzella, H. (2014) Enzymatic hydrolysis of steryl glucosides, major contaminants of vegetable oil-derived biodiesel. *Appl. Microbiol. Biotechnol.* **98**, 4033-4040
- 74. Klionsky, D. J., Herman, P. K., and Emr, S. D. (1990) The fungal vacuole: composition, function, and biogenesis. *Microbiol. Rev.* **54**, 266-292
- 75. Weber, R. W. S. (2002) Vacuoles and the fungal lifestyle. *Mycologist* **16**, 10-20
- 76. Li, S. C., and Kane, P. M. (2009) The yeast lysosome-like vacuole: endpoint and crossroads. *Biochim. Biophys. Acta* **1793**, 650-663
- 77. Richards, A., Gow, N. A., and Veses, V. (2012) Identification of vacuole defects in fungi. *J. Microbiol. Methods* **91**, 155-163
- 78. Mellman, I., Fuchs, R., and Helenius, A. (1986) Acidification of the endocytic and exocytic pathways. *Annu. Rev. Biochem.* **55**, 663-700
- 79. Preston, R. A., Murphy, R. F., and Jones, E. W. (1989) Assay of vacuolar pH in yeast and identification of acidification-defective mutants. *Proc. Natl. Acad. Sci. U. S. A.* **86**, 7027-7031
- 80. Yamashiro, C. T., Kane, P. M., Wolczyk, D. F., Preston, R. A., and Stevens, T. H. (1990) Role of vacuolar acidification in protein sorting and zymogen activation: a genetic analysis of the yeast vacuolar proton-translocating ATPase. *Mol. Cell. Biol.* **10**, 3737-3749
- 81. Plant, P. J., Manolson, M. F., Grinstein, S., and Demaurex, N. (1999) Alternative mechanisms of vacuolar acidification in H<sup>+</sup>-ATPase-deficient yeast. *J. Biol. Chem.* **274**, 37270-37279
- 82. Martinez-Munoz, G. A., and Kane, P. (2008) Vacuolar and plasma membrane proton pumps collaborate to achieve cytosolic pH homeostasis in yeast. *J. Biol. Chem.* **283**, 20309-20319
- 83. Kane, P. M. (2006) The where, when, and how of organelle acidification by the yeast vacuolar H<sup>+</sup>-ATPase. *Microbiol. Mol. Biol. Rev.* **70**, 177-191
- 84. Klionsky, D. J., Nelson, H., and Nelson, N. (1992) Compartment acidification is required for efficient sorting of proteins to the vacuole in *Saccharomyces cerevisiae*. *J. Biol. Chem.* **267**, 3416-3422
- 85. Klionsky, D. J., Nelson, H., Nelson, N., and Yaver, D. S. (1992) Mutations in the yeast vacuolar ATPase result in the mislocalization of vacuolar proteins. *J. Exp. Biol.* **172**,

- 83-92
- 86. Ohsumi, Y., and Anraku, Y. (1981) Active transport of basic amino acids driven by a proton motive force in vacuolar membrane vesicles of *Saccharomyces cerevisiae*. *J. Biol. Chem.* **256**, 2079-2082
- 87. Booth, J. W., and Guidotti, G. (1997) Phosphate transport in yeast vacuoles. *J. Biol. Chem.* **272**, 20408-20413
- 88. MacDiarmid, C. W., Milanick, M. A., and Eide, D. J. (2002) Biochemical properties of vacuolar zinc transport systems of *Saccharomyces cerevisiae*. *J. Biol. Chem.* **277**, 39187-39194
- 89. Poltermann, S., Nguyen, M., Gunther, J., Wendland, J., Hartl, A., Kunkel, W., Zipfel, P. F., and Eck, R. (2005) The putative vacuolar ATPase subunit Vma7p of *Candida albicans* is involved in vacuole acidification, hyphal development and virulence. *Microbiology* 151, 1645-1655
- 90. Peters, C., Bayer, M. J., Buhler, S., Andersen, J. S., Mann, M., and Mayer, A. (2001) Trans-complex formation by proteolipid channels in the terminal phase of membrane fusion. *Nature* **409**, 581-588
- 91. Bayer, M. J., Reese, C., Buhler, S., Peters, C., and Mayer, A. (2003) Vacuole membrane fusion: V<sub>0</sub> functions after trans-SNARE pairing and is coupled to the Ca<sup>2+</sup>-releasing channel. *J. Cell Biol.* **162**, 211-222
- 92. Baars, T. L., Petri, S., Peters, C., and Mayer, A. (2007) Role of the V-ATPase in regulation of the vacuolar fission-fusion equilibrium. *Mol. Biol. Cell* **18**, 3873-3882
- 93. Kato, M., and Wickner, W. (2001) Ergosterol is required for the Sec18/ATP-dependent priming step of homotypic vacuole fusion. *EMBO J.* **20**, 4035-4040
- 94. Fratti, R. A., Jun, Y., Merz, A. J., Margolis, N., and Wickner, W. (2004) Interdependent assembly of specific regulatory lipids and membrane fusion proteins into the vertex ring domain of docked vacuoles. *J. Cell Biol.* **167**, 1087-1098
- 95. Weisman, L. S. (2006) Organelles on the move: insights from yeast vacuole inheritance. *Nat. Rev. Mol. Cell Biol.* 7, 243-252
- 96. Efe, J. A., Botelho, R. J., and Emr, S. D. (2005) The Fab1 phosphatidylinositol kinase pathway in the regulation of vacuole morphology. *Curr. Opin. Cell Biol.* **17**, 402-408
- 97. Efe, J. A., Botelho, R. J., and Emr, S. D. (2007) Atg18 regulates organelle morphology and Fab1 kinase activity independent of its membrane recruitment by phosphatidylinositol 3,5-bisphosphate. *Mol. Biol. Cell* **18**, 4232-4244
- 98. Tamura, N., Oku, M., Ito, M., Noda, N. N., Inagaki, F., and Sakai, Y. (2013) Atg18 phosphoregulation controls organellar dynamics by modulating its phosphoinositide-binding activity. *J. Cell Biol.* **202**, 685-698

- 99. Byrnes, E. J., 3rd, Bildfell, R. J., Frank, S. A., Mitchell, T. G., Marr, K. A., and Heitman, J. (2009) Molecular evidence that the range of the Vancouver Island outbreak of *Cryptococcus gattii* infection has expanded into the Pacific Northwest in the United States. *J. Infect. Dis.* 199, 1081-1086
- 100. Michaelson, L. V., Zauner, S., Markham, J. E., Haslam, R. P., Desikan, R., Mugford, S., Albrecht, S., Warnecke, D., Sperling, P., Heinz, E., and Napier, J. A. (2009) Functional characterization of a higher plant sphingolipid Δ4-desaturase: defining the role of sphingosine and sphingosine-1-phosphate in Arabidopsis. *Plant Physiol.* 149, 487-498
- 101. Ito, M., and Yamagata, T. (1986) A novel glycosphingolipid-degrading enzyme cleaves of the linkage between the oligosaccharide and ceramide of neutral and acidic glycosphingolipids. *J. Biol. Chem.* **261**, 14278-14282
- 102. Ito, M., and Yamagata, T. (1989) Purification and characterization of glycosphingolipid-specific endoglycosidases (endoglycoceramidases) from a mutant strain of *Rhodococcus* sp Evidence for 3 molecular-species of endoglycoceramidase with different specificities. *J. Biol. Chem.* 264, 9510-9519
- 103. Izu, H., Izumi, Y., Kurome, Y., Sano, M., Kondo, A., Kato, I., and Ito, M. (1997) Molecular cloning expression, and sequence analysis of the endoglycoceramidase II gene from *Rhodococcus* species strain M-777. *J. Biol. Chem.* 272, 19846-19850
- 104. Nakagawa, T., Tani, M., Kita, K., and Ito, M. (1999) Preparation of fluorescence-labeled GM1 and sphingomyelin by the reverse hydrolysis reaction of sphingolipid ceramide *N*-deacylase as substrates for assay of sphingolipid-degrading enzymes and for detection of sphingolipid-binding proteins. *J. Biochem.* **126**, 604-611
- Laemmli, U. K. (1970) Cleavage of structural proteins during assembly of head of Bacteriophage T4. *Nature* 227, 680-685
- 106. Hayashi, Y., Zama, K., Abe, E., Okino, N., Inoue, T., Ohno, K., and Ito, M. (2008) A sensitive and reproducible fluorescent-based HPLC assay to measure the activity of acid as well as neutral β-glucocerebrosidases. *Anal. Biochem.* **383**, 122-129
- 107. Kim, M. S., Kim, S. Y., Yoon, J. K., Lee, Y. W., and Bahn, Y. S. (2009) An efficient gene-disruption method in *Cryptococcus neoformans* by double-joint PCR with NAT-split markers. *Biochem. Biophys. Res. Commun.* **390**, 983-988
- 108. Cox, G. M., Rude, T. H., Dykstra, C. C., and Perfect, J. R. (1995) The actin gene from *Cryptococcus neoformans*: structure and phylogenetic analysis. *J. Med. Vet. Mycol.* **33**, 261-266
- 109. Perfect, J. R., Rude, T. H., Penning, L. M., and Johnson, S. A. (1992) Cloning the *Cryptococcus neoformans TRP1* gene by complementation in *Saccharomyces cerevisiae*. *Gene* 122, 213-217

- 110. McDade, H. C., and Cox, G. M. (2001) A new dominant selectable marker for use in *Cryptococcus neoformans. Med. Mycol.* **39**, 151-154
- Davidson, R. C., Cruz, M. C., Sia, R. A. L., Allen, B., Alspaugh, J. A., and Heitman, J.
   (2000) Gene disruption by biolistic transformation in serotype D strains of Cryptococcus neoformans. Fungal Genet. Biol. 29, 38-48
- 112. Bligh, E. G., and Dyer, W. J. (1959) A rapid method of total lipid extraction and purification. *Can. J. Biochem. Physiol.* **37**, 911-917
- 113. Cabrera, M., and Ungermann, C. (2008) Purification and *in vitro* analysis of yeast vacuoles. *Methods Enzymol.* **451**, 177-196
- 114. Zinser, E., Paltauf, F., and Daum, G. (1993) Sterol composition of yeast organelle membranes and subcellular distribution of enzymes involved in sterol metabolism. *J. Bacteriol.* 175, 2853-2858
- 115. Sakon, J., Adney, W. S., Himmel, M. E., Thomas, S. R., and Karplus, P. A. (1996) Crystal structure of thermostable family 5 endocellulase E1 from *Acidothermus cellulolyticus* in complex with cellotetraose. *Biochemistry* **35**, 10648-10660
- 116. Idnurm, A., Warnecke, D. C., Heinz, E., and Howlett, B. J. (2003) Characterisation of neutral trehalase and UDP-glucose: sterol glucosyltransferase genes from the plant pathogenic fungus *Leptosphaeria maculans*. *Physiol. Mol. Plant Pathol.* 62, 305-313
- 117. Harrison, T. S., Chen, J., Simons, E., and Levitz, S. M. (2002) Determination of the pH of the *Cryptococcus neoformans* vacuole. *Med. Mycol.* **40**, 329-332
- 118. Cornet, M., Bidard, F., Schwarz, P., Da Costa, G., Blanchin-Roland, S., Dromer, F., and Gaillardin, C. (2005) Deletions of endocytic components VPS28 and VPS32 affect growth at alkaline pH and virulence through both RIM101-dependent and RIM101-independent pathways in *Candida albicans*. *Infect. Immun.* **73**, 7977-7987
- Johnston, D. A., Eberle, K. E., Sturtevant, J. E., and Palmer, G. E. (2009) Role for endosomal and vacuolar GTPases in *Candida albicans* pathogenesis. *Infect. Immun.* 77, 2343-2355
- 120. Franke, K., Nguyen, M., Hartl, A., Dahse, H. M., Vogl, G., Wurzner, R., Zipfel, P. F., Kunkel, W., and Eck, R. (2006) The vesicle transport protein Vac1p is required for virulence of *Candida albicans*. *Microbiology* **152**, 3111-3121
- 121. Zhang, Y. Q., and Rao, R. (2012) The V-ATPase as a Target for Antifungal Drugs. *Curr. Protein. Pept. Sc.* **13**, 134-140
- 122. Saitou, N., and Nei, M. (1987) The neighbor-joining method: a new method for reconstructing phylogenetic trees. *Mol. Biol. Evol.* **4**, 406-425
- 123. Thompson, J. D., Higgins, D. G., and Gibson, T. J. (1994) CLUSTAL W: improving the sensitivity of progressive multiple sequence alignment through sequence weighting,

- position-specific gap penalties and weight matrix choice. *Nucleic Acids Res.* **22**, 4673-4680
- 124. Gouet, P., Robert, X., and Courcelle, E. (2003) ESPript/ENDscript: extracting and rendering sequence and 3D information from atomic structures of proteins. *Nucleic Acids Res.* **31**, 3320-3323
- 125. Caines, M. E. C., Vaughan, M. D., Tarling, C. A., Hancock, S. M., Warren, R. A. J., Withers, S. G., and Strynadka, N. C. J. (2007) Structural and mechanistic analyses of endo-glycoceramidase II, a membrane-associated family 5 glycosidase in the Apo and G<sub>M3</sub> ganglioside-bound forms. *J. Biol. Chem.* **282**, 14300-14308
- 126. Weete, J. D., Abril, M., and Blackwell, M. (2010) Phylogenetic distribution of fungal sterols. *PLoS One* **5**, e10899
- 127. Benveniste, P. (2004) Biosynthesis and accumulation of sterols. *Annu. Rev. Plant Biol.* **55**, 429-457
- 128. Janke, C., Magiera, M. M., Rathfelder, N., Taxis, C., Reber, S., Maekawa, H., Moreno-Borchart, A., Doenges, G., Schwob, E., Schiebel, E., and Knop, M. (2004) A versatile toolbox for PCR-based tagging of yeast genes: new fluorescent proteins, more markers and promoter substitution cassettes. *Yeast* 21, 947-962
- 129. Sheff, M. A., and Thorn, K. S. (2004) Optimized cassettes for fluorescent protein tagging in *Saccharomyces cerevisiae*. *Yeast* 21, 661-670
- 130. Naewbanij, M., Seib, P. A., Burroughs, R., Seitz, L. M., and Chung, D. S. (1984) Determination of ergosterol using thin-layer chromatography and ultraviolet spectroscopy. *Cereal Chem.* **61**, 385-388
- Watanabe, T., Ito, T., Goda, H. M., Ishibashi, Y., Miyamoto, T., Ikeda, K., Taguchi, R., Okino, N., and Ito, M. (2015) Sterylglucoside catabolism in *Cryptococcus neoformans* with endoglycoceramidase-related Protein 2 (EGCrP2), the first steryl-β-glucosidase identified in fungi. *J. Biol. Chem.* **290**, 1005-1019
- 132. Akiyama, H., Kobayashi, S., Hirabayashi, Y., and Murakami-Murofushi, K. (2013) Cholesterol glucosylation is catalyzed by transglucosylation reaction of β-glucosidase 1. *Biochem. Biophys. Res. Commun.* **441**, 838-843
- 133. Mayer, A., Scheglmann, D., Dove, S., Glatz, A., Wickner, W., and Haas, A. (2000) Phosphatidylinositol 4,5-bisphosphate regulates two steps of homotypic vacuole fusion. *Mol. Biol. Cell* 11, 807-817
- 134. Mima, J., Hickey, C. M., Xu, H., Jun, Y., and Wickner, W. (2008) Reconstituted membrane fusion requires regulatory lipids, SNAREs and synergistic SNARE chaperones. *EMBO J.* 27, 2031-2042
- 135. Seeley, E. S., Kato, M., Margolis, N., Wickner, W., and Eitzen, G. (2002) Genomic

- analysis of homotypic vacuole fusion. Mol. Biol. Cell 13, 782-794
- 136. Ishibashi, Y., Kohyama-Koganeya, A., and Hirabayashi, Y. (2013) New insights on glucosylated lipids: metabolism and functions. *Biochim. Biophys. Acta* **1831**, 1475-1485
- 137. Kolter, T., and Sandhoff, K. (2005) Principles of lysosomal membrane digestion: stimulation of sphingolipid degradation by sphingolipid activator proteins and anionic lysosomal lipids. *Annu. Rev. Cell Dev. Biol.* **21**, 81-103
- 138. Matern, H., Boermans, H., Lottspeich, F., and Matern, S. (2001) Molecular cloning and expression of human bile acid β-glucosidase. *J. Biol. Chem.* **276**, 37929-37933
- 139. Hayashi, Y., Okino, N., Kakuta, Y., Shikanai, T., Tani, M., Narimatsu, H., and Ito, M. (2007) Klotho-related protein is a novel cytosolic neutral β-glycosylceramidase. *J. Biol. Chem.* 282, 30889-30900
- 140. Kobayashi, T., and Suzuki, K. (1981) The glycosylceramidase in the murine intestine. Purification and substrate specificity. *J. Biol. Chem.* **256**, 7768-7773
- 141. Sumida, T., Sueyoshi, N., and Ito, M. (2002) Molecular cloning and characterization of a novel glucocerebrosidase of *Paenibacillus* sp TS12. *J. Biochem.* **132**, 237-243
- 142. Siafakas, A. R., Wright, L. C., Sorrell, T. C., and Djordjevic, J. T. (2006) Lipid rafts in *Cryptococcus neoformans* concentrate the virulence determinants phospholipase B1 and Cu/Zn superoxide dismutase. *Eukaryot. Cell* **5**, 488-498
- 143. Laloi, M., Perret, A. M., Chatre, L., Melser, S., Cantrel, C., Vaultier, M. N., Zachowski, A., Bathany, K., Schmitter, J. M., Vallet, M., Lessire, R., Hartmann, M. A., and Moreau, P. (2007) Insights into the role of specific lipids in the formation and delivery of lipid microdomains to the plasma membrane of plant cells. *Plant Physiol.* 143, 461-472
- 144. Peng, L., Kawagoe, Y., Hogan, P., and Delmer, D. (2002) Sitosterol-β-glucoside as primer for cellulose synthesis in plants. *Science* **295**, 147-150
- 145. Vandeputte, P., Ferrari, S., and Coste, A. T. (2012) Antifungal resistance and new strategies to control fungal infections. *Int. J. Microbiol.* **2012**, 713687
- 146. Do, E., Hu, G., Caza, M., Oliveira, D., Kronstad, J. W., and Jung, W. H. (2015) Leu1 plays a role in iron metabolism and is required for virulence in *Cryptococcus neoformans*. Fungal Genet. Biol. 75, 11-19
- 147. Kretschmer, M., Wang, J., and Kronstad, J. W. (2012) Peroxisomal and mitochondrial β-oxidation pathways influence the virulence of the pathogenic fungus *Cryptococcus neoformans*. *Eukaryot*. *Cell* **11**, 1042-1054

### **ACKNOWLEDGMENTS**

The author would like to express my gratitude to Dr. Makoto Ito, Professor of Kyushu University Graduate School, for enthusiastic instruction, stimulating discussions, and warm encouragements throughout of this study.

The author would like to express my gratitude to Dr. Nozomu Okino, Associate Professor of Kyushu University Graduate School, for invaluable help and encouragements throughout of this study.

The author extends sincere appreciation to Dr. Kaoru Takegawa, Professor of Kyushu University Graduate School, for making a thorough review of the thesis.

The author expresses hearty thanks to Dr. Yohei Ishibashi, Assistant Professor of Kyushu University Graduate School, for constructive advice, technical assistance throughout of this study.

The author appreciates Mr. Tomoharu Ito for providing the valuable information about EGCrP2.

The author expresses gratitude to Dr. Hatsumi M Goda, Kyushu University, and Dr. Tomofumi Miyamoto, Associate Professor of Kyushu University Graduate School, for NMR analysis of EG.

The author appreciates Dr. Motohiro Tani, Associate Professor of Kyushu University Graduate School for kindly donating the various yeast strains, and valuable advice throughout of this study.

The author expresses gratitude to Dr. Kazutaka Ikeda, Keio University, Dr. Ryo Taguchi, Professor of Chubu University, and Ms. Emiko Matsunaga, Center for Advanced Instrumental and Educational Supports, Faculty of Agriculture, Kyushu University for MS analysis of EG.

The author appreciates Dr. Ken Matsuoka, Professor of Kyushu University Graduate School for valuable suggestion about vacuole morphology.

The author expresses heartfelt thanks to Mr. Kei Hashida, Dr. Yoshiki Itoh, and Dr. Yasuyuki Ishii, Sato Pharmaceutical Inc. for helpful advice.

Thea author would like to thank Dr. Kuniko Yamaguchi, Ms. Noriko Nakahara, and all members in this laboratory for providing joyful days and encouragements throughout of this work.

My deep graduate is due to my family for support and warm encouragements throughout of my student life.